CONJUGATED POLYMER NANOPARTICLES FOR BIOMEDICAL APPLICATIONS INCLUDING BIOIMAGING AND DRUG DELIVERY

A THESIS

SUBMITTED TO THE DEPARTMENT OF CHEMISTRY

AND THE GRADUATE SCHOOL OF ENGINEERING AND SCIENCE

OF BİLKENT UNIVERSITY

IN PARTIAL FULFILLMENT OF THE REQUIREMENTS

FOR THE DEGREE OF

MASTER OF SCIENCE

By

ÖZLEM ÜNAL

July, 2013

I certify that I have read this thesis and that in my opinion it is fully adequate, in scope and in quality, as a thesis for the degree of Master of Science.

…….

Assoc. Prof. Dr. Dönüş TUNCEL (Advisor)

I certify that I have read this thesis and that in my opinion it is fully adequate, in scope and in quality, as a thesis for the degree of Master of Science.

…….

Prof. Dr. Engin Umut AKKAYA

I certify that I have read this thesis and that in my opinion it is fully adequate, in scope and in quality, as a thesis for the degree of Master of Science.

…….

Assist. Prof. Dr. Özlen KONU

Approved for the Graduate School of Engineering and Science:

…….

Prof. Dr. Levent ONURAL

Director of the Graduate School

ABSTRACT

CONJUGATED POLYMER NANOPARTICLES FOR BIOMEDICAL APPLICATIONS INCLUDING BIOIMAGING AND DRUG DELIVERY

Özlem Ünal

M.S. in Department of Chemistry

Supervisor: Assoc. Prof. Dr. Dönüş TUNCEL

July, 2013

In this study, the ability of fluorene-based conjugated polymer nanoparticles in the delivery of anticancer therapeutics and bioimaging was investigated through *in vitro* cytotoxicity assessments and fluorescence imaging. In order to prepare the nanoparticles, green light emitting polymer,poly[(9,9-bis{6-dimethylaminohexyl}fluorenyl-2,7-diyl)-co-(1,4-benzo-{2,1,3}-thiodiazole)] (PDAFBT),was synthesized via Suzuki coupling reaction and characterized by nuclear magnetic resonance (NMR), electrospray ionization mass spectroscopy (ESI-MS), matrix assisted laser desorption ionization mass spectroscopy (MALDI), fourier transform infrared spectroscopy (FT-IR), UV-visible absorption spectroscopy (UV-Vis) and fluorescence spectroscopies. PDAFBT nanoparticles were synthesized through reprecipitation method which is based on the injection of the polymer solution in a good solvent into a poor solvent for the polymer to enhance the collapse of polymer chains in the form of spherical nanoparticles. Anti-cancer drug, camptothecin (CPT), was entrapped into the PDAFBT nanoparticles via hydrophobic interaction during the nanoparticle formation. Size, surface charge, morphology and optical characterizations of blank and CPT loaded nanoparticles were investigated by dynamic light scattering (DLS), scanning electron microscopy (SEM), transmission electron microscopy (TEM), UV-Vis and fluorescence spectrocopies. In order to investigate the properties of nanoparticles as drug carrier, drug encapsulation efficiency (EE) and drug loading efficiency (LE) were determined and EE was found to be as 92% and 75% for the 1:35 and 1:25 polymer to drug ratios, respectively, while LE of PDAFBT nanoparticles was determined as 2.67±0.3 %. Preliminary drug release profile which needs to be strengthen statistically, of PDAFBT nanoparticles was analyzed and showed that almost 100% of the loaded CPT was

released steadily during first 48h time period indicating that the release of CPT is not a burst process. Stability of blank and CPT loaded PDAFBT nanoparticles was examined in different biological media including cell culture medium, bovine serum albumine (BSA) andhuman serum. The precipitation in nanoparticle dispersion was observed due to adsorption of proteins onto the surface of polymers.

In vitro dose dependent cytotoxicity of blank and CPT loaded PDAFBT nanoparticles was assessed through 3-[4,5-dimethylthiazol-2-yl]-2,5-diphenyl tetrazoliumbromide (MTT) toxicology assay on human carcinoma breast cancer cell lines, namely,MDA-MB-231, MDA-MB-157 and MCF-7 cells. The blank PDAFBT nanoparticlesdo not exhibit significant toxicity to MDA-MB-231 and MDA-MB-157 cells up to 40 μM, however, a linear decrease on the viability of MCF-7 cells was detected ata concentration higher than 2.5 μM and nearly 40% of the cells were dead at 40 μM.The half maximal inhibitory concentration (IC_{50}) values of free CPT and CPT loaded PDAFBT NPs were calculated to be 4.50μM and 1.35μM for MDA-MB-157 cell line, respectively, and 1.97μM and 1.05μM for MDA-MB-231 cells, respectively. These results indicate clearly that the CT-loaded nanoparticles are more efficient than free CPT in destroying the cancer cells. Fluorescent microscope images show also the efficient internalization of blank and CPT-loaded nanoparticles by MDA-MB-157 and MDA-MB-213 cell lines. Preliminarily *in vivo* studies have been performed on embryonic zebra fish and C. Elegans animal models using these nanoparticles and the efficient uptake of nanoparticles by the tissues have been observed by fluorescent microscopy. This results indicate that CPNs are promising for imaging and delivery vehicles for time and dose dependent treatments.

Keywords: Conjugated polymer nanoparticles, drug delivery, bioimaging.

ÖZET

KONJUGE POLİMER NANOPARÇACIKLARIN İLAÇ TAŞINIMI VE BİYOLOJİK GÖRÜNTÜLEME İÇEREN BİYOMEDİKAL UYGULAMALARI

Özlem Ünal

Kimya Bölümü Yüksek Lisans Tezi

Tez Yöneticisi : Doç. Dr. Dönüş TUNCEL

Temmuz, 2013

Bu çalışmada, floren tabanlı konjuge polimer nanoparçacıkların antikanser terapatik taşınımı ve biolojik görüntüleme verimi, canlı dışı toksik inceleme ve floresan görüntüleme yöntemleriyle incelenmiştir. Nanoparçacıkların hazırlanmasında yeşil ışıyan poli[(9,9-bis{6-dimetilaminohekzil}florenil-2,7-dil)-ko-(1,4-benzo-{2,1,3}-tiyadiazol)](PDAFBT**)** polimeri kullanılmıştır. PDAFBT polimeri, Suzuki kenetleme reaksiyonu ile sentezlenmiş, karekterizasyonu nükleer manyetik rezonans spektroskopileri (H^1-NMR, C^{13}-NMR), elektrosprey ionizasyon kütle spektroskopisi (ESI-MS), matris destekli lazer salınımlı kütle spektroskopisi (MALDI), fourier transformu kızılötesi spektroskopisi (FT-IR), UV-Vis absorbans ve floresans spektroskopileri ile yapılmışmıştır. PDAFBT nanoparçacıkları, çözücünün hidrofilikliğinin azaltılmasına dayanan ve polimer zincirlerinin çökerek küresel forma dönüşmesine dayanan geriçöktürme yöntemi ile hazırlanmıştır. Anti-kanser terapatiği olarak kullanılan kamptotesin, PDAFBT nanoparçacıklarının içerisine nanoparçacık oluşumu sırasında etkin olan hydrofobik etkileşimle yüklenmiştir. Nanoparçacıkların boyut, yüzey yükü, şekilsel ve ışıksal karekterizasyonları dinamik ışık saçılımı (DLS), geçirimli elektron (TEM), taramalı elektron mikroskopileri (SEM), UV-Vis absorbans ve fluoresans spektroskopileri ile yapılmıştır. Nanoparçacıkların ilaç taşıyıcı olarak özelliklerinin incelenmesi amacıyla, ilaç kapsülleme (EE) ve ilaç taşıma (LE) verimleri analiz edilmiş ve ilaç kapsülleme verimi 1:35 ilaç-polimer oranında % 92, 1:25 ilaç-polimer oranında % 75 olarak bulunurken, ilaç taşıma verimi ise % 2.67±0.3 olarak belirlenmiştir. Öncül bir çalışma olan ve sonuçları istatiksel olarak güçlendirilecek PDAFBT

nanoparçacıkların ilaç salınım profili analiz edilmiş ve ilaç miktarının yaklaşık % 100 ünün 48 saat içinde salındığı gözlenmiştir.

Boş ve kamptotesin yüklü PDAFBT nanoparçacıkların hücre kültürü ortamı, bovin serum albumin (BSA) ve insan serumu içeren farklı biyolojik ortamlardaki stabilitesi test edilmiş, insan serumu ve bovin serum albumin ortamında proteinlerin polimer yüzeyine tutunması nedeniyle nanoparçacık solusyonunda çökme gözlenmiştir.

Boş ve ilaç yüklü nanoparçacıkların canlı dışı (in vitro) doza bağlı toksik incelenmesi, tetraazolyum boyasının redüklenmesine dayanan MDA-MB-231, MDA-MB-157, MCF-7 insan göğüs kanseri hücre hatları üzerinde MTT toksikoloji testi ile yapılmıştır. Sadece kamptotesin ve kamptotesin yüklü PDAFBT nanoparçacıklar için % 50 inhibe edici konsantrasyon (IC_{50}) değerleri MDA-MB-157 hücreleri için 4.50 μM ,1.35 μM ve MDA-MB-231 hücleri için 1.97μM ve 1.05μM'dır ve polimer kapsuller sayesinde ilacın hücrerele etkin alınımı gösterir. PDAFBT ve PPFBT nanoparçacıkların yaşayan canlı modelleri olan zebra balığı ve C. Elgans üzerindeki yapılan görüntülemeleri nanoparçacıkların dokulara etkin bir şekilde nüfuz ettiğini desteklemektedir ayrıca zamana ve doze bağlı uygulamalar için umut vericidir.

Anahtar Kelimeler: Konjuge polimer nanoparçacıklar, ilaç taşıma, biyolojik görüntüleme

Dedicated to the memory of

Burak Alisir

ACKNOWLEDGEMENT

First of all, I would like to express my sincere appreciation to my research supervisor Assoc. Prof. Dönüş Tuncel for her guidance, support, trust and encouragement for not only my reseach project, but also for my academic plans. Her positive attitude towards my studies have helped me to ahead, despite all the academic challenges and huddles I faced.

I would also thank examining committee members, Prof. Engin Umut Akkaya and Assist. Prof. Özlen Konu, for their time and valuable suggestions on my thesis.

I am deeply grateful to Prof. Özlen Konu and her PhD student Ermira Jahja for their worthy colaboration and and significant support to biological part of the study. Moreover I would like to thank to Prof. Arzu Atalay and Selen Güçlü due to their trainings for *C. Elegans* experiments.

I would like to extend special thanks to Vusale İbrahimova for her guidance in the laboratory and her valuable friendship.

I also would like to express my appreciation to all of those with whom I have had the pleasure to work within the past three years. I am sincerely grateful to my old and new colleagues Meltem Aygüler, Müge Artar, Şeyma Ekiz, Eda Kocak, Özlem Gezici, Muazzam Idris, Josheed PK., Hamidou Keita, Esra Soner and Sinem Gürbüz.

I have to express my thanks to Alp Özgün for donation of his blood for the experiments with "human serum" in my research and sharing his ideas.

I would like to thank to my close friends, Gözde Barım, Merve Doğaç, Tuğçe Durgut, Tuba Yaşar, Duygu Demircioğlu, Melis Tunalı, Menekşe Koca, Seda Selçuk, Merve Taner, Merve Şahinsoy, Gülşen Uğrar, Mert Demirdelen, Yiğit Altay, Aykut Aydın, and Yiğit Can Yüceyurt for their worthy fellowship and significant contrubition to my life.

Lastly, I wish to sincerely thank to my mother, father and brother for their encouragement, trust and motivation. It is very important for me to feel their love and suppot during my life.

CONTENTS

CHAPTERS

LIST OF FIGURES

LIST OF SCHEMES

LIST OF TABLES

LIST OF ABBREVIATIONS

CPs Conjugated Polymers

CPNs Conjugated Polymer Nanoparticles

HOMO Highest Occupied Molecular Orbital

LUMO Lowest Unoccupied Molecular Orbital

PDAFBT Poly[(9,9-bis{6-dimethylaminohexyl}fluorenyl-2,7-diyl)-co-(1,4-benzo-{2,1,3}-thiodiazole)

PPFBT Poly[9,9-bis{propenyl}fluorenyl-2,7-diyl))- co-(1,4-benzo{2,1,3}-thiodiazole)]

PDAFBT NPs Poly[(9,9-bis{6-dimethylaminohexyl}fluorenyl-2,7-diyl)-co-(1,4-benzo-{2,1,3}-thiodiazole) Nanoparticles

CPT Camptothecin

THF Tetrahydrofuran

$CDCl_3$ d-Chloroform

NMR Nuclear magnetic resonance

UV-VIS Ultraviole Visible

MALDI Matrix-Assisted Laser Desorption/Ionization

ESI Electrosprey Ionization

MS Mass Spectroscopy

TEM Transmittance Electron Spectroscopy

SEM Scanning Electron Microscopy

MTT 3-[4,5-dimethylthiazol-2-yl]-2,5-diphenyl tetrazoliumbromide

BrdU 5-Bromo-2-deoxyuridine

CHAPTER 1

1. INTRODUCTION

Recent developments in nanotechnology provide special biomedical tools which are capable to deliver pharmaceuticals and biological agents with high efficiency, in a controlled time-scale and a safe way.These nano devices have an importance for drug delivery, molecular imaging and biomarkers. Traditional therapeutic approaches provide only non-specific drug mixtures but an efficient delivery needs more attention to design smart systems through a multifunctional aspect which target to visualize the carriers with an effective screening and increase the bio-compatibility. Nanoparticles improve the bio-availability of water-insoluble drugs, protect the drugs from physiological barriers and increase the body tolerability to the drugs and thereby, enhance the efficiency of drug delivery. Tracking the bio-distribution of nanocarriers is crucial to investigate the interaction of therapeutics with the sections of tissues and cells. Among a number of screening methods, fluorescence imaging has important impact to control the bio-distributions of pharmaceutical carriers in drug delivery research.

Typical fluorescent imaging agents containing conventional dyes have photobleaching and toxicity problems. Although quantum dots have high brightness and photostability, they are cytotoxic due to heavy metals from their nanocrystal core and their bio-compatibility is not high enough for biological applications.These limitations urgethe design of new fluorescent materials in drug delivery research. Development of fluorescent conjugated polymer materials is very promising in imaging guided drug delivery applications due their high brightness, good photostability and lower toxicity. Fluorene based conjugated polymer nanoparticles which are prepared through miniemulsion[57] or reprecipitation[59] methods have wide range of applications from nanomedicine [70,78,79] to molecular electronics.[63-64]

CHAPTER 2

2. BACKROUND

2.1. Conjugated Polymers

Broad range of polymers exhibit insulating properties, however if polymers are designed in such a way that having conjugated backbone, they could conduct the electricity (Figure 1). These polymers are called conjugated polymers and consist of unsaturated sp^2 or sp hybridized carbon atom chains including p_z orbitals which forms π overlap with adjacent unsaturated carbon atom and these overlaps form delocalization of π electrons along the polymer chain.[1-2]

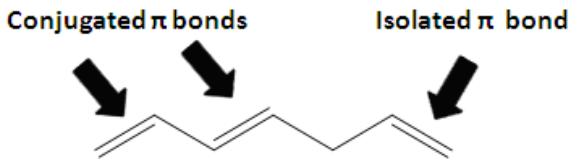

Figure 2. 1. Conjugated and isolated π bonds in 1,3,6heptene..

This πstateformation leads to a frontier electronic gap, named as π-band gap which is relatively smaller than σ-band gap and varies from 1.5 eV to 4 eV depending on the structure.The energy spacing between highest occupied molecular orbital (HOMO) and lowest unoccupied molecular orbital (LUMO) is defined as band gap energy and identifies the level of conductivity (Figure 2). The ability of semiconducting behaviours of conjugated polymers come from this low energy band gap between conduction band (HOMO) and valence band (LUMO).[1-4] Density of charge carriers affects the conductivity. Small band gaps in conjugated polymers provide ease in doping,which corresponds to partial oxidation or reduction, and charge carrier generation.[4-6]

The first conducting polymer was poly(acetylene) and synthesized using Ziegler-Natta catalyst in 1958 by K. Ziegler , G. Natta who were awarded 1966 Nobel Prize

in Chemistry.[7] However only conjugation is not enough for being conductive, thus charge carriers which contains holes (missing electrons or positive charge) or electrons, have to be added to system (doping) to allow charge to migrate along the long distance. In 1974, Shirakawa and coworkers discovered that treatment with halogen vapour increases the conductivity of polyacetylene 10^9 times more than its natural form and were awarded the Nobel Prize 2000 "*for the discovery and development of electrically conductive polymers*" [8-9]

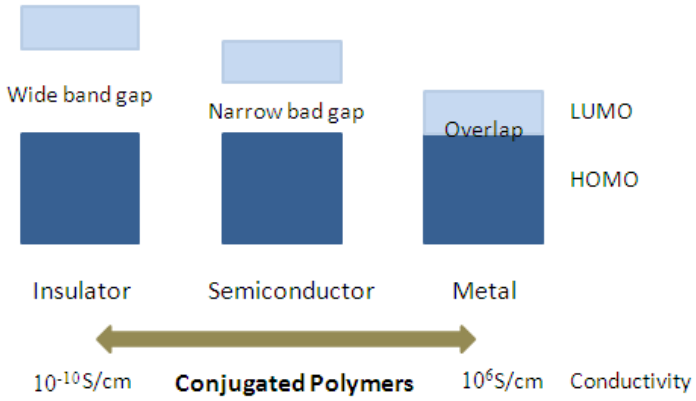

Figure 2.2. General band picture of an insulator, a semiconductor,a metal and conductivity of conjugated polymers compared to those of materials.

Conjugated polymers could also exhibit photoluminescence (PL) properties when they are excited with a suitable wavelength of a light. Luminescence is the spontaneous emission of light from electronically excited states in the substances under optical excitation and it can be named as fluorescence when light emits from singlet excited states and phosphorescence when light emits from triplet excited states.[10] Jablonski Diagrams are used to explain light absorption and emission phenomena through illustrating electronic ground and excited states with a number of vibrational energy levels (Figure 3). When a photon at particular energy is absorbed by the fluorophore (fluorescent molecule) which is excited to higher vibrational levels of S_1 or S_2,several pathways can be followed including vibrational relaxation, internal conversion, fluorescence, intersystem crossing, and phosphorescence to dissipate the energy. Conjugated polymers exhibit allowed absorptions and emissions and generally luminescence efficiency changes with the delocalization and

polarization of the electronic structure. For example, highly delocalized and polarizable polymers are weakly luminescent due to dissociation of photo-generated electron-hole pairs through the chain in order to generate charge carriers, then combination of these free carriers to form triplet or deactivation by non-radiative relaxations occur.[11]

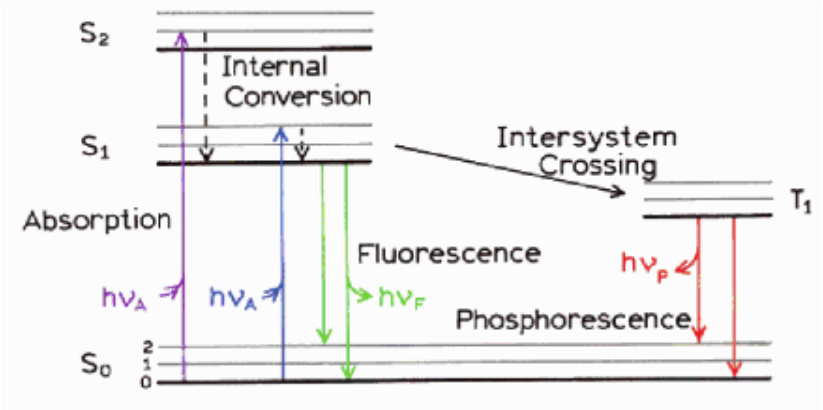

Figure 2.3. Ilustration of radiative and nonradiative transitions between the electronic states in a molecule after absorption of a photon by Jablonski diagram.[12]

Electroluminescence, emitting light due to excitation by the flow of electric current, became another important feature of conjugated polymers with the discovery of electroluminescent property of semiconductive conjugated polymer poly(p-phenylenevinylene) by Friend *et al* in 1990.[13] In the last decade, polymer light emitting diodes (PLEDs) (Figure 4a), which produce light by the fast decay of excited molecular states in the polymers, have been under great interest and polythiophenes[14], polyphenylenes[15], polyfluorenes[16] were used for various electroluminescent applications due to their comparable efficiency and brightness to their inorganic analogs.[17] In the area of photovoltaics which is based on producing electrolytic cells to generate electrical current when exposed to light[18] (Figure 4b), conjugated polymers are widely preferred semiconductors due to their ability of absorbing significant fraction of sun light and ease of processing on flexible films at low cost.[19] With the discovery of bulk heterojunction, the improvements in conjugated polymer based photovoltaic cells (PV) through the attempts to achieve smaller band gaps, wider band widths,higher carrier mobilities have been obtained

and their power efficiency enhanced 100 folds greater in the past decade.[20] As another photonic application, conjugated polymers are unique class of solid state laser materials due to their emission spectrum which involves entire visible spectrum.[21]

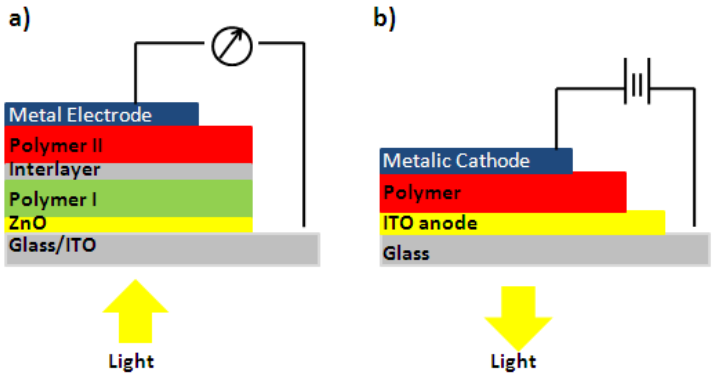

Figure 2.4. Schematic representation of a) photovoltaic cell b) light emitting diode based on conjugated polymer.

Apart from being *high performance plastic photonic devices*, conjugated polymers are versatile chemosensors performing for variety of sensing methods such as conductrometric sensors due their conductivity, potentiometric sensors which is developed on the basis of their reversible nature of redox processes, calorimetric sensors based on the sensitivity of CP's band gap with respect to polymer conformation[22]. Moreover, CPs are preferred significantly for the applications as fluorescent chemosensors to detect the substances from biomolecules to explosives[23-24] due to their direct fluorescent response to the analytes in the environment, conformational change of backbone by the interaction with analyte, ease of substitution of flexible backbones with receptor groups to achieve molecular recognition and amplify the fluorescence signals.[25] Furthermore, conjugated polymers have applications also in the new emerging areas such as artificial muscles and nano-electromechanical systems.[26-27]

2.1.1 Fluorene Based Conjugated Polymers

Polyfluorenes (PFs) are stepladder types polyphenylenes, being very promising for the fabrication of LED[28-29]and PV diodes[30-31]. The most important advantage in the

area of optoelectronics of these polymers is their high photoluminescence efficiency both in solution and in solid films with the emission of blue light in the visible spectrum due to their rigid biphenyl units providing a large band gap for blue emission.[32-33] They show better thermal- and photo-stability than their analogs in the optoelectronics.[34] Moreover, highly reactive protons at C-9 position of the fluorene unit allow substitutions at this position without destroying their electrochemical properties and provides the opportunities to improve the solubility and processability of these polymers.[35-36] Various fluorene copolymers are synthesized, in order to obtain wide range of emission colors in the entire visible spectrum and tune their band gaps as shown in Figure 5.[28] Apart from applications in optoelectronics, PFs are widely used in bioimaging[37]and chemosensory[38]applications.

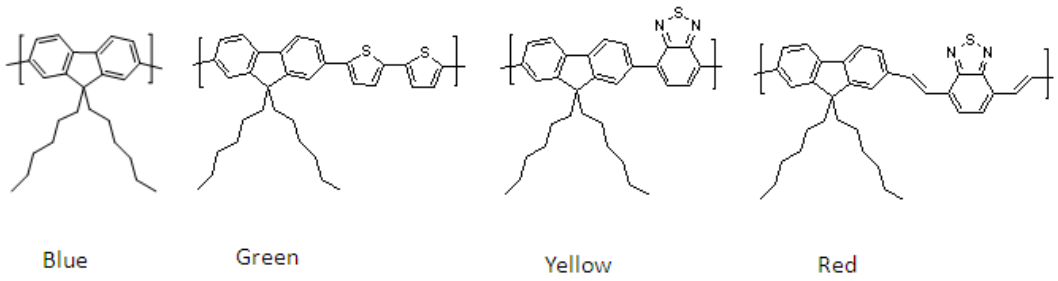

Figure2.5. Different emission colors based on backbone structure of co-polyfluorenes.

2.1.2. Synthesis methods of conjugated polymers

Polymerization is the process of combination of desired monomers through stepwise oligomer formation to long chains or adding unsaturated monomers onto the active site of the growing polymers in a controlled manner.[39] Synthetic methods are significant to obtain polymers including well defined molecular weight and polydispersity. Various methods have been developed to synthesize conjugated polymers and tried to design pure, soluble, efficient electrochemical features containing polymers by preserving delocalized pi states in the polymer chain. One of these methods is electrochemical polymerization which is based on deposition of polymer thin films from monomers such as aniline, pyrole, thiophene on the anode.[40] Experimentally, polymerization is carried outin a single compartment electrochemical cell with three electrodes configuration and electrochemical bath

consists of monomer and electrolyte in an appropriate solvent.[41] When going into a literature research in this area, it can be seen that, the electrochemical synthesis of conducting polypyrole by Diaz *et al.* provided a new synthetic way in the polymer science and triggered various studies in the field.[42] Polythiophene and poly(isothionaphthalene) have been other electrochemically prepared conductive polymers which is carried out Wuld et al.[43] Electrochemical synthesis of polythiophenes in microemulsion medium by using cationic surfactant has been reported by Murugan and his co-worker.[44] Electrochemical synthesis of these conductive polymers consists of especially polypyroles and polythiophenes provides many enhanced applications in the field of optoelectronics.[41] Besides, catalytic chain polymerization, which is mainly used for the synthesis of polyvinylenes and polyphenylenevinylenes[45], chemical oxidation polymerization for the preparation of polyacetylenes and polyanilines unfortunately with high amount of side products[40], photochemical polymerization typically for the synthesis of polydiacetylenes[46], are other feasible approaches for the synthesis of conjugated polymers.

Transition metal mediated cross coupling reaction is one of the most powerful techniques to synthesize conjugated polymers via carbon-carbon bond formation between sp^2-sp^2 or sp^2-sp hybridized carbon atoms and recently was awarded with the Nobel Prizes in Chemistry 2010 for *palladium catalyzed cross couplings in organic synthesis*.[47] Nucleophilic substitutions at sp^2 and sp carbons are not easy and need transition metal catalysts.The theory of cross coupling reactions is basically, assembling of carbon atoms of two reactants on the transition metal through the metal-carbon bonds and resulting carbon-carbon bonds between these couples after introducing them into very close proximity as shown schematically in Figure 6. Generally, palladium (or nickel) catalyst couplings are believed to follow the similar catalytic cycle with some changes in the steps including activation of the catalyst and release of the product.The reactions start with oxidative addition, reacting of Pd(0) catalyst with organohalide and changing to Pd(II) with the formation of organopalladium compound via C- Pd bonding, after that step there are some differences in different type of couplings but transmetallation is the common step consisting of the co-ordination of nucleophile (second carbon source) to Pd and assembling of two reagents on the Pd and followingly reacting of these couples with

each other. After carbon carbon bond formation is achieved then regeneration of Pd(0) and releasing of newly formed organic compound occur at the final step which is called as reductive elimination.

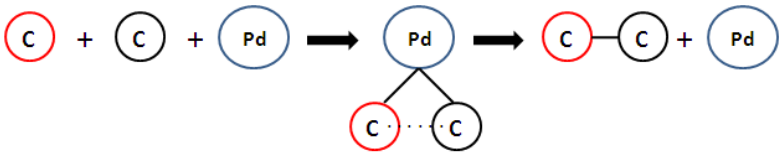

Figure 2. 6. Basic representation of metal catalyzed C-C bond formation.

Discoveries in cross coupling reactions are triggered by publications of Kumada *et. al*in the beginning of 1972, including carbon-carbon bond formation by cross coupling of Grignard reagents with organic halides through Ni catalyst.[48] Again in 1972, a new cross coupling reactions of aryl, vinyl halides and olefins in the presence of Pd catalyst has been reported by Heck *et al*.[49] and it became the most important carbon-carbon bond forming reaction under the truth that palladium salts are mostly useful. In the case of Heck coupling, general catalytic cycle is followed between organohalide and olefin but differently carbon-carbon bond forms via migratory insertion including migration of carbon atom on Pd to one of the carbon atoms of the coordinated olefin and release of newly formed organic compound through β-H elimination (Figure 7).

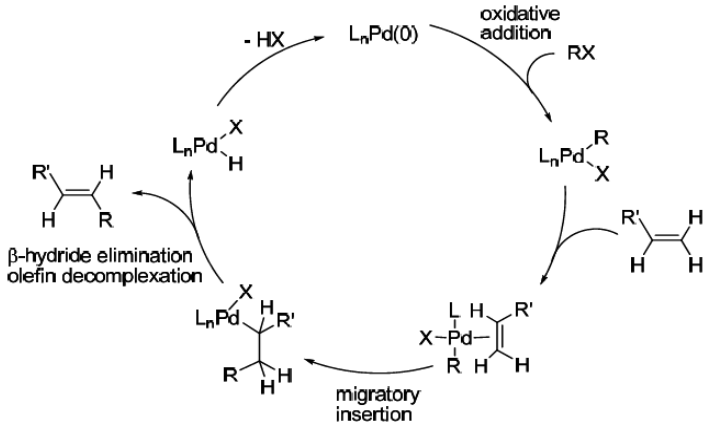

Figure 2. 7. Reaction Mechanism of Heck[47] cross-coupling.

In 1979, another most attractive approach to carbon-carbon bond formation has been discovered by Suzuki and Miyaura including trans metal catalyzed cross coupling between an organoboron compound and organic halide.[50] Differently from Heck coupling, reaction mechanism of Suzuki coupling involves the activation of organoboronic acid through a base and facilitation of transmetallation. Choosing the organoboronic compounds provides various advantages such as making coupling reactions more practical due to the weak nucleophilicity and stability of organoborones, having high chemoselectivity, providing to run the reaction at mild conditions and non-toxicity of boron compounds. Moreover, the most important benefit of this coupling is to tolerate many different functional groups and providing efficient couplings between biaryl, aryl-vinyl, alkyl-aryl and alkyl-alkyl compounds.[47]Due to these advantages, Suzuki cross-coupling reaction was preferred for the synthesis of polymers in this thesis.

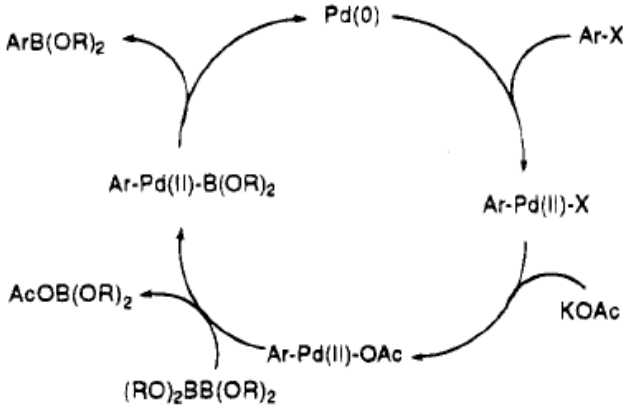

Figure 2. 8. Reaction Mechanism of Suzuki Cross Coupling[51]. (Reprinted with the permission from ref 51. Copyrigth (1995) American Chemical Society)

In 1977, Negishi and coworkers reported using organozinc ligands as nucleophiles in the palladium catalyzed couplings containing organozinc and organoaliminum compounds.[52]

One of the most versatile organometallic reagent in Pd catalyst cross coupling reactions is organotin which is used as a novel method for carbon-carbon bond generation between an organohalide and organostanne developing through Stille and

coworkers.[53] The most important advantage of this reaction is to tolerate variety of functional groups containing alcohols, ketones, enones, esters, nitriles, nitro groups.

In the reaction, Pd catalyst is coupled with an electrophile with a vinyl or a aryltin compound through oxidative addition. After transmetallation with organostanne, functional group of organostanne replaces the halide anion on Pd(II) complex and finally coupled product is released with the reductive elimination (Figure 8).

Sonogashira[54] reaction which is based on the reaction between aryl and alkynes under Pd and Cu catalysis, Yamamato[55] obtaining biaryl from aryl halides in the presenceof Ni catalyst, are other coupling reactions to synthesize conjugated polymers.

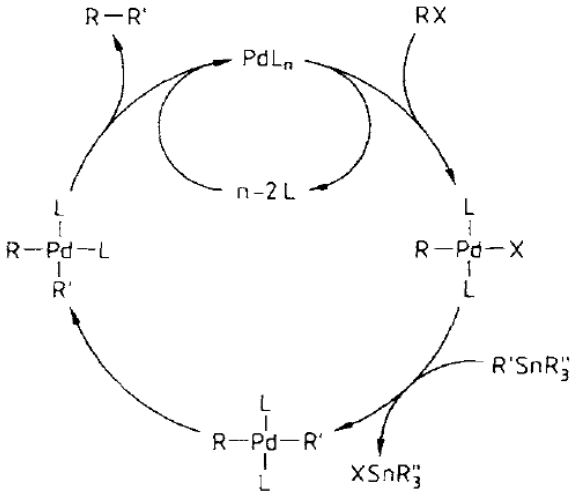

Figure 2. 9. Reaction Mechanism of Stille Cross Coupling.[53] (Reprinted with the permission from ref 53. Copyrigth (1986) Wiley)

2.2. Conjugated Polymer Nanoparticles

Conjugated polymer nanoparticles (CPNs) can be termed as colloidal dispersions of lyophobic polymers surrounded by low molecular weight solvents. First colloidal dispersions of CPs have been reported in 1980's from polyacetylene, polyaniline and polypyroles.[56] In order to benefit conjugated polymers in biological applications, water soluble forms have to be prepared of these resulting polymers through substitutions with hydrophilic or ionic side chains. However this method can cause decrease in quantum yields or aggregations of the polymers in water. In order to

avoid these undesired situations, conjugated polymers can be converted into the water soluble nanoparticles through several physical steps. Conjugated polymer nanoparticles are highly versatile tools in wide range of applications from optoelectronics to biological fields due to their major advantages including mechanical and photostability, ease in surface functionalization and emissions in a wide range of wavelengths.

2.2.1 Preparation Methods of Conjugated Polymer Nanoparticles

CPNs could be prepared through miniemulsion or reprecipitation methods. Among them, miniemulsion method is based on generating emulsions from conjugated polymers dissolved in organic solvent.[57] Figure 9 shows the preparation CPNs through miniemulsion method. High stability of aqueous dispersion of nanoparticles can be preserved through combined effects of surfactant and co-stabilizer molecules which builds osmatic pressure in the droplets. With this technique, submicron polymer nanoparticles (75-250 nm) can be obtained by adjusting amount of surfactants and the concentration of the polymer solution. Landfester and coworker reported stable miniemulsions from ultra-hydrophobe methyl substituted ladder type poly(para phenylene) by using sodium dodecyl sulfate as surfactant in the size range about 150 nm and also it was investigated that the size of nanoparticles can decrease to nearly 75 nm by increasing the surfactant.[58]

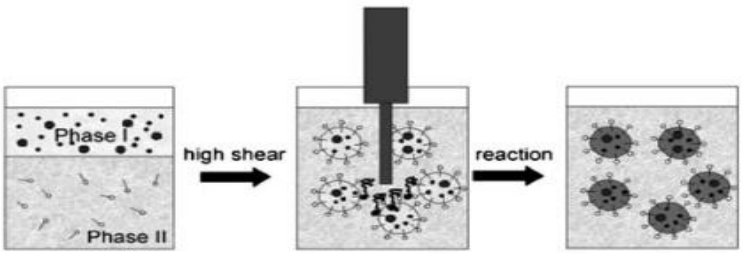

Figure2.10. Miniemulsion method for the preparation of polymer nanoparticles.[57] (Reprinted with the permission from ref 57. Copyrigth (2009) Wiley)

Another developed method to obtain conjugated polymer nanoparticles is reprecipitation.[59] This method is based on hydrophobic effect through the decrease in the hydrophobicity of solvent. After dissolving polymer in a solvent such as tetrahydrofuran (THF) which dissolves polymer well, then the polymer solution is rapidly injected into to excess amount of water having poor solvent quality for the

polymer (Figure 10). Polymer chainstend to collapse down triggered by the decrease in contact area with solvated molecules due to decrease in solvent property.[56,60] Through this method, it is possible to prepare spherical nanoparticles in a wide range of sizes (3-150 nm) by adjusting the concentration, chemical structure and molecular weight of the polymer. There are many examples in the literature for the preparation of conjugated polymer nanoparticles based on reprecipitation method. One of them consist of polymer nanoparticles from poly(phenylene ethynylene) derivatives which are sensitive to labeled oligonucleotides and used to detect them by fluorescence quenching.[61] Resulting polymer nanoparticles were prepared through injection of the polymer solution in dimethyl sulfoxide into the excess amount of SSED (saline, sodium phosphate, EDTA) buffer.

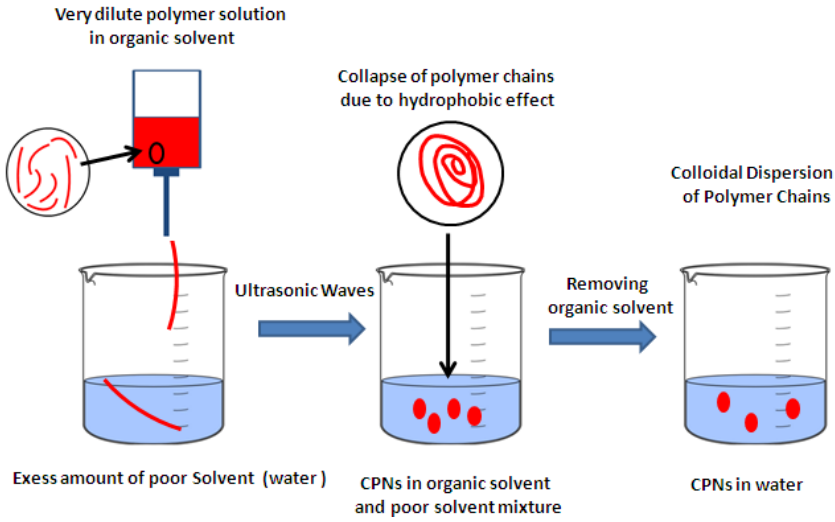

Figure 2. 11. Reprecipitation method for the preparation of polymer nanoparticles.

.

2.2.2 Photophysical Properties and Optoelectronic Applications of CPNs

Nanoscale organic electronics became more attractive with the development in nanoscience. The use ofconjugated polymer nanoparticles in organic devices have been demonstrated successfully in many studies. Applicability of these polymer nanospheres in organic electronics provides controlled multilayer deposition and high throughput capacity to the surface without consuming high amount of materials and most importantly environmental friendly processing.[61-62] The fabrication process consists of printing of polymer dispersion to a non-emitting matrix through deposition from an organic solvent and spreading on a large area as single or

multilayer (Figure11). The effect of fabrication process of polymer nanoparticle on devices was studied by Piok et al and reported that there is no significant difference in quantum yields for bulk and polymer nanoparticle states.[62] In the study, single layer methyl substituted poly(para phenylene) dispersion in water based OLED was fabricated by spin coating methods and it was observed that emission and absorption spectra of CPN dispersion, CPN film and polymer bulk in organic solvent are not intensely different from each other.

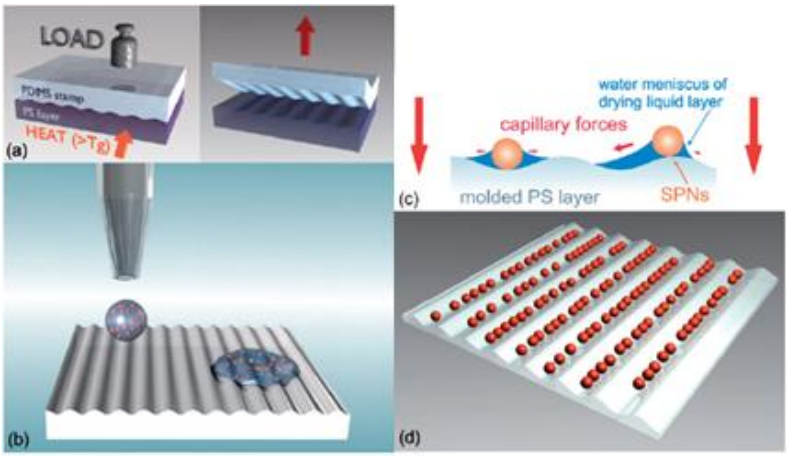

Figure 2.12. Schematic representation showing fabrication process of semiconducting polymer nanoparticles for optoelectronic applications.[61] (Reproduced with the permission from ref 61. Copyrigth (2008) Royal Chemical Society)

Another novel approach to LED applications was to generate white light via the tunability of emission color of CPNs containing cross-linkable functional groups.[63] Crosslinking enhances both the mechanical stability of polymer nanoparticles and forms a core shell structure which contains blue emitting layer in the core and yellow-green emitting layer in the shell. Through the energy transfer between these layers at different emissions wavelength with the control of the shell formation white light generation was obtained.

Applicability of conjugated polymer nanoparticles in photovoltaic cells was reported by Sherf and coworker.[64] The study is based on nanoparticle solar cell application through PFB and F8BT polymers which have high hole and electron mobility and it

was investigated that nanoparticles in photovoltaic cells provide controlling phase separation in polymer blend layer which effects to performance of the cell.

2.2.3 Conjugated Polymer Nanoparticles in Nanomedicine

Delivering of small molecules such as DNA, proteins and pharmaceuticals is one of the most important areas in the nanotechnology. Drug industries begin to give high attention to the novel drug carrier technologies. Recent developments in nanotechnology have provided new biological tools which are able to deliver pharmaceuticals in high efficiency, long time delivery and in a safe way of the drug loaded structures. Traditional therapeutic methods prepare only non-specific drugmixtures while these nano devices have important roles not only for drug delivery but also for molecular imaging and biomarkers.

CPNs in bioimaging

Molecular tracking of drug carriers plays a crucial role in target specific drug therapy because controlling biodistrubution of drug molecules is an important issue in drug delivery studies. In order to investigate spatial and temporal interactions of therapeutic agents with cellular compartments, bioimaging techniques have to be applied. Application of fluorescence technology in especially cell biology provides the enhancements in real time measurements in high sensitivity and high efficiency Therefore drug delivery science seek developments in fluorescence microscopy since 1970's.[65] In the same aspect, application of live cell imaging has a significant potential for drug delivery research through providing the understanding of dynamic events, such as intracellular trafficking.[66] Conventional fluorescent dyes have been used initially in this area but recent developments in the fluorescent nanoparticles made them significant candidate in imaging guided drug delivery. Encapsulation of organic dye with silica or polymeric nanoparticles are used in theranostic therapies due their mechanical stability and ability to amplify signal considerably. Significant advantages of encapsulation of dye with nanoparticles is to reduce photobleaching via polymer coating which penetrates the interaction with the oxygen.[67-68] Quantum dots another bioimaging tools which provides extended visualization of cells under multicolor imaging. Quantum dots are semiconductor crystals in the nanometer size

with broad absorption and narrow emission spectrum and also tunability of emission spectra by controlling of their size. The best applicable quantum dots fluorophores for biological applications are CdSe coated with ZnS which protects core layer from oxidation and prevent photobleaching of the CdSe.[69] Typical fluorescent imaging agents containing conventional dyes have photobleaching and toxicity problems. Although quantum dots have high brightness and photostability, they are cytotoxic due to heavy metals from their nanocrystal core and their biocompability is not high enough for biological applications. These limitations necessitates for the design of new fluorescent materials. One promising strategy is to develop fluorescent conjugated polymer materials which are useful sensing tools via the signal amplification. Several conjugated polymers have been used for live cell imaging due to their high brightness, good photostability and lower toxicity. One of them is reported by Wu and coworkers including new size controlled polymer dots from fluorene derivatives which exhibit much higher emission rate and no bleaching with respect to their conventional dye molecules[70]. It was investigated that these polymer dots are very promising for single molecule imaging and tracking of live cells due to their high absorption cross section, bright fluorescence and high photon numbers (Figure 12). Furthermore, cytotoxicity of the polymer nanoparticles was not in an appreciable extent givenresulting incubation time and concentration.

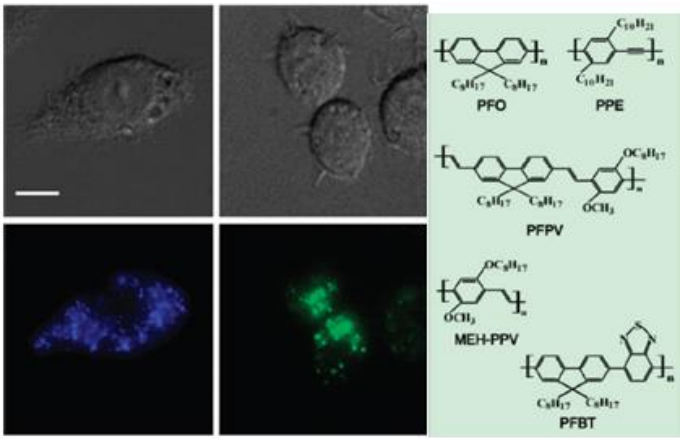

Figure 2. 13. Differential contrast (top) and fluorescence (bottom) images of macrophage cells labeled with PFO PFBT polymer dots.[70] (Reproduced with the permission from ref 70. Copyrigth (2008) American Chemical Society)

Targetted drug delivery via CPNs

Nanoparticles improve the bio-availability of water- insoluble drugs,protect the drugs From physiological barriers and increase tolerability ofthe body to the drugs and in turn, this enhances the efficiency of drug delivery. However, although these nanocarriers increase the therapeutic index of drugs, they are generally simple and lack of efficient targeting and improved with the design of multifunctional nanoparticle platforms which enhances cell or tissue targeting.

In principal, delivery of anticancer drugs by nanocarriers is achieved by active or passive targeting. In passive targeting long circulating nanoparticles accumulate passively on solid tumor tissue by enhanced permeability and retention effect (EPR). EPR effect is result of angiogenesis in tumor tissues. Blood vessels in tumor tissues have gaps with the sizes of between 600 and 800 nm.[71-72] Passive targeting takes advantages of size of nanoparticles. Nanoparticles can enter the tissue through these defects and accumulate on tumor tissues. It has been demonstrated that 10 fold greater increase occurs in the drug accumulation on tumor tissue when drug is delivered by nanoparticles rather than as free drug.[73] Passive targeting generally uses EPR effect and this delivery does not have an effective targeting and has some limitations of distribution of drug. Drug molecules can outflow from the cells due to osmotic pressure in the intervascular side and this prevents efficient distribution of drug molecules to the cancer tissue.[74] These limitations in passive targeting can be alternated with the conjugation of targeting ligand or antibody to the nanoparticle. Ligand targeted approach is expected to deliver drug molecules in a high selectivity. [75]Active targeting is based on the ability of targeting agent to bind to tumor tissue surface to trigger receptor mediated endocytosis. A variety of tumor targeting ligands such as antibodies, growth factors or cytokines have been used as targeting agents.[76-77] In brief, efficient targeting is based on size, surface modification of nanocarriers and the presence of the targeting ligand.A novel targeted delivery of conjugated polymers is reported by Rong et al in which the design of conjugated polymer nanoparticles is based on fluorene and benzothiodiazole units containing boron dipyromethene (BODIPY).[78] Highly bright and narrow emissive polymer dots which exhibit emission full width at half- maximum varying from 40-55 nm were obtained through the intra-chain energy transfer between the polymer and BODIPY units.

Cellular labeling with these highly fluorescent marker was demonstrated by fluorescence imaging and flow cytometry experiments.The bio-conjugation of streptavidin to the carboxylate functional groups of the nanoparticle surfaces through covalent bond linkage provides cell specific targeting based on interaction between biotinylated antibodies and streptavidin conjugated polymer nanoparticles (Figure 13).

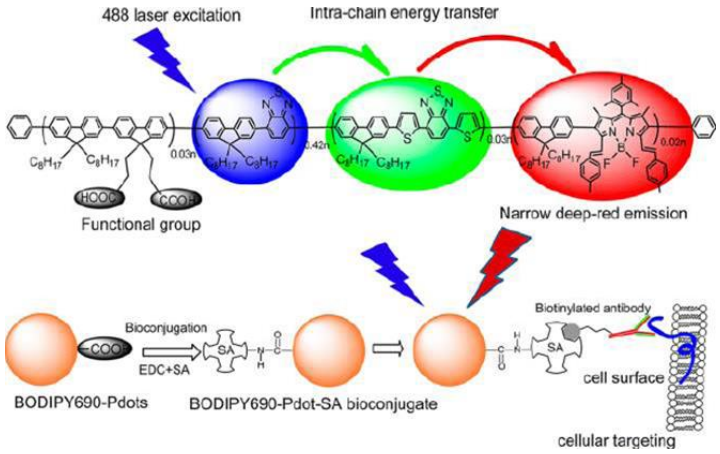

Figure 2. 14. Schematic illustration of narrow emissive CPN bioconjugates for specific cellular targeting.[78] (Reprinted with the permission from ref 78. Copyrigth (2013) American Chemical Society)

Wang *et a l*reported a facile multifunctional drug delivery system consisting of a complex of positively charged conjugated polymer (PFO) with negatively charged poly(L-glutamic acid) (PG) loaded with the anticancer drug doxorubicin (DOX).[79] Conjugated Polymer (PFO) exhibited a high quantum yield and photostability. Delivering Dox to lung cancer cells and release process were monitored by using fluorescence signal of PFO. When PFO/PG-DOX complex was internalized by the cells, the PFO remained in 'turn off' state, however, after 24 hours bright fluorescence of PFO was observed inside the cells due to release of DOX and weak fluorescence of DOX also was seen (Figure 14).

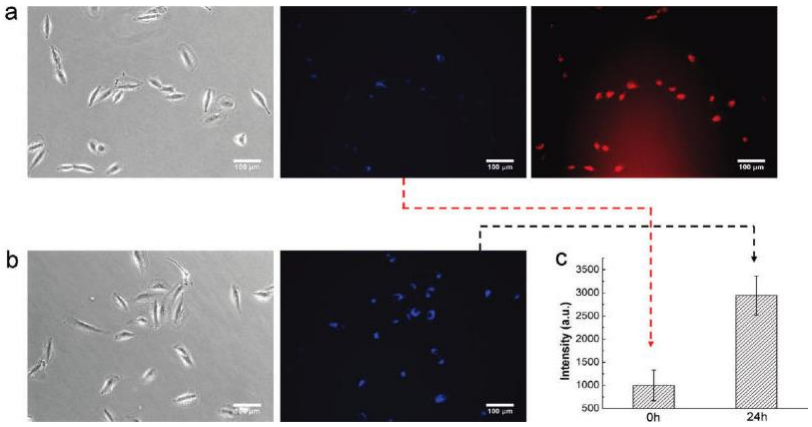

Figure 2. 15. Light and fluorescence miscroscopy images of A549 cell after incubation with PFO/PG-DOX for (a) 0 and (b) 24 h and (c) the fluorescence recovery of PFO.[79] (Reprinted with the permission from ref 79. Copyrigth (2010) American Chemical Society)

Fernando and coworker investigated therate, efficiency and mechanism of uptake of PFBT polymer dots through the cell line, J774A, which have similarities with macrophages.[80] To analyze the rate of nanoparticle uptakes, cells are incubated in different time scales and resulting intercellular fluorescence was measured by flow cytometry. It was also exhibited that the rate of nanoparticle uptake depends on the concentration of nanoparticle and temperature. The results indicate that very low amount of nanoparticles (155 pM) is enough for efficient labeling and low temperatures decrease the rate of uptake. Furthermore, live cell imaging highlights the entry routes of nanoparticles and their final locations in cellular compartments, it was hypothesized that endocytotic mechanism is responsible for PPFT dots uptake. The routes of nanoparticles was determined by using specific cellular markers such as protein lysosomal associated membrane protein (LAMP-1) taken up by the membranes of late endosomes and remains in the lysosomes and it was confirmed that nanoparticles localized in LAMP-1 containing organelles.

CPNs as nucleic acid therapeutics carriers

Nucleic acid therapeutics are important tools to treat many diseases, especially cancer. Synthetic small interference RNAs (siRNA) are important class of nucleic acid therapeutics including gene silencing mechanism with 21-25 nucleotides which degrade target mRNA.[81] siRNAs have significant therapeutic potential however

inefficient delivery systems due to stiff structure of siRNA limits their biomedical applications, thereby, a feasible and smart delivery systems should be developed to achieve a successful internalization by the desired tissue through protecting the stability of siRNAs in the body and facilitating cellular uptake.[82] It was investigated that many cationic species can make polyelectrolyte complexes with negatively charged RNA through electronic interactions, hence this complex formation provides the protection of siRNA from extracellular enzymes and mild cellular uptake. Liposomes, lipids, peptides, polymers, virus based vectors have been studied as delivery carriers in order to improve the efficiency of targeted delivery, enhance the biodegradability of vesicles and increase the circulation time in the body. However severe toxic effects of cationic species result limitations in the clinical applications.[83] Recently, several hydrophobic compounds are tried to be incorporated into the delivery vesicles to increase the complexation efficiency and to decrease the toxicity. Conjugated polymers have high potential in the area of nucleic acid delivery due to their flexible side chains which can be substituted with positive charges enabling to attract negatively charged nucleic acids and rigid backbones which provides facile cellular uptake.[84] Moon et al reported siRNA for actine B gene delivery to the HeLa cell via CPNs from amine containing poly(phenylene ethylene) through taking advantage of their low toxicity (Figure 15).[85] Fluorescent visualization and significant down regulation of target protein was observed. Hence, it was investigated that polymer nanoparticles make stable complex with siRNAs due to their large surface area which is the result of hydrodynamic volume rather than solid form and showed that increase in hydrodynamic volume of nanoparticles also increases the efficiency of complex formation with siRNA.

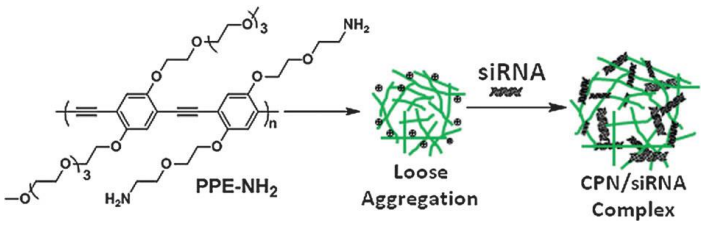

Figure 2. 16. Shematic representation of complex formation between poly(phenylene ethylene) CPNs and siRNA for actine B gene delivery.[85] (Reprinted with the permission from ref 85. Copyrigth (1995) Royal Chemical Society)

Hydrophobic polymers have aggregated nature in a poor solvent, and this feature of polymeric nanoparticles can provide using them as efficient delivery agents after entrapping with nucleic acids derivatives. Zare and coworkers published a study of siRNA delivery which consist of encapsulation of hydrophilic nucleic acid tRNA into copolymer (L-lactic acid)-polyethylene glycol for sustained release *in vivo*. [86] Nanoparticles were prepared through solution enhanced dispersion method with non-toxic supercritical carbondioxide as anti-solvent which provides efficient encapsulation and protection of nucleic acids by the polymers.

In vivo applications of CPNs

Fluorescence imaging methods remain generally *in vitro* studies or small animal models and not improve to clinical applications due to limitations in absorbance, scattering and autofluorescence phenomena. However using near infrared (NIR) excitation is less harmful for biological samples resulting minimum photodamag and has greater sample penetration depths with minimum autofluorescence.[87] However, there are several drawbacks in *in vivo* applications of conjugated polymer nanoparticles despite of their excellent brightness and nontoxic features. One of them is decreasing of their fluorescence quantum yield in red or NIR region through nanoparticle formation. Through this aspect, Kim et al developed water dispersed cyanovinylene-backboned polymer dots show bright fluorescence and synthesizing directly with *in situ* polymerization in the aqueous phase and showed their *in vivo* applications in a mouse model.[88] Furthermore, chemical and mechanical stability of nanoparticles in bodily fluid and strong NIR suggest their utilizations in *in vivo* applications. As an another novel approach to obtain deep red emitting polymer dots for in vivo applications, Chiu and coworkers designed polymer blend nanoparticle system which is based on an intra-particle energy transfer between a light harvesting polymer (PPFT) as donor and an efficient deep red emitting polymer (PF-DBT5) as an acceptor.[89] Fluorescence intensity distribution shows that fluorescence intensity of polymer blend dots is 15 times higher than QDs. Moreover, those polymer blend dots can be used to label specific cellular parts through polymer blend-streptavidin bioconjugate forms.

Caenorhabditis Elegans (C. Elegans) as model organisms for in vivo applications

C. Elegans is a transparent soil nematode with well-defined anatomy which is 1 mm long as being adult and consist of invariable number of 959 cells. The most feasible feature of C. Elegans as model organism in biological applications is its completely sequenced genome which enables to study biological processes in molecular level. Moreover, being optically transparent allows to image whole organism and track biodistribution of fluorescent markers. Alternatively, C. Elegans provides easy handling with their short life cycles and analyzing the results of various type of stress factors due to their sensitivities to these stimulants.[90-91]

In the area of bioimaging, several fluorescent markers were analyzed in vivo studies by using C. Elegans. For instance, Austin and coworkers published a preliminary work including imaging up-conversion phosphors (non-aggregated nanocrystals in the size of 50-200 nm) in the digestive systems in C. Elegans by using near infrared spectrum.[92] Moreover, survival rate of organisms was analyzed over 6h and it was investigated that there is little toxic effects of these nanoparticles in the organisms.

Another study about the biomaging through C. Elegans,which demonstrates the internalization of novel fluorescent nanodiamonds from nanocarbon family through the worms, was reported by Mohan et al.[93] The nanodiamonds were introduced to both with microinjection into the gonads of the worms and with feeding method to investigate the interactions between the nanomaterial and C. Elegans. The toxicity assessments were applied by life span and reproductivity assays and it was reported that these nanomaterials are nontoxic and not cause any reasonable stress for the worms. Additionally, it was also showed that the treated worms exhibit similar feeding behaviour with untreated worms and nanodiamonds do not cause any defect in natural behaviours (Figure 16).

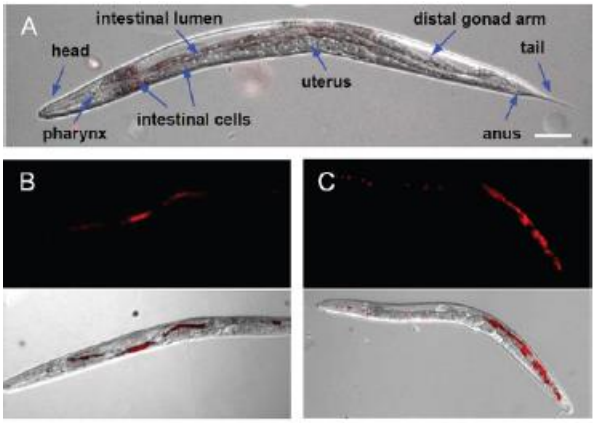

Figure 2. 17. Epifluorescence and epifluorescence/ DIC merged images of wild type C. Elegans A) untreated young adults, worms fed with fluorescent nanodiamonds for B) 2 h and C)12 h.[93] (Reprinted with the permission from ref 85. Copyrigth (2010) Royal Chemical Society)

Camptothecin as an Anti-Cancer Therapeutic

(S)-Camptothecin(CPT) is a pentacyclic alkoloid which is isolated firstly by Wall and coworkers in 1966 and promising in clinic activities of cancer treatment due to its anti-tumor activity.[94] The structure of the CPT is given in Figure 17. First total synthesis of CPT was reported by Stork and Shultz in 1971.[95] CPT gained a significant attraction as anticancer drug and this leads to synthesize its water soluble analogs to improve therapeutic applications limited due to its insolubility in aqueous medium.Topotecan and irinotecan are FDA approval camptothecin analogs and used in ovarian, small cell lung, refractory colorectal cancer treatments.[96] Primary cellular target of CPT is DNA topoisomerease I, a nuclear enzyme which modifies the topological state of DNA through breaking phosphodiester backbones of DNA. It was suggested that CPT binds non-covalently to topoisomerase I-DNA complex to break DNA strands upon replication to trigger cell death during the S-phase in the cell cycle.[97] Targeted and controlled delivery systems were developed for theinternalization of CPT into the cancer cells. One of them is reported by Yokoyama et al, consisting of CPT loaded polymeric micelles based on poly(ethylene glycol)- poly(benzyl L aspartate-69) block copolymer.[98]

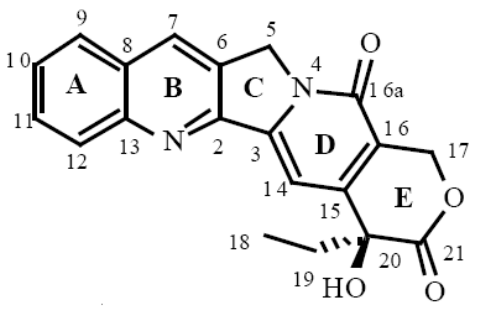

Figure 17. Structure of Camptothecin[97]

CHAPTER 3

3.EXPERIMENT RESULTS

3.1. General

All reagents were purchased from Sigma Aldrich Chemical Co. And were used as received. Column chromatography with silica gel (Kiegesel 60, 0.063-0.200 nm) was used for the purification of monomers. Thin layer chromatography (TLC) was performed by using silica gel plates (Kieselgel 60 F254, 1mm) to identify the products and impurities and determine the purity of the desired products. For structural characterization, nuclear magnetic resonance (NMR, Bruker Avance III 400 MHz spectrometer) and fourier transform infrared spectroscopy (FT-IR, Bruker Tensor 27) were performed. CDCl3-d_6 solvent was used for NMR measurements. For the FT-IR measurements, KBr pellets were prepared. The data were recorded at 25^{o}C, in the spectral range of 4000-400 cm^{-1}, by accumulating 25 scans with a resolution of 4 $cm^{-1.}$ For the optical characterization, a UV-Vis spectrophotometer (Cary Uv-Vis) and a fluorescence spectrophotometer (Cary Eclipse) equipped with a xenon lamp as the excitation source were used. Molecular mass of the monomers were determined via a liquid chromatography mass spectroscopy (TOF LC/MS, Agilent 1200/6210). Autoclaved ddH_2O was used to prepare the nanoparticles. The sizes of nanoparticles were measured by dynamic light scattering (DLS, Zetasizer Nano-ZS). Measurements were carried out at 633 nm and the laser, as a light sources, was used at room temperature. The avarage particle diameters were calculated by the Marquardt method. The DLS measurements were usually repeated at least three times and the avarage values were reported. Morphological characterization was done by transmission electron microscopy (TEM, FEI Tecnai G2 F30) and scanning electron microscopy (SEM, Quanta 200 FEG).

Preparation of cells and culture : Human Breast Adenocarcinoma cell lines MCF 7 , MDA-MB-231, MDA-MB-157 were maintained in Dubelcco's Modified Eagle's Medium (DMEM) (HyClone with 1000mg/L glucose, 4 mM L-Glutamine and 110 mg/Lsodiumpyruvate).MTT (3-(4,5-dimethylthioazol-2-yl)-2,5-diphenyltetraazolium bromide (Sigma Alrich) was used for MTT cell proliferation assay. Cells were

incubated at 37ºC with 5% CO_2. DMSO (Sigma Aldrich) was used as solvent for camptothecin (Calbiochem) at a concentration less than 1% in the cell culture medium. In order to detect cell proliferation BrdU reagent (Sigma Aldrich B9285) was used with primer antibody BrdU mouse- mAB #5292S (Cell Signaling Technology) and seconder antibody anti-mouse IgG (H+L), $F(ab')_2$Fragment (Alexa Fluor 555 Conugate) #4409 (Cell Signaling Technology). To quantify the amount of adsorbed proteins on the nanoparticles in the human blood serum environment Bradford reagent (Coomasive blue G-250) was used and the absorbance values of the samples were obtained through a spectrometry at 595 nm (Beckman-DU 640). Zebrafish embryos were purchased from Wisconson Madison University (US) and kept through Bilgen Zebrafish Facility in Bilkent University, Department of Moecular Biology and Genetics. Zebrafish experiments were approved by Ethic Comittee in Bilkent University. C. Elegans were purchased from C. Elegans Stock Center.

3.2 Syntheses of Monomers and Polymer

3.2.1. Synthesisof 2,7-dibromo-9,9-bis-(6-bromo-hexyl)-9H-fluorene (M1)

2,7 Dibromofluorene (2.0 g, 6,17 mmol) and tetrabutylammoniumbromide (0.40 g, 1.20 mmol) were dried under vacuum and nitrogen for 30 min. DMSO (10 ml) which was degased with Argon was added to the solid mixture. To this mixture, degassed DMSO (15ml), 50% NaOH (15 ml) and 1,6 dibromohexane (9.5 ml, 60 mmol) were added, respectively. The resulting mixture was stirred at room temperature for 2 hours. Work-up was done with diethyl ether (125 ml) and water (50 ml) to the reaction. The reaction was exothermic and an ice bath was needed to control the temperature. For the work-up, the organic layer was extracted in diethyl ether and washed with 1x100 ml water, 1x2N HCl 100 ml, 1x100 ml water, 4x100 ml brine solution, 3x100 ml water. The diethyl ether was removed under reduced pressure. Vacuum distillation was applied to the liquid product in order to remove DMSO. The final product was purified with column chromatography packed with silica using cyclohexane as an eluent. For further purification, the desired monomer was dissolved in minimum amount of cyclohexane and precipitated into cold methanol, filtered and dried under vacuum. Yield: 1.62g 40 %.

^{1}H-NMR (400 MHz, $CDCl_3$, δ ppm):7.5 (m, 6H), 3.30 (t,4H), 1.87 (t,4H), 1.79 (t, 4H), 1.22 (t,4H), 1.12 (t,4H), 0.61 (t, 4H)

^{13}C-NMR (400 MHz, $CDCl_3$, δ ppm):144.1**,** 140.1,135.5, 132.2, 130.1, 129.8, 122.5, 43.5, 42.9, 32.9, 34.1, 29.9, 28.1, 23.1.

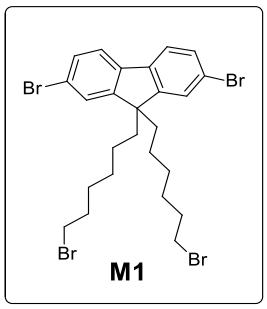

M1

3.2.2. The Synthesis of {6-[2,7-Dibromo-9-(6-dimethylamino-hexyl)-9H-fluoren-9-yl]-hexyl}-dimethyl-amine

2,7-Dibromo-9,9-bis(6-bromo-hexyl)-9H-fluorene **(M1)**(1.00g,1.54 mmol) was dissolved in dry THF (5 ml) and flushed with argon. The solution was cooled down to -78^{o}C. 2 M solution of dimethylamine in THF was added under argon. The mixture was brought to room temperature and stirred for 24 hours at room temperature. THF was removed under reduced pressure and 0.1 M NaOH (5 ml) and chloroform (10 ml) were added. The mixture was stirred for 30 minutes and organic layer was separated and washed with 50 ml brine solution. The solvent was removed under reduced pressure to obtain an oily solid in which water was added and the suspension was stirred for 10 min and the precipitateswere collected through suction and dried. The yield is 0.71 mg, 80 %.

^{1}H-NMR (400 MHz, $CDCl_3$, δ ppm): 7.55 (m,6H), 2,17 (t, 4H), 1.95 (m,12H), 1.28 (m,4H), 1.09 (m,8H), 0.61 (t,4H) .

^{13}C-NMR (400 MHz, $CDCl_3$, δ ppm):141.1, 135.5, 132.2, 129.8, 122.5, 58.6, 43.5, 42.9, 41.5, 30.6, 29.4, 28.0, 25.1.

TOF-MS: $[M2]^{+}$m/z : 579.17

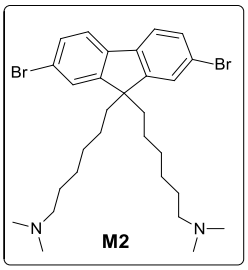

M2

3.2.3. Synthesis of Poly[(9,9-bis{6-dimethylaminohexyl}fluorenyl-2,7-diyl)-co-(1,4-benzo-{2,1,3}-thiodiazole)] (PDAFBT)

{6-[2,7-Dibromo-9-(6-dimethylamino-hexyl)-9H-fluoren-9-yl]-hexyl}-dimethyl amine (500 mg, 0.864 mmol), 2,1,3-Benzothiadiazole-4,7-bis(boronic acid pinacol ester) (307.404 mg, 0.864 mmol), $Pd(Ph_3P)_4$ (17.68 mg, 0.0153 mmol) and K_2CO_3 (625 mg, 4.513 mmol) were placed in a 25 ml round-bottom flask an dried under vacuum remove for about 30 min. Then, degassed THF (8 ml) and water (5 ml) were and added to the reaction vessel under argon and freeze-pump-thaw method was applied three times for further removal of the oxygen. The mixture was stirred at 80^{o}C for 5 h under argon. After cooling to the room temperature, the mixture was diluted with chloroform and water. The insoluble part was removed by filtering through glass filter funnel and soluble part was redissolved in THF and precipitated into water. The solid residue was washed again with deionized water. The orange precipitates were collected by suction and dried under vacuum. Yield : 0.2g, 25 %.

^{1}H-NMR (400 MHz, $CDCl_3$, δ ppm):7.6-7.7 (m,6H), 7.5 (m,2H), 2,36 (m, 4H), 2.27 (m,12H), 1.39 (m,4H), 1.29 (m,8H), 1.87 (m,4H) .

^{13}C-NMR (400 MHz, $CDCl_3$, δ ppm):156.4, 154.0, 142.4, 141.8, 137.1, 136.0, 135.4, 133.5, 130.2, 129.6, 128.4, 127.8, 127.2, 126.7, 58.6, 45.5, 42.9, 41.5, 30.6, 29.4, 28.0.

FT-IR (KBr, pellet,υ_{max}(cm^{-1})): 3074(-C-H, m), 2918 (-C-H,s), 1500 (-C-C in ring, m), 1265 (-C-N, m).

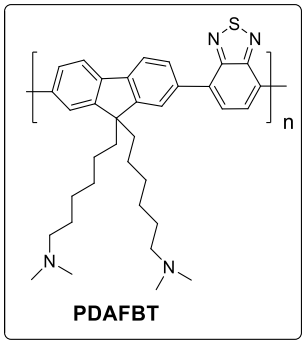

PDAFBT

3.2.4.Synthesis of PDAFBT Nanoparticles

PDAFBT (2.0 mg, 3,6×10^{-3} mmol, based on per repeat unit) was dissolved in THF (5ml) then solution was filtered through syringe filter (0,45μm PFFT) and sonicated for 30 min. The resulting solution was injected rapidly into the autoclaved double disttiled water (50ml) in the ultrasonic bath. It was stirred for further 30 min. THF was removed under reduced pressure. The resulting nanoparticle solution was concentrated under reduced pressure to obtain the desired concentration for the experiments.

3.2.5. Synthesis of Drug Loaded PDAFBT Nanoparticles and Determination of Drug Loading Capacity of PDAFBT Nanoparticles

For the drug loaded nanoparticles preparations drug to polymer ratios were selected as 1:10, 1:25, and 1:35, weight to weight (w/w). To prepare the drug loaded nanoparticles for the 1:10 (drug to polymer) ratio, 2.0mg (3.6 x 10^{-3} mmol, based on per repeat unit) of PDAFBT and 2.0 x10^{-1}mg CPT (5.7 x 10^{-4} mmol) was dissolved in 5 ml of THF and for the 1:25 (drug to polymer) ratio, 2.0 mg (3.6 x10^{-3} mmol, based on per repeat unit) of PDAFBT and 8.0 x10^{-2}mg CPT (2.3 x 0^{-4} mmol) was dissolved in 5 ml of THF. In the similar manner, to prepare for the 1:35 (drug to polymer) ratio, 2.0 mg (3.6 x10^{-3} mmol, based on per repeat unit) of PDAFBT and 5.5x10^{-2} mgCPT (1.6 x 10^{-4} mmol) was dissolved in 5 ml of THF. The resulting solutions were sonicated for 30 min and injected into the autoclaved double distilled water (50ml) in the ultrasonicbath. They were stirred for further 30 min. THF was removed under reduced pressure. The resulting nanoparticle dispersions were transferred into a dialysis tube (cellulose tubular membrane, 3.47 mm,Cellu Sep) with molecular weight cut-off 3000 Da and dialyzed against water for 24 hours at

room temperature while providing a gentle stirring. After 24 hours,the dialysates of each set of experiments were evaporated to dryness and the remaining residues weredissolved in 3 ml of THF. Subsequently, the concentration of CPT in the release medium was measured by using absorption spectroscopy (λ_{ex}= 366 nm). As a control experiment, the dialysis of free CPT was carried out by keeping the concentration of CPT as the same as used in the drug-loaded nanoparticle cases.

3.2.6. Drug Release Study

To determine the drug release profile of the CPT encapsulated nanoparticles, the drug-loaded nanoparticles with the drug to polymer ratio of 1:35, w/w was prepared and the solution was concentrated down to 2 ml and the final volume was made upto 10 ml with 10 M PBS solution. This solution was transferred into a dialysis tube (cellulose tubular membrane, 3.47 mm, Cellu Sep) with molecular weight cut-off 3000 Da. The dialysis tube was placed into a beaker containing 100 ml of PBS buffer and 2% Tween 20 and dialyzed at 37^{o}C while shaking at 60 RPM. 1ml of aliquots were withdrawn from the medium at different time intervals during 50 hours time period and at each time, equal amount of fresh PBS was added to the release medium to prevent the sink condition.The concentration of CPT in the release medium was measured by using absorption spectroscopy (λ_{ex}= 366 nm). 5 samples at known concentrations in THF were used to obtain a calibration curve to determine the concentration of unknown sample.

3.2.7. Sample Preparation from PDAFBT Nanoparticles for TEM imaging

Negative staining with phosphotungstic acid to PDAFBT nanoparticle dispersions (7.2×10^{-5}M) was donein order to obtain TEM images. Nanoparticle-phosphotungstic acid solution was prepared in the 8:1 ratio from 1 % (w/w) solution of phosphotungstic acid in distilled water. 15 ul was taken and dropped onto the surface of the grid. After waiting for adhesion of the nanoparticles on the surface in 5 minutes, drop was removed from the surface. After the complete dryness of sample on the grid, the images were taken.

3.2.8. Preparation of PDAFBT Nanoparticle Solutions in Bovine Serum Albumin and Human Serum Media

PDAFBT (2.0 mg, $3{,}6\times10^{-3}$ mmol, based on per repeat unit) was dissolved in THF (5ml) then solution was filtered through syringe filter (0,45μm PFFT) and sonicated for 30 min. The resulting solution was injected rapidly into the autoclaved double disttiled water (50ml) in the ultrasonic bath. It was stirred for further 30 min. THF was removed under reduced pressure. The resulting nanoparticle solution was concentrated under reduced pressure to 22.5×10^{-5} M with three replications. Then concentrated PDAFBT nanoparticle solutions were rediluted with stock solutions of bovine serum albumine (BSA) (10 mg in 10 ml of water) and human serum (10% (v/v)) to $7{,}2\text{x}10^{-5}$M. Prepared nanoparticles solutions were incubated at 37ºC and 60 RPM and 1 ml of aliquotes were taken at 0, 30 and 120 min time periods to measure their size by DLS.

3.3 Biological Assays

3.3.1.3-[4,5-dimethylthiazol-2-yl]-2,5-diphenyl tetrazoliumbromide (MTT) In Vitro Toxicology Assay for Culture Cells Treated with Blank and Drug Loaded Nanoparticles

MCF-7, MDA-MB-231, MDA-MB-157 cell were inoculated (2000 cells /well in 300 μL) in 96 well plates. The next day, the media were refreshed and the CPT and CPT loaded PDAFBT nanoparticles were placed in the range of concentration between 0,125 and 2μM in parallel with DMSO-only and CPN-only treated cells as negative controls. At the end of 48 h of treatment resulting cells were treated with MTT reagent for 4 h at 37ºC then after treating with Sodium Dodecyl- HCl was treated cell were incubated 18h at 37ºC . After incbation well plate was shaken and the absorbance values were obtained through microplate reader at 570 nm.

3.3.2. 5-Bromo-2-deoxyuridine (BrdU) Cell Labeling and Proliferations Assay for Culture Cells Treated with Blank and Drug Loaded Nanoparticles

MCF-7 cells were inoculated (100000 cells / well in 1000 μL) in 6 well plates and treated with blank PDAFBT nanoparticles (30μM, concentration of 2μM CPT loaded nanoparticles) 48h later, BrdU reagent (12μL for 12 mL DMEM) was treated with the cells for 2h. After the exposure time, the cells were washed with phosphate buffer saline (PBS) (0.02M) and fixed with slowly added methanol (in -20ºC) after 10 min

cells were washed with PBS again. Washed cells were exposed to HCl (2N) for 30 min at 37^{o}C then add with borate buffer and washed PBS (0,03 M). After 30 min primary antibody (α-BrdU) diluted in blocking solution was apllied for 1h. After exposure, cells were washed with %0.5 tween 20 containing PBS (PBS-T) 3 times then secondary antibody diluted in PBS-T only was treated for 2h washed again PBS-T 3 times.After treatments, cell were placed onto the slide with mounting medium with DAPI and cells screening under the fluorescence microscope through the blue, red and yellow filters at 40X magnification.

3.3.3. Bradford Protein Assay to Determine the Quantitative Amount of Human Plasma Proteins Adsorbed on the Surface of Nanoparticles

Bradford reagent without protein (900 μL), 98 μL ddH_2O and 2μL human plasma serum (1X) at the 0.5 X, 0.25X, 0.125X, 0.0625X dilutions were prepared as reference solutions, and the intensityof absorbance was read at 595 nm through a spectrometer. Human plasma serum added nanoparticles solution was precipitated through centrifugation at 4000 rpm for 15 min and washed with ddH_2O three times. Then, 2 μL of nanoparticles dispersion (0,8 μg in 2 ml water) was mixed with bradford reagent (900 μL) and 98μL and their intensity of absorbance read at 595nm.

3.3.4 PDAFBT Nanoparticle Staining Protocol on Embryonic Zebra Fish

0.5 and 2 μM CPT loaded and blank PDAFBT nanoparticles prepared in the system of used for zebrafish maintanence at BILGEN Bilkent University Department of Molecular Biology and Genetics. Zebra fish embryos (48h postproliferation, hbf) were kept in these nanoparticle medium at 28^{o}C for 24h. After treatment embryos were fixed with 4% paraformaldehyde for 48h then washed with PBS-t two times. After washing, fixed embryos were treated with glycerol (50%) for 30 min at 4^{o}C then transferred onto a microscope slide and slide was covered with a coverslip and the periphery of it was sealed with a nail polish. Prepared slides were checked under fluorescence microscope with multidimensional acquisition under GFP lamb.

3.3.5 PPFBT Nanoparticle Staining protocol on C. Elegans

Synchronized worms at L4 stages in the plates were washed with 10 ml of phosphate buffer salinebuffer (PBS (1X) and spun in the centrifuge at 2500 RPM for 2 min. Supernatant was taken and washing step was replicated three times then worms were re-suspended in 1ml of 0.01 mM PPFBT nanoparticle solution in PBS buffer during 30 min. Then worms were settled down in centrifuge at 2500 RPM for 2 min. Stainingsolution was aspirated and pellet of worms washed three times with PBS buffer. In order to fix the worms, 1 ml of cold methanol (100%) was exposed for 5 min. 600 µL of PBTw (PBS containing 0.1 % tween-20) was added and the resulting solution was spun in the centrifuge at 2500 RPM. Supernatant was aspirated then worm pellets were washed with 500 µL of PBTw. Settled worms were transferred onto a microscope slide using a capillary pipette and after removing excess liquid with a tissue paper, slide was covered with a coverslip and the periphery of it was sealed with a nail polish. Prepared slides were imagedunder a fluorescence microscope with multidimensional acquisition under GFP lamb.

CHAPTER 4

4. EVALUATION

This chapter consists of two parts. In the first section, synthesis and characterization of monomers and polymer are discussed. The second section reports the preparation of blank and drug loaded nanoparticles, their modifications and characterizations as well as their biomedical applications including stability tests in different biological media, toxicological analysis through cell culture studies, *in vitro* and *in vivo* imaging for different cell lines and different model organisms.

The content of thesis work is illustrated in Figure 4.1.

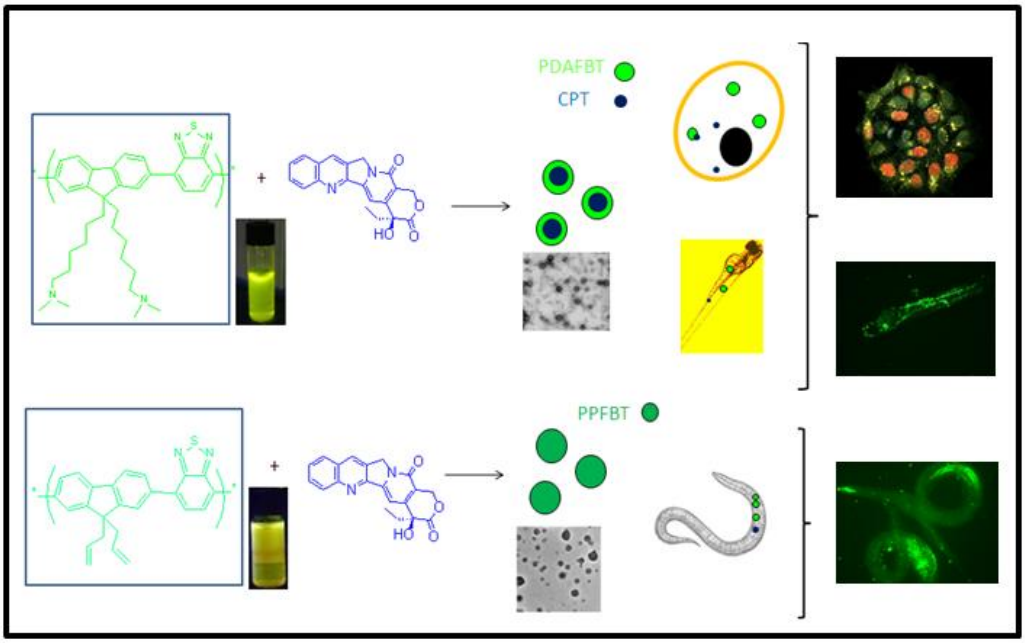

Figure 4. 1.Schematic illustration of thesis work.

4.1. Synthesis and Characterization of Monomers

4.1.1.Synthesis and Characterization of 2,7-dibromo-9,9-bis-(6-bromo-hexyl)-9H-fluorene (M1)

2,7-dibromo-9,9-bis-(6-bromo-hexyl)-9H-fluorene (M1) was synthesized from 2,7-dibromofluorene by removing the weakly acidic hydrogens at the C9 position with 50% (w/w) NaOH solution. After the abstraction of mentioned protons, nucleophilic susbstitiution of 1,6-dibromohexane was achieved (Scheme 4.1). Due to addition of NaOH in aqueous phase, interaction between the aqueous and the organic phases was enhanced by the phase transfer catalyst tetrabutylammonium bromide (TBAB). Moreover, temperature control is important because the substitution and elimination reactions might be in competition in this reaction and to decrease the probability of elimination reaction leading to side products, reaction has to be conducted at room temperature. In order to prevent temperature raising due to addition of NaOH, the reaction vessel was kept in an ice bath during the addition of base. The isolation of the product was achieved by the extraction with diethyl ether, distilled water and 2N HCl (aq) followed by column chromatography (cyclohexane as eluent). M1 was obtained in white powders with 40% yield.

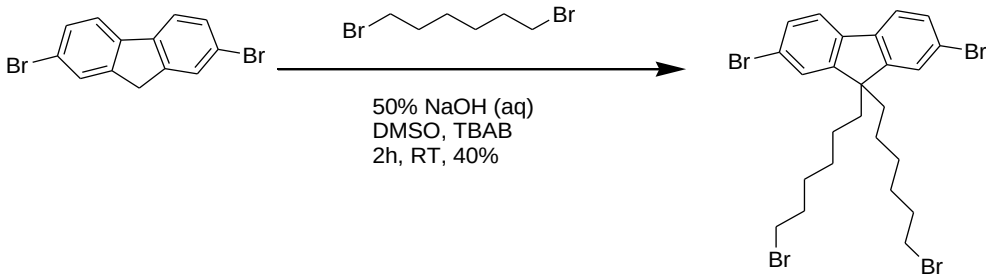

Scheme 4.1 Synthesis mechanism of the monomer 2,7-dibromo-9,9-bis-(6-bromo-hexyl)-9H-fluorene **(M1).**

The structural characterization of the monomer M1 was done by ^{1}H-NMR and ^{13}C-NMR spectroscopies shown in the Figure 4.2. In the ^{1}H-NMR spectrum, the integrations and the chemical shifts of the peaks confirm the expected structure. A multiplet at 7.5 ppm belongs to the fluorene rings protons and triplet at 3.30 ppm is due to $–CH_2$ protons adjacent to bromine which is relatively downfield shifted comparing to the rest of the methylene protons of the alkyl chain because ofthe effect of electron withdrawing bromine atoms. In the ^{13}C-NMR spectrum peaks at between

the 122.5 and 144.1 ppm were observed due to carbons in the aromatic part of fluorene and peaks in the upfield region belong to the carbon atoms of alkyl chain (122.5, 43.5, 42.9, 32.9, 34.1, 29.9, 28.1, 23.1 ppm) and are in convenience with the expected structure.

(a)

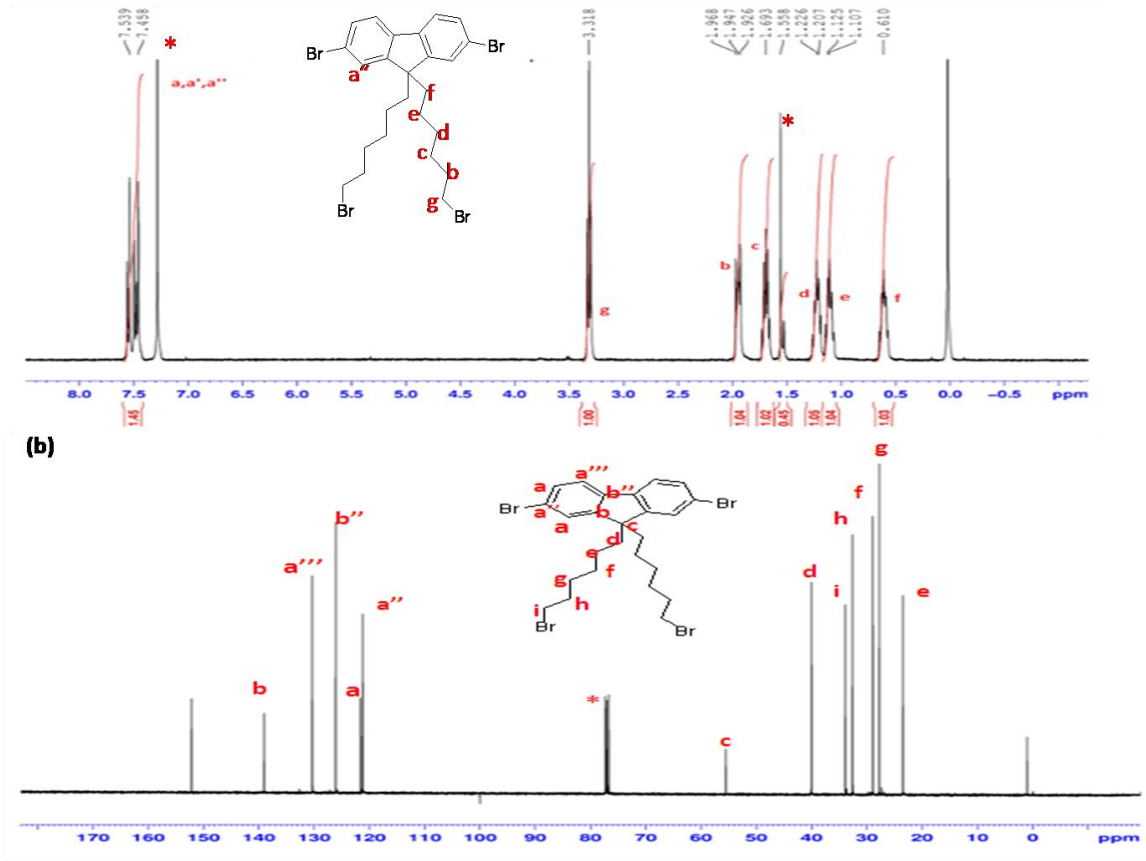

Figure 4.2. (a) ^{1}H-NMR (400 MHz, CDCl3, 25^{o}C) and (b)^{13}C-NMR (400 MHz, CDCl3, 25^{o}C) spectra of 2,7-dibromo-9,9-bis-(6-bromo-hexyl)-9H-fluorene **(M1).**

* Denotes solvent peak and other impurities from the solvent.

4.1.2.The Synthesis and Characterization of The Synthesis of {6-[2,7-Dibromo-9-(6-dimethylamino-hexyl)-9H-fluoren-9-yl]-hexyl}-dimethyl-amine (M2)

{6-[2,7-Dibromo-9-(6-dimethylamino-hexyl)-9H-fluoren-9-yl]-hexyl}-dimethyl-amine (M2) was obtained through amination reaction of **(M1)** as shown in the Scheme 4.2.Since dimethylamine is highly reactive, the reaction was carried out at low temperature during its addition and after the addition was over the mixture was stirred at room temperature for 24h. The isolation of the product was done through

the extraction with chloroform and aqueous NaOH solution was used to neutralize the reaction mixture.After the removal of solvent, an oily solid residue was obtained in which water was added to obtain precipitates. Precipitates were collected by suction and dried under vacuum to obtain a yellowish powder with the yield of 80 %.

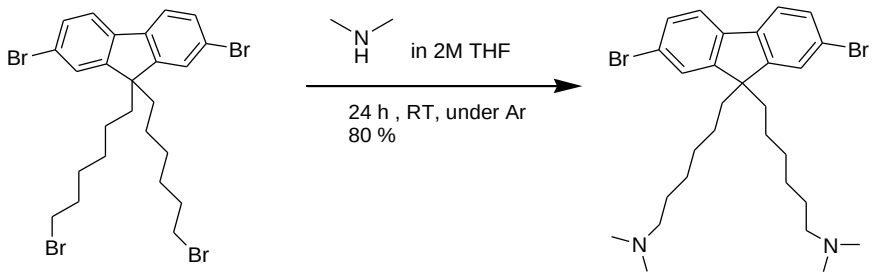

Scheme 4.2. Synthesis mechanism of the monomer {6-[2,7-Dibromo-9-(6 dimethylamino-hexyl)-9H-fluoren-9-yl]-hexyl}-dimethyl-amine **(M2).**

The structural characterization of the monomer M2 was done by ^{1}H-NMR,^{13}C-NMR spectroscopies and mass spectroscopy (TOF-MS) shown in the Figure 4.3 and Figure 4.4. In the ^{1}H-NMR spectrum, the integrations and the chemical shifts of the peaks confirm the expected structure. The ^{1}H-NMR of monomer M2 differentiates from M1 through the disappearance of the peak at 3.30 ppm which belongs to $–CH_2$ protons near bromine due to replacing of –Br with $-N(CH)_2$ group. Differently, chemical shifts of protons in ($-N-CH_3$) group was observed as a multiplet at 1.95 ppm and protons in ($-N-CH_2$) was shown as triplet at 2.17 ppm. In the ^{13}C-NMR spectrum, chemical shifts between the 122.5 and 144.1 ppm were observed due to carbons in the aromatic part of fluorene. Chemical shifts at 41.5 ppm and 58.6 ppm belong to methylene carbons of dimethylamine group and carbons at CH_2-. Other signals are similar with the monomer M1 and confirm the expected structure.

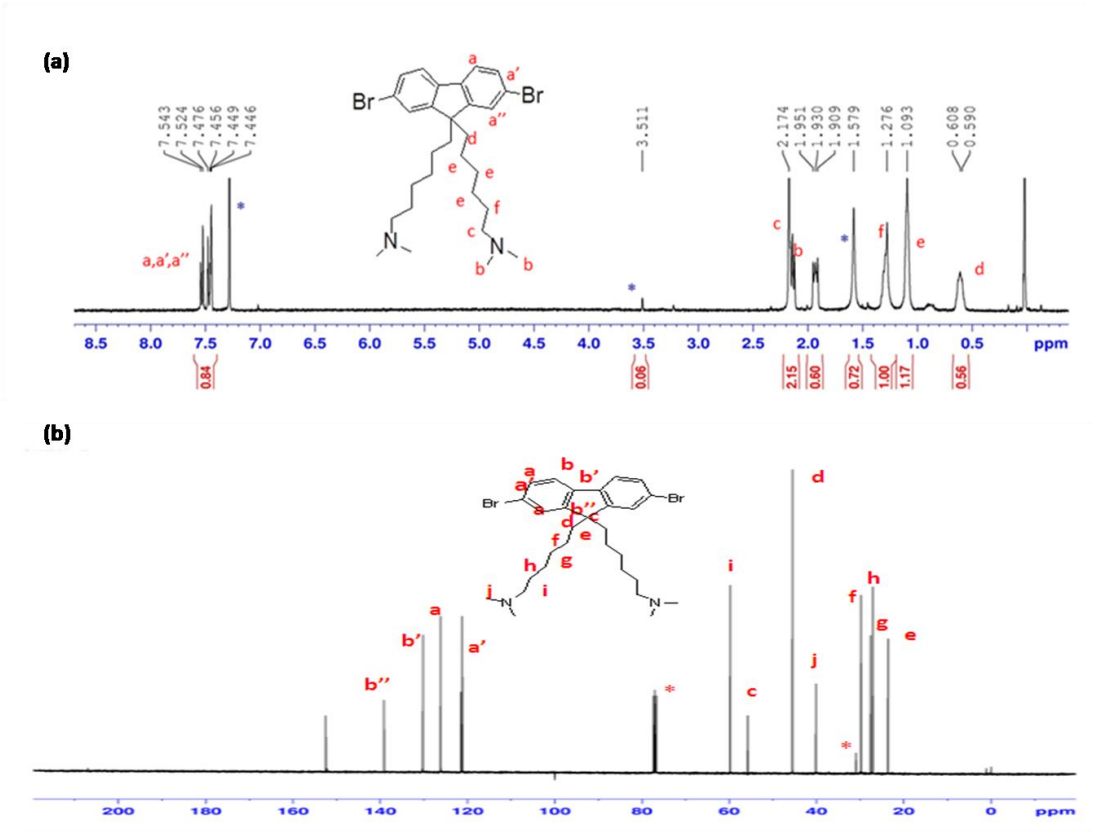

Figure 4.3. (a) ^{1}H-NMR (400 MHz, CDCl3, 25^{o}C) and **(b)** ^{13}C-NMR (400 MHz, CDCl3, 25^{o}C) spectra of {6-[2,7-Dibromo-9-(6-dimethylamino-hexyl)-9H-fluoren-9-yl]-hexyl}-dimethyl-amine (M2). *Denotes solvent peak and other impurities from the solvent.

The molecular mass of M2 was determined by using time of flight mass spectroscopy (TOF-MS). This method determines the mass to charge ratio of ions by measuring the traveling time for the distance to the detector under an electric field. Basically, this time depends on mass to charge ratio, namely heavier particles have low acceleration. For these large molecules, due to fragmentation many different ions can be formed but relative molecular mass of the molecule can be obtained. In the TOF-MS spectrum of M2 given in the Figure 4.4, the peak at 579.17 indicates the presence of molecular ion of M2 confirming the expected structure.

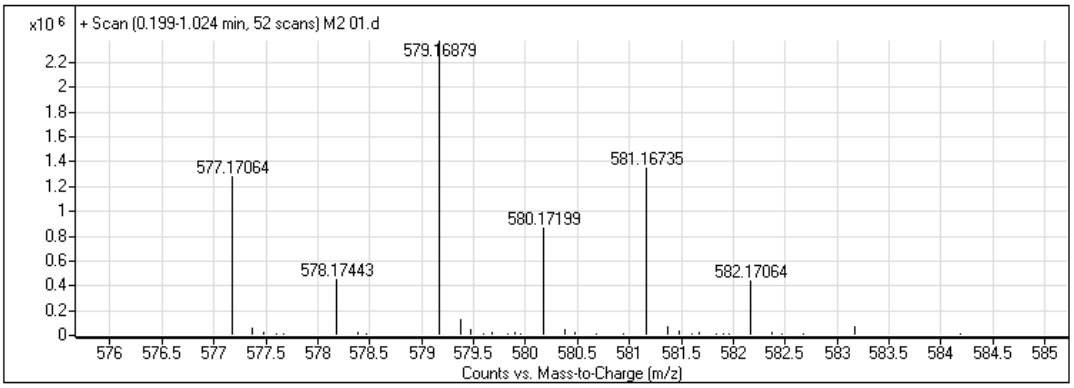

Figure 4.4. TOF-MS spectrum of M2. (m/z $[M2]^+$: 579.17)

4.1.3. Synthesis and Characterization of Poly[9,9-bis{6-dimethylaminohexyl} fluorenyl-2,7-diyl)-co-(1,4-benzo-{2,1,3}-thiodiazole)] (PDAFBT)

The polymer PDAFBT was synthesized through the Suzuki Coupling reaction of {6-[2,7-Dibromo-9-(6-dimethylamino-hexyl)-9H-fluoren-9-yl]-hexyl}-dimethylamineas alkyl halide and 2,1,3-benzothiadiazole-4,7-bis(boronic acid pinacol ester) as organoboronic compound under $Pd(Ph_3P)_4$ catalyst which is given in the Scheme 4.3. Reaction has to be conducted under inert atmosphere because in the presence of oxygen, palladium catalyst can be oxidized readily and reaction do not start. The reaction time was kept relatively short in order to prevent high molecular weight polymer formation as the high molecular weight could be difficult to dissolve and process. Moreover, in order to obtain smaller nanoparticles low molecular weight polymer might be suitable. The polymer was isolated and purified by the by precipitation polymer solution in THF to water. The product was obtained as orange powder with 25% yield.PDAFBT was characterized by ^{1}H-NMR, ^{13}C-NMR, ESI-MS,MALDI, FT-IR, UV-Visand Fluorescence spectroscopies.

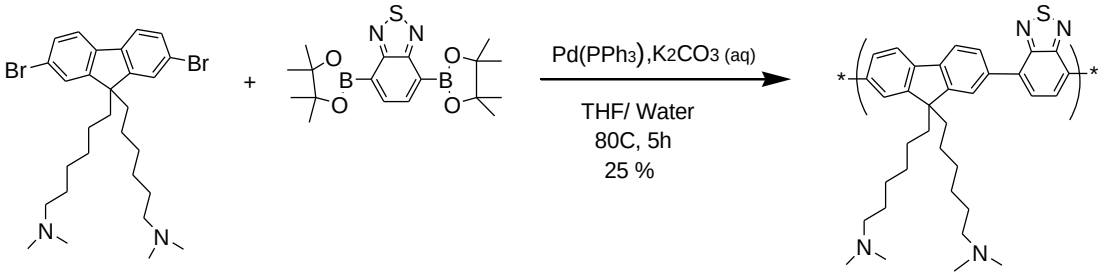

Scheme 4.3. The synthesis mechanism of poly[9,9-bis{6-dimethylaminohexyl} fluorenyl-2,7-diyl)-co-(1,4-benzo-{2,1,3}-thiodiazole)] **(PDAFBT).**

In the ^{1}H-NMR spectrum of PDAFBT, it was observed that signals become more broader than ^{1}H-NMR spectra of the monomers because monomer units are converted into long chains in which the mobility of the whole molecule is reduced. Signals observed at around 8.2 ppm as multiplets and 7.5 ppm as triplet are for aromatic protons of fluorene and benzothiodiazole units. The multiplets at 2.1 ppm are due to the protons $–CH_2$-N and methylene protons belonging to the dimethylamine groups. Resonance peaks at 0.79 and 1.59 ppm belong to the proton of the alkyl chain in the polymer. In the ^{13}C-NMR spectrum, chemical shifts between the 122.5 and 156.2 ppm were observed due to carbons in the aromatic part of fluorene. Chemical shifts at 41.5 ppm and 58.6 ppm and belong to methylene carbons of dimethylamine group and carbons at -CH_2.

Molecular mass of the PDAFBT was determined through electrospray ionization mass spectroscopy (ESI-MS) which applies soft ionization technique to produce charged gaseous species without causing high level of structural destruction for large biomolecules and synthetic polymers. In the spectrum given in the Figure 4.6 most intense peaks at 1683.2 and 1331.5 m/z indicate mainly the presence of dimer and trimer, respectively. However, in this technique it is not so possible to see molecular masses higher than 3000 even increasing the voltage because it is difficult to ionize larger molecules. Matrix-assisted laser desorption ionization mass spectroscopy (MALDI) is another useful analytical tool which gives mainly accurate m/z ratio values with efficient energy transfer during matrix assisted laser induced desorption process. The spectrum given in the Figure 4.6(b) indicates that m/z ratio of PDAFBT concentrates mainly in the region up to 4000 Da. ESI-MS and MALDI-MS results show that number of repeating units of the PDAFBT is around 5.

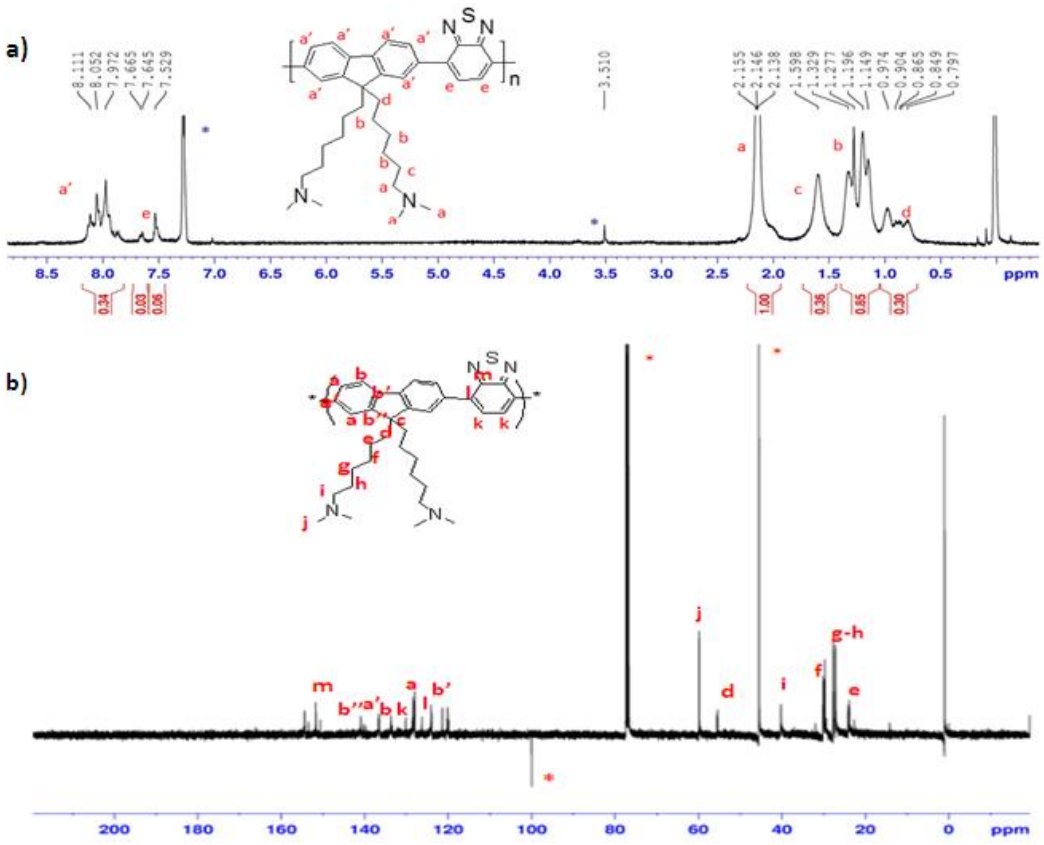

Figure 4.5. (a) ^{1}H-NMR (400 MHz, CDCl3, 25^{o}C) and **(b)** ^{13}C-NMR (400 MHz, CDCl3, 25^{o}C) spectra of Poly[9,9-bis{6-dimethylaminohexyl} fluorenyl-2,7-diyl)-co-(1,4-benzo-{2,1,3}-thiodiazole)] **(PDAFBT).***Denotes solvent peak and other impurities from the solvent

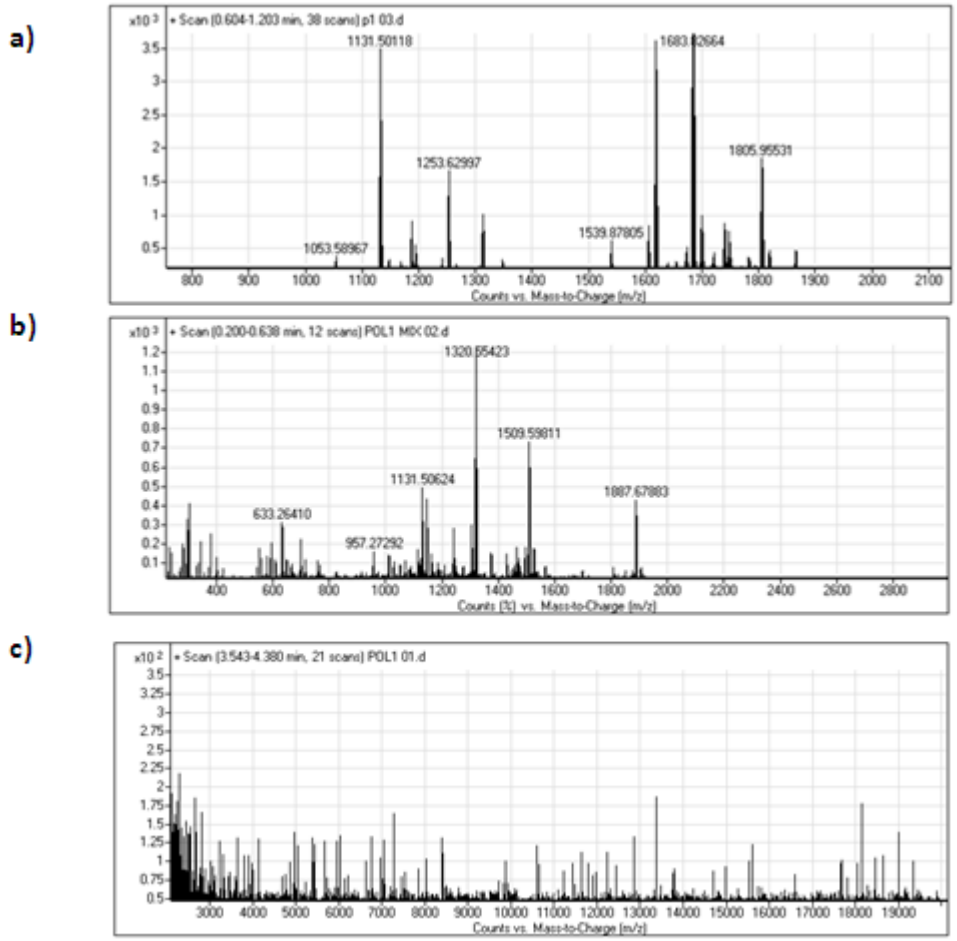

ü

Figure 4.6. (a) ESI-MS of PDAFBT m/z [3M2]+ =1683.8 **(b)** MALDI-MS of PDAFBT m/z [2M2]+ =1331.5 **(c)** MALDI-MS of PDAFBT in the wide spectrum.

FT-IR spectrum of the polymer PDAFBT is shown in the Figure 4.7. Spectrum shows peaks at 3074 cm^{-1} and 1500 cm^{-1} which belong to C-H and C-C stretching in the ring. The characteristic peak of C-N for aliphatic amines was shown at 1265 cm^{1}.

Optical properties of PDAFBT were determined by UV-Vis absorbance and fluorescence spectroscopiesand their absorption and emission spectra are shown in the Figure 4.8. The maximum absorption bands at 320 nm 446 nm and the maximum fluorescence emission band at 541 nm were observed in the region of green light.

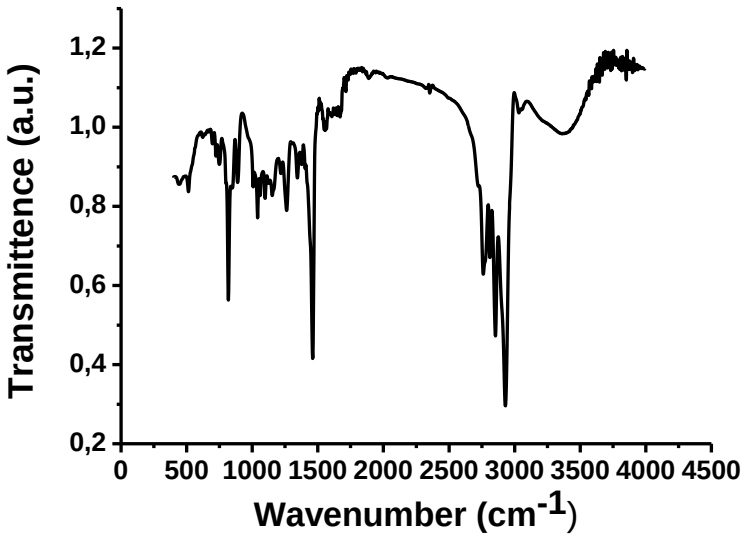

Figure 4. 7. FT-IR spectrum of poly[9,9-bis{6-dimethylaminohexyl}fluorenyl-2,7-diyl)-co-(1,4-benzo-{2,1,3}-thiodiazole)] **(PDAFBT).**

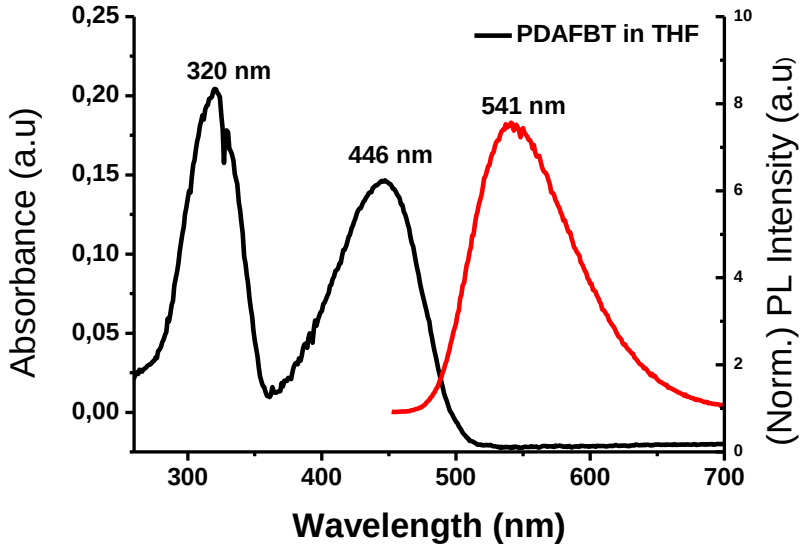

Figure 4.8. UV-Vis absorption and fluorescence emission spectra of poly[9,9-bis{6-dimethylaminohexyl}fluorenyl-2,7-diyl)-co-(1,4-benzo-{2,1,3}-thiodiazole)] (PDAFBT) in THF. (λ_{ex}= 446 nm)

4.2. Synthesis and Characterization of Blank and Drug Loaded Water Dispersible Conjugated Polymer Nanoparticles (CPNs)

Blank and drug loaded conjugated polymer nanoparticles were prepared through reprecipitation method. Polymer solution was dissolved in a relatively low amount of THF which dissolves the polymer well then this hydrophobic polymer solution rapidly injected during the sonication into excess amount of water which is a poor solvent for the polymer. This leads to collapse of polymer chains in order to decrease the contact area with water due to hydrophobic effect. After the removal of THF under reduced pressure spherical polymer dots were obtained. The characterization of nanoparticles was done by DLS and Zeta Potential to determine their size and stability. UV-Vis and Fluorescence spectroscopies are used to reveal their optical properties and their morphologies and sizes were investigated by SEM and TEM.

4.2.1. Synthesis and Characterization of poly[9,9-bis{6-dimethylaminohexyl} fluorenyl-2,7-diyl)-co-(1,4-benzo-{2,1,3}-thiodiazole)] (PDAFBT) Nanoparticles

In the preparation of PDAFBT nanoparticles, polymer solution was dissolvedin minimum amount of THF to obtained concentrated polymer solution and sonicated for 30 min, then the resulting polymer solution was injected rapidly into double distilled water. It was stirred with sonication for further 30 min. THF was removed under reduced pressure. For different experiments which will be mentioned further, different concentrations of nanoparticle solutions were adjusted by removing water.

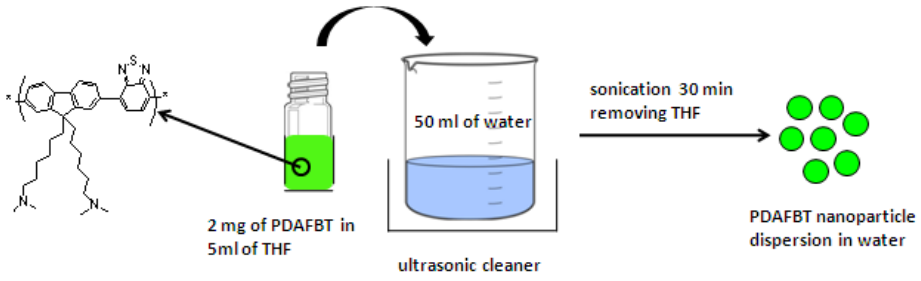

Figure 4.9. Cartoon representation of the preparation of PDAFBT nanoparticles.

Particle size is an important information about nanoparticles which could affect the biodistribution in tissues. Mean particle size, the homogenity of the distribution of nanoparticles and the zeta potential values were determined by DLS and zeta sizer

which measures the random motion of particles due to effect of solvent molecules and relates this measurement averagely with the size of nanoparticles. The number average size distribution of nanoparticles were measured as 24 nm, shown in the Figure 4.10a. Polydispersity index is the parameter which shows homogenity of the size distribution. PDI values from 0.1 to 0.25 indicates narrow distributions and values greater than 0.5 shows broad distribution. In the following result, PDI index of 0.29 shows that size distribution of PDAFBT nanoparticles is nearly broad. Zeta potential value is obtained through the evaluation of electrophoretic mobility of nanoparticles dispersion in the medium and shows the ionic strength and colloidal stability of dispersion. Zeta potential values more positive than +30 mV and more negative than -30 mV indicates that nanoparticle solution are stable enough due to the repulsive forces. Zeta potential value of +35.5 given in the Figure 4.10.b is the result of partial positive charge on dimethylamine groups of the polymer and shows that nanoparticle dispersion have colloidal stability.

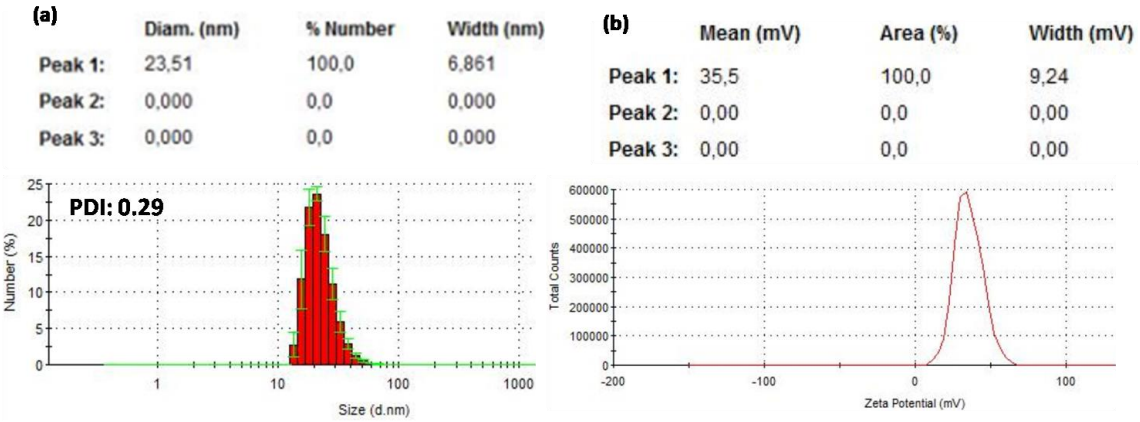

Figure 4.10. (a) Number avaragesize distrubution by histogram from DLS masurement and **(b)** zeta potential measurement of PDAFBT nanoparticles.

It is possible to adjust the size of the nanoparticles by changing concentration of the polymer. To investigate that, different amount of polymers containing 1.25, 2.5 and 5 mg was dissolved in the same amount of THF (5ml) and injected into the same volume of water (50 ml). It was observed that, as concentration of polymer increases from 1.25 mg to 5 mg, size of the nanoparticles doubles from 34nm to 62 nm (Table 1), because polymer chains in more dilute solution were solvated much better by water molecules than in concentrated solution and hydrophobic effectprocesses more

efficiently in dilute polymer solutions. It was also observed that zeta potential values of nanoparticles do not indicate concentration dependent trend. Another important parameter which effects the size of nanoparticles is sample preparation.The results can vary even though using the same method due to aggregations. Obtaining well dispersion by sonication before the measurement affects the DLS result. This detail highlights differences of size and zeta potential values between two measurements of the same samples given in the following table (Table 1).

PDAFBT CPNs	1st Preparation Size (nm)	PDI	2nd Preparation Zeta Potential (mV)	1st Preparation Size (nm)	PDI	2nd Preparation Zeta Potential (mV)
1.25 mg in 5 ml THF	34	0.239	28	33	0.182	51
2.5 mg in 5 ml THF	47	0.142	49	40	0.201	33
5 mg in 5 ml THF	62	0.132	45	53	0.125	36

Table 1. Number average size and zeta potential values of PDAFBT nanoparticles at different polymer concentrations.

Optical properties of PDAFBT nanoparticles were determined by UV-Vis and fluorescence spectroscopies and compared with the polymer solution in THF given in the Figure 4.11. Maximum absorption peaks were observed at 317 nm and 444 nm for polymer solution in THF. While converting polymer into nanoparticle absorption wavelengths do not change significantly (1-3 nm red shift), however, 10 nm red shift was observed in the fluorescence emission spectrum upon the formation of nanoparticles from the polymer. The red shift in the emission wavelength shows the collapse of polymer chains which leads to π- π stacking, decrease in the band gap and lower in the energy.

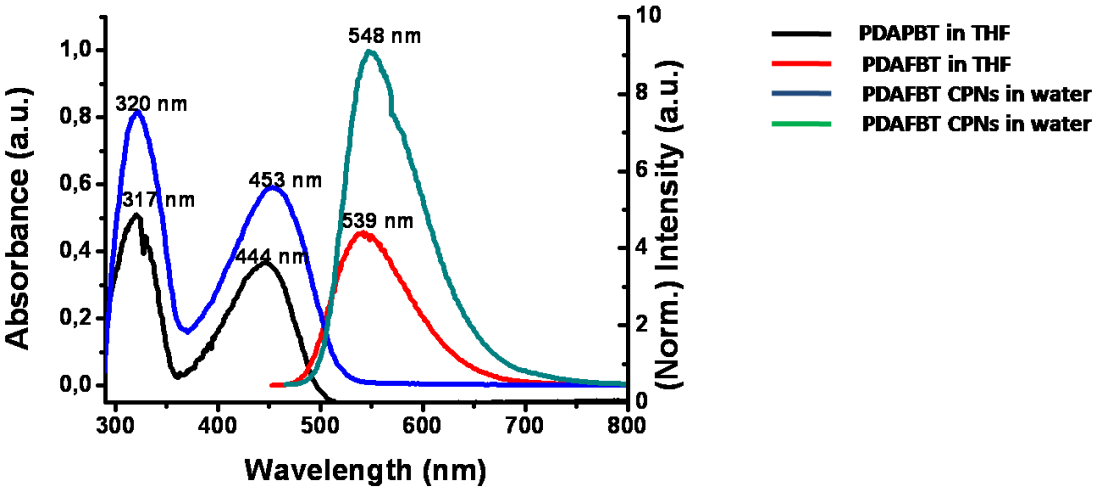

Figure 4.11. UV-Vis absorption and fluorescence emission spectra of PDAFBT in THF (λex= 446 nm) and dispersion of PDAFBT nanoparticles in water (λex= 446 nm).

Microscopic techniques give precise information about the size, morphology and the state of aggregation of the nanoparticles.Morphological characterization of PDAFBT nanoparticles was done by SEM and TEM methods. Their micrographs are shown in the Figure 4.12 which indicate the formation of spherical polymer dots. It was also noted that the sizes of nanoparticles observed in the SEM and TEM are in good agreement with the DLS results.

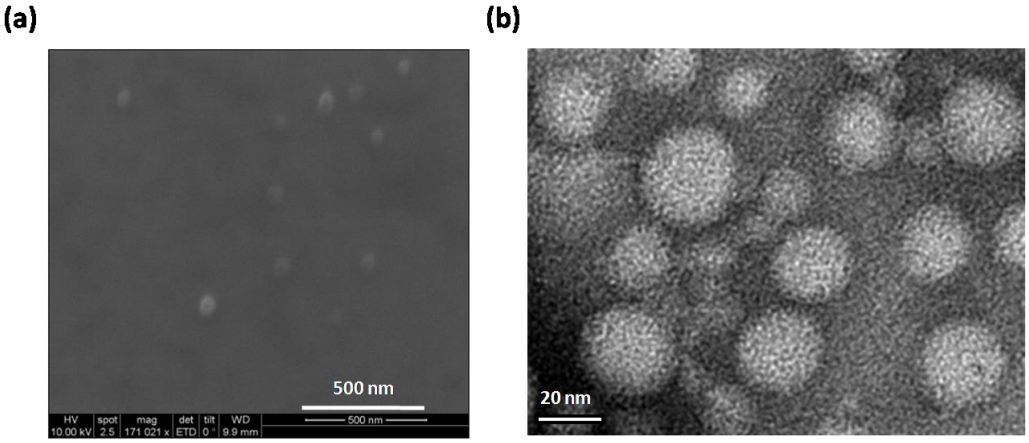

Figure 4.12. (a) SEM **(b)** TEM images of PDAFBT nanoparticles.

4.2.2 Synthesis and Characterization of Drug Loaded poly[9,9-bis{6-dimethyl aminohexyl}fluorenyl-2,7-diyl)-co-(1,4-benzo-{2,1,3}-thiodiazole)](PDAFBT) Nanoparticles

Drug loaded nanoparticles were synthesized with the similar method used in preparation of blank nanoparticles. Camptothecin (CPT) was used as a model anticancer therapeutic to investigate the drug carrying ability of PDAFBT nanoparticles. CPT was encapsulated into polymer nanoparticles through hydrophobic interaction. PDAFBT and CPT dissolved in THF and injected into rapidly to the excess amount of water. During this addition, hydrophobic CPT tends to escape from water droplets and is encapsulated by collapsed polymer chains.

4.2.3 Determination of the Drug Encapsulation Efficiency of PDAFBT Nanoparticles

In order to investigate the drug encapsulation efficiency of PDAFBT nanoparticles,at different polymer to drug ratios including 1:15 and 1:25 were selected. Forthis purpose,dialysis membrane diffusion method was used. The amount of the non-encapsulated drugs which is diffused out of the dialysis tube into the dialysate was measured after dialyzing the drug loaded nanoparticle for 24h at room temperature(Figure 4.13).

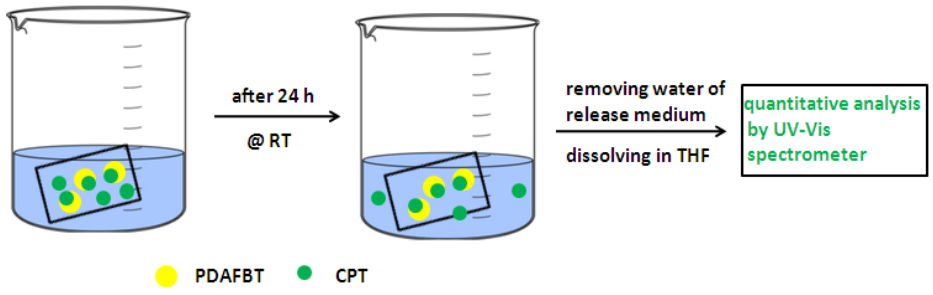

Figure 4.13. Schematic representation of the study about determination of drug encapsulation efficiency.

The theory of the study is based on the tendency of decreasing the concentration gradient of drug molecules through the diffusion from the membrane to the release medium. Drug loaded nanoparticles are not able to pass through the membrane due to their size.

Before analysis of the drug loading capacity of PDAFBT nanoparticles, molecular diffusion of CPT was tested by placing only CPT dispersion in water in the membrane and its release medium was quantitatively analyzed by UV-Vis spectroscopy after 24h. It was observed that whole of the CPT was diffused from the membrane into the release medium. Dialysis membrane and the release medium are two different environments and in order to lower the concentration gradient, CPT molecules have to diffuse from the membrane to the release medium. The volume of water in the membrane is 5 ml while the volume of water in the release medium being 100 ml. It means 5% of CPT has to remain in the membrane while 95% of CPT diffuses to the higher volume to obtain equal chemical potentials. It was calculated nearly 100% of CPT was diffused out of the membrane. The results are given in the Figure 4.13 and Table 2.5% error was observed maybe due to little differences in volumes of THF during the UV-Vis absorption measurements.

(a) **(b)**

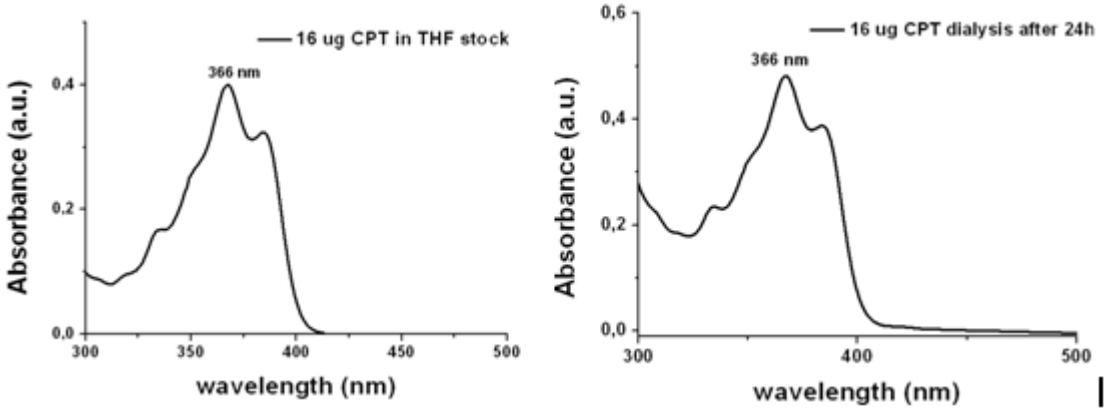

Figure 4.14. UV-Vis absorption spectra of **(a)** 16µg CPT stock in 3ml of THF and **(b)** 16 µg dialyzed CPT (after removing releasing medium and dissolving in 3 ml of THF).

Sample	Absorbance	Concentration (mM)	Total CPT (mg)	Diffused CPT to water(mg)	Diffused CPT (%)
Dialyzed CPT (16 µg)	0.24	0.0153	0.016	0.016	100
CPT stock in THF (16 µg)	0.24	0.0153	0.016	No measurement	No measurement

Table 2. Percentage of diffused CPT from the membrane to the release medium.

Determination of optimum drug loading efficiency of PDAFBT was expressed in the following Figure 4.15 and Table 3. In the first step, CPT solutions with respect to the same amount of loaded CPT in to the PDAFBT nanoparticles were prepared and the intensities of their absorbance were measured to plot a calibration curve. At the second step, the absorbance intensity of the free CPTsin the dialysate which are diffused out from the dialysis tube filled with CPT-loaded nanoparticles dispersion was measured. To obtain accurate result, the dialysate was evaporated to dryness and the remaining residue was dissolved in THF and the measurement was carried out in THF. It was observed that for the drug to polymer ratio of 1:35, respectively, 92% of the drug was encapsulated by the PDAFBT nanoparticles while for 1:25 (drug to polymer) ratio, 75% of the drug being encapsulated.

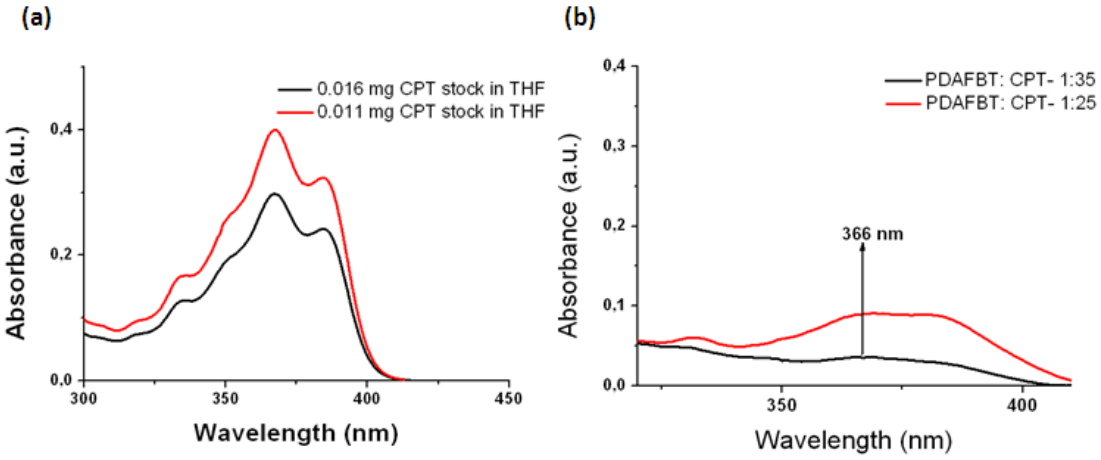

Figure 4.15. UV-Vis absorption spectra of **(a)** 0.011 mg and 0.016 mg CPT stocks in THF as references (with respect to amount of CPT at 1:35 and 1:25 drug to polymer ratios). **(b)** dialyzed CPT which is loaded in PDAFBT at 1:35 and 1.25 drug to

polymer ratios.(After the removal of the releasing medium and dissolving in 3 ml of THF).

Sample	Absorbance max of dialyzed CPT (λmax: 366nm)	Absorbance max of stock CPT (λmax: 366nm)	Amount of total CPT (mg)	Amount of diffused CPT to the water (mg)	Percentage of loaded CPT
Dialyzed CPT (1:35)	0.033	0.297	0.011	0.0009	92%
Dialyzed CPT (1:25)	0.096	0.400	0.016	0.0040	75%

Table 3. Percentage of loaded CPT by the PDAFBT nanoparticles for the CPT to PDAFBT, 1:35 and 1:25 : CPT ratios, respectively.

Drug loading ability of nanoparticles was expressed in terms of ensapsulation efficiency (EE) defining the ratio of the amount of encapsulated drug to the total drug, and loading efficiency (LE) gives the ratio of amount of encapsulated drug to the total drug and nanoparticles as percentage shown in the following equations.

$$EE = \frac{actualamountofdrugloadedinNP}{theorethicalamountofdrugloadedinNP} \times 100$$

$$LE = \frac{actualamountofdrugloadedinNP}{theorethicalamountofdrugloadedinNP + totalamountofNP} \times 100$$

Based on these equations, drug encapsulation efficiencies (EE) of PDAFBT nanoparticles are calculated to be as 92% and75% for the 1:35 and 1:25, respectively,for drug to polymer ratio. Drug loading efficiency of PDAFBT (LE) nanoparticles is calculated as 2.45% and 2.88% for the 1:35 and 1:25 respectively, for drug to polymer ratio. It can be concluded that the average drug loading efficiency of PDAFBT nanoparticles is 2.67±0.3 %. In order to achive maximal therapeutic effect drug loading efficiency has an significant role. In the literature there are various studies investigating the factors which affect drug loading efficiency. In the case of polymer nanoparticles polymer concentration, polymer solubility, interactions between polymer and drug, preparation methods are important parameters for loading efficiency and generally polymeric nanoparticles. For intance

it was reported, poly(lactic glycolic acid) nanoparticles which have high drug loading efficiency have high loading of CPT with 25%.

4.2.4. Characterization of Drug Loaded PDAFBT Nanoparticles

The number average size distributionof CPT loaded PDAFBT nanoparticles were measured as 20.3 and 24.4 for 1:35 and 1:25, respectively for drug to polymer ratios indicating that loading of polymers with drug does not cause significant size change in the nanoparticles.

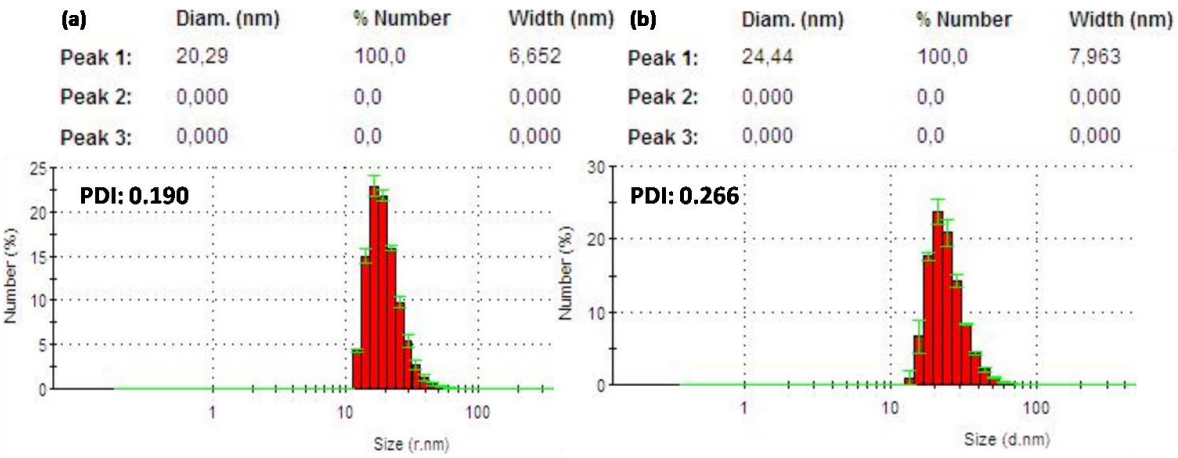

Figure 4.16. Number averagesize distribution by histogram from DLS measurements of CPT loaded PDAFBT nanoparticles for **(a)** 1:35 and **(b)** 1:25 drug to polymer ratios.

Optical characterizations of drug loaded nanoparticles was obtained by UV-Vis absorption and fluorescence spectroscopies. CPT loaded PDAFBT nanoparticles have the same absorption maxima with the blank nanoparticles as shown in the Figure 4.15(a). In order to analyze their encapsulation efficiency by optically, absorption spectra of 1:35, 1:25 and additionally 1:10 drug to polymer ratios of PDAFBT nanoparticles solution were measured and observed that increasing amount of CPT results occurrence of a shoulder at 365 nm in the spectra due to CPT and those peak can be detected strongly for the highest CPT ratio (1:10) which shows non-encapsulated CPT. In the fluorescence spectrum emission band of CPT was seen at 440 nm when it is excited at 365 nm. As the polymer ratio increases, a shoulder at around 570 nm begins to appear which belongs to PDAFBT. The reason to observe emission intensity of CPT much more higher than PDAFBT nanoparticles could be

due to a minimum interaction of loaded CPT with the local environment caused by the protection of CPTs from the solvent molecules due to the surrounded polymer shell and that can lead to a high fluorescence intensity at the 365 nm excitation wavelength.

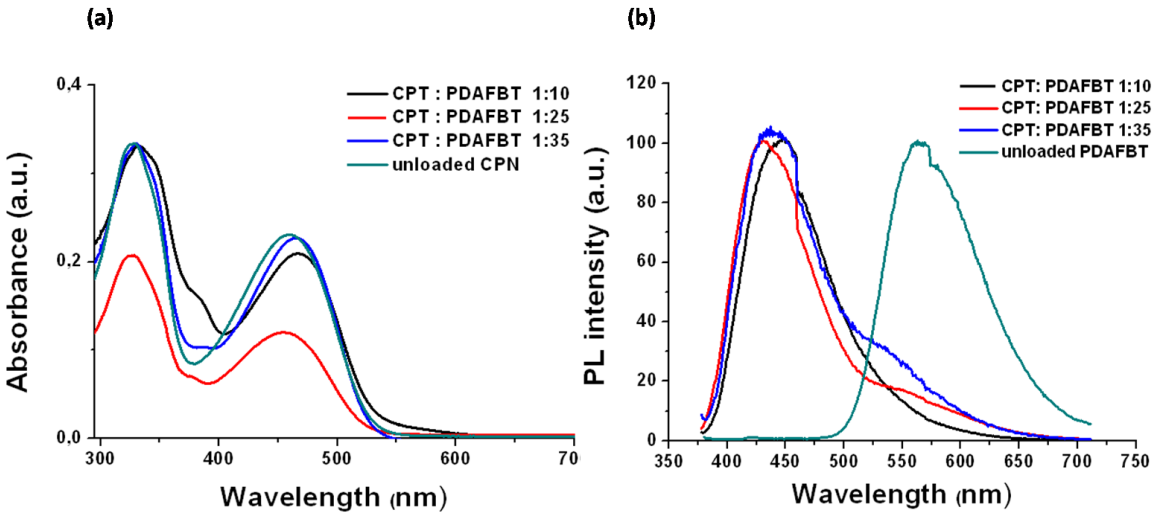

Figure 4.17. (a) UV-Vis absorption **(b)** normalized fluorescence spectra of CPT loaded PDAFBT nanoparticles in water at different ratios.(λ_{ex}= 366 nm).

The images of blank and drug loaded nanoparticles under day light and UV light in the Figure 4.18 also suggest the high fluorescence intensity of CPT in drug loaded nanoparticles under UV light. Fluorescence emission is much more sensitive to the local environment than the UV-Vis absorption, thus nearly only absorption band of PDAFBT nanoparticles on the outer shell was detected in the UV-Vis spectrum while emission band of the protected CPT was observed much intensely in the fluorescence spectrum.

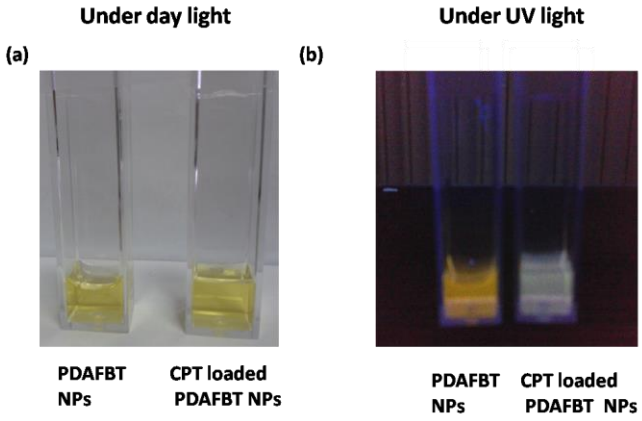

Figure 4.18. Photographic images of blank and CPT loaded PDAFBT nanoparticles under **(a)** day and **(b)** UV light.

Morphological characterization of CPT loaded PDAFBT nanoparticles was done by TEM and the images are shown in the Figure 4.19 which reveal a correlation in sizes of nanoparticles measured by DLS and TEM.

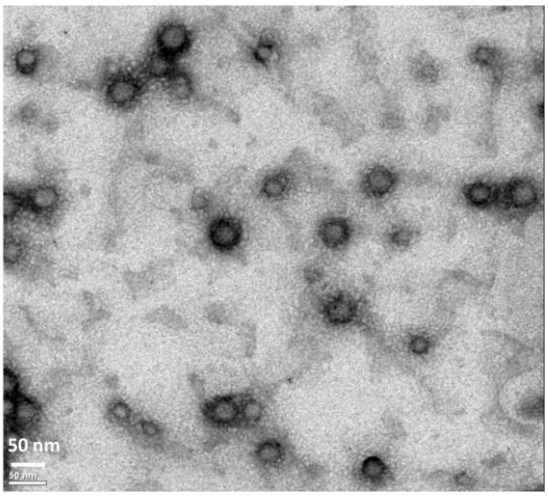

Figure 4.19. TEM image of CPT loaded PDAFBT nanoparticles.(CPT:PDAFBT is 1:25)

4.2.5. Determination Drug Release Profile of CPT Loaded PDAFBT Nanoparticles

Drug release profile evaluates ability of nanoparticles to release drug over specific time period which is significant for therapeutic efficiency of drug carriers. Drug

release ability of PDAFBT nanoparticles was analyzed with the technique of dialysis membrane diffusion by supplying simple biological conditions (incubation at 37^{o}C and 60 RPM) to force the diffusion of drug molecules from the polymer capsules. To study drug release profile, solution of CPT loaded PDAFBT nanoparticles at the 1:35 drug to polymer ratio was placed in to the cellulose membrane and excess amount of phosphate buffer saline (PBS) with a few percent of Tween 20 was used as drug release medium. PBS buffer was used as release medium to mimic preliminarily conditions of human body because it provides desired isotonic environment and its osmolarility and ion concentrations resemble to the human body and tween 20 enhances the solubility of released CPT in PBS buffer. To determine the amount of released drug, aliquots at specific volume were withdrawn from the release medium at different time intervals during the 50 hours-time period The concentration of the camptothecin in the release medium was measured by using UV-Vis absorption spectroscopy (λ_{ex}=366 nm). 5 samples at known concentrationsin THF were used to obtain calibration curves to determine the concentration of unknown samples which is given in the Figure 4.20.

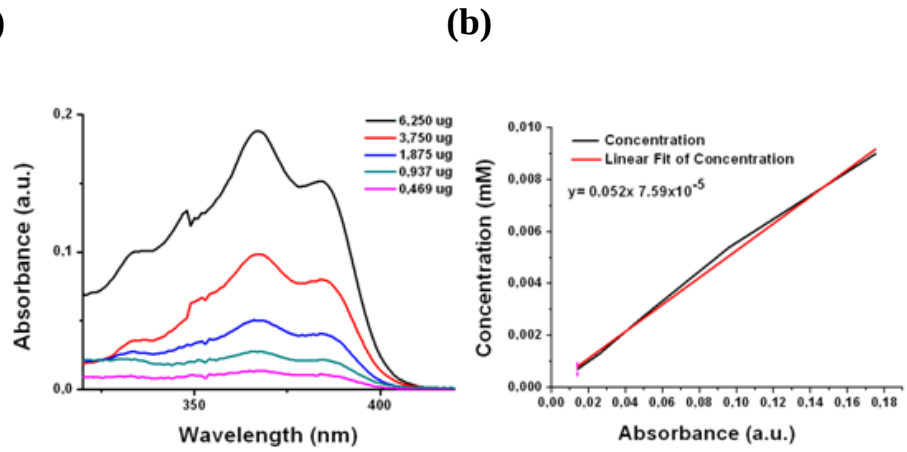

Figure 4.20. (a) UV-Vis absorption spectra of reference CPT stocks while increasing its amount (ex = 366 nm). **(b)** Fit curve which represent the absorption curves of CPT stock.

Sample	Concentration (mM)	Amount (µg)	Absorbance
Reference 1	0.0090	6.25	0.175
Reference 2	0.0050	3.75	0.096
Reference 3	0.0030	1.87	0.049
Reference 4	0.0013	0.94	0.026
Reference 5	0.0007	0.47	0.014

Table 4. Percentage of loaded CPT by the PDAFBT nanoparticles for the CPT to PDAFBT, 1:35 and 1:25 : CPT ratios, respectively.

UV-Vis absorption spectra of the withdrawn aliquots from the media were given in the Figure 4.21. The spectra was not clear and smooth like the spectra of reference CPT stocks due to effect of PBS and Tween 20 however it can be observed the intensity of peaks at 366 nm increases from 0 to 48 h time period.

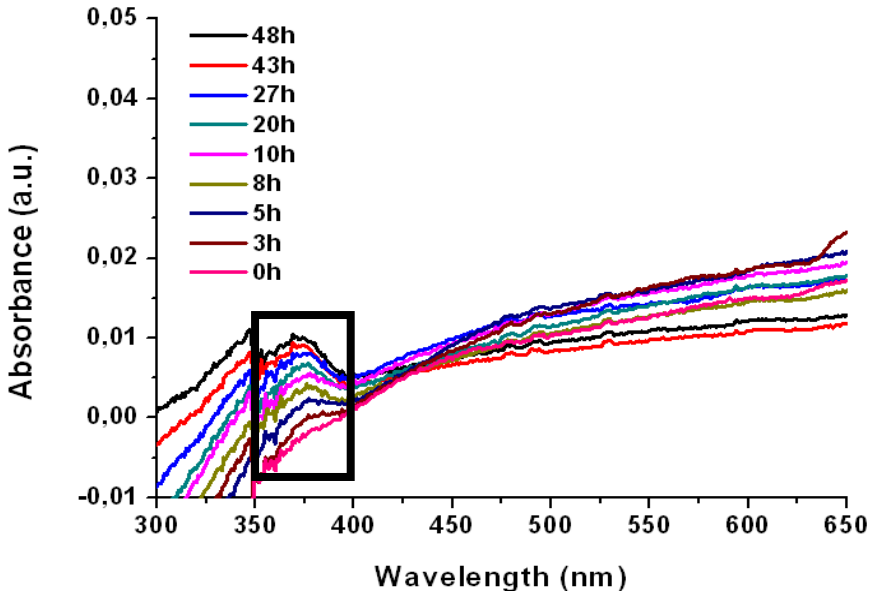

Figure 4.21. UV-Vis absorption spectra of samples withdrawn from the release medium at given time intervals.

.

Time of Release	Absorbance	Concentration (mM) *	Amount (mg)	Percentage (%)
0. hour	0	0	0	0
3. hour	0.00023	17.56×10^{-5}	0.0061	30
5. hour	0.00040	19.34×10^{-5}	0.0067	34
8.hour	0.00084	2.350×10^{-4}	0.0082	41
10. hour	0.00110	2.660×10^{-4}	0.0093	47
20. hour	0.00200	3.598×10^{-4}	0.0125	63
27. hour	0.00300	4.638×10^{-4}	0.0162	81
43. hour	0.00370	5.366×10^{-4}	0.0187	94
48. hour	0.00380	5.470×10^{-5}	0.0190	95

*Concentration values obtained from absorbance values are duplicated due to taking into consideration of dilution effect.

Table 5. UV-Vis absorbance, concentration values and percentage of released CPT at 48h time period.

Concentration values of withdrawn samples from release medium in Table 4 were calculated by using linear fit curve of reference CPT stocks then concentration of released CPT in 100 ml of medium was obtained during 48h time period. In the drug release profile shown in the Figure 4.22, it was observed that after 20 hours 63% of total CPT was released and 95% of drug was diffused from the nanoparticles at 48. hours which shows there is no sudden, and burst release of CPT by polymer matrix degradation. The main mechanism of release of CPT from the PDAFBT nanoparticles has to be diffusion. Polymer matrix allows to leak of uniformly distributed drug molecules in the sphere. This is a preliminarily demonstration of drug release profile of PDAFBT, in order to improve the study, experiment will be repeated two more times and statistical outcome (with error bars) has to be obtained. However, this preliminary study is promising and suggests that release of CPT is not a sudden process and the result will be strengthen with two other measurements and detection over long time period.

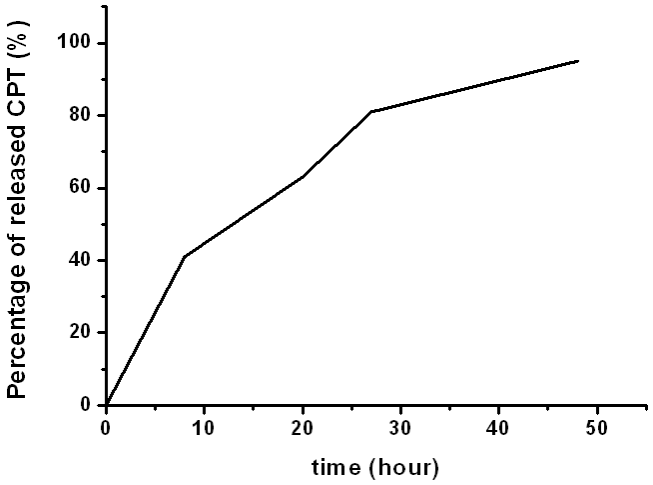

Figure 4.22. Percentage release of CPT from PDAFBT nanoparticles during 48h.

4.3. Biological Applications of Blank and Drug Loaded PDAFBT Nanoparticles

This part consists of three major studies to investigate the efficiency of PDAFBT nanoparticles as drug carriers, imaging probes and understand the interactions of those nanoparticles with biological environments. In the first part,the stability of PDAFBT nanoparticles was analyzed at different biological media. In the second part,*in vitro*cytotoxicity assessment of blank and drug loaded nanoparticles was conducted; third part deals with exploring the ability of those nanoparticles as fluorescent probe*in vitro* and *in vivo* assays.

4.3.1 Determination of the Stability of Blank and Drug Loaded Nanoparticles in the Biological Media

For the biological applications, interaction between material and biological system has to be understood and the level of biocompability should be determined especially to minimize the cytotoxicity of nanomaterial because when biomaterials are contact with cellsthey are encountered with an immunogenic response and recognized as a foreigner body. Herein, the interaction of PDAFBT nanoparticles with the human serum and bovine serum albumine (BSA) media was analyzed and the stability profile in those media was obtained. Firstly,stability of blank nanoparticles in water was analyzed by measuring their sizes with DLS during one week time period and observed that there is no significant change in the number average size distributions of blank nanoparticles over seven days. The results are given in the Figure 4.23.(a).

Secondly, those non-loaded nanoparticles were incubated in the BSA and human serum media by providing simple biological conditions (at 37^{o}C, 60 RPM) then subsequently, the samples were taken at 0, 30 and 120 min. time intervals. As shown in the Figure 4.21 (b), a sudden increase in the size was observed for both samples incubated in BSA and human blood serum media due to adsorption of the proteins on the surface of nanoparticles via either protein layer formation or aggregation on the surface of nanoparticles. Hydrophobic interaction plays a major roles for the adsorption of the proteins on the surfaces of nanoparticles. Fluorene backbone in the PDAFBT nanoparticles provides desired hydrophobic surface for proteins in the media. Moreover, ion-dipole interaction between the local positive charges on proteins and lone pairs on the dimethylamine groups of nanoparticles has to be considered protein-polymer interaction.

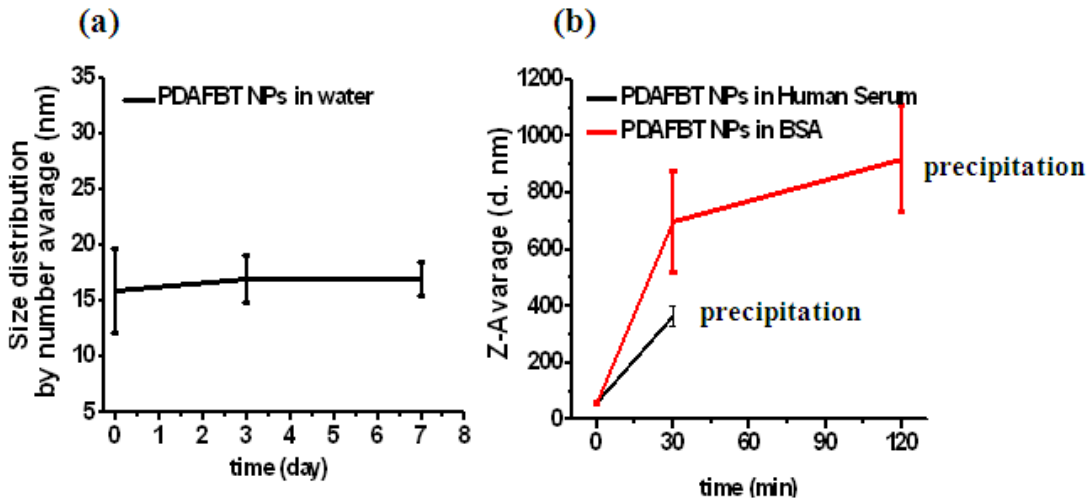

Figure 4.23. (a) Number avarage size change of blank PDAFBT nanoparticles in **(b)** Z-Avarage value (nm) of blank PDAFBT nanoparticles in human serum and BSA media masured by DLS.

.

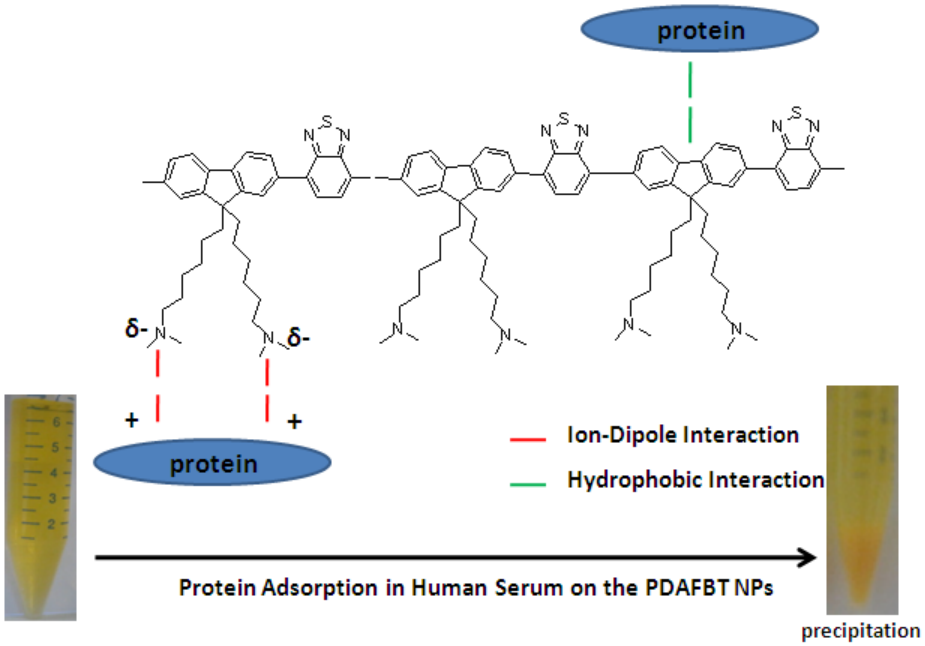

Figure 4.24. Schematic representation of interaction PDAFBT with proteins.

The percentage amount of absorbed proteins in human serum was detected by using Bradford assay, which is a quantitative protein determination method by using coomassie brilliantblue G 250 dye. Under acidic conditions this dye exists in doubly protonated red cationic form but when it binds to a protein it forms a stable unprotonated blue form ($A_{max=}$ 595 nm). Thus, the intensity of the blue protein-dye complexwas detected by using spectrometer at the 595 nm excitation. To detect the percentage adsorption of human serum proteins on the nanoparticles, the concentration of stock solution of human serum was accepted as 1X, several dilutions of this human serum stock was made and their absorbance maximum values were taken as reference. The calculated result indicates that only nearly 2.2% of proteins human serum adsorbed on the PDAFBT nanoparticles triggers the precipitation of nanoparticle solution dispersion.

(a)

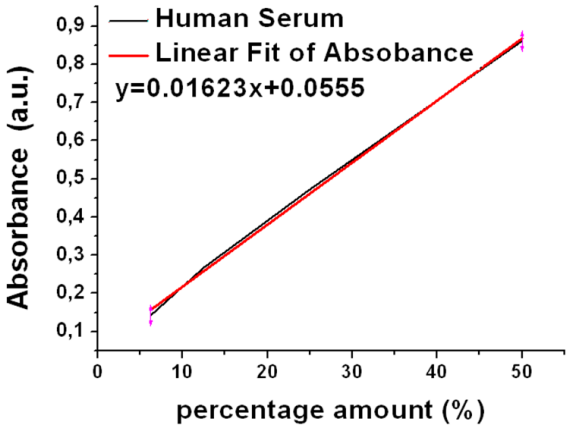

(b)

Sample	Amount	Absorbance
PDAFBT NP in Human Serum	0.6 mg polymer in 0.5 ml water	0.0919
Human Serum Reference 1	50% (from stock solution)	0.8611
Reference 2	25%	0.4724
Reference 3	12.5%	0.2675
Reference 4	6.25%	0.1428

Figure 4.25. Calculation of adsorbed proteins on surface of PDAFBT NPs in human serum through **(a)** calibration curve of stock solutions of human serum with respect to **(b)** absorbance values.

Stability of CPT loaded PDFAFBT nanoparticles was investigated in water and cell culture medium (DMEM) during one week time period by DLS. It was observed that there is not significant size change of drug loaded nanoparticles in water over days in their storage conditions (5^{o}C, 0 RPM). This also suggest that drug loaded nanoparticles preserve their shape and size unless encountering any destruction of polymer matrix which carries the drug. Before conducting the cell culture experiments of nanoparticles for different cell lines, stability of drug loaded nanoparticles in cell culture medium was determined and it was shown that the size of nanoparticles were nearly duplicated in DMEM given in the Figure 4.26 (b). DMEM supports the basal medium for growth of mammalian cells. Glucose and glycine in the content of DMEM can surround mildly the surface of nanoparticles and cause increase in size. Because the size of glycine and glucose are much lower than proteins, an acceptable size increase was observed rather than precipitation.

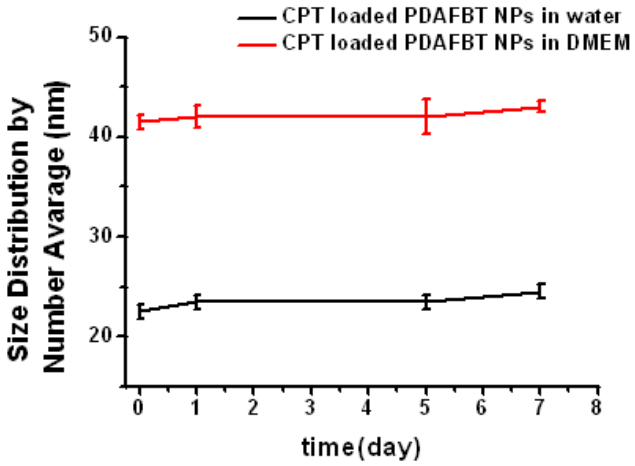

Figure 4.26. Calculation of adsorbed proteins on surface of PDAFBT NPs in human serum through **(a)** calibration curve of stock solutions of human serum with respect to **(b)** absorbance values.

Stability experiments including interactions of drug loaded and blank PDAFBT nanoparticles with several media basically show that nanoparticles are almost stable in their non-treated, storage conditions, but in the case of protein environment, adsorption of proteins on the surface of nanoparticles is at the high level which leads decrease in their compatibility in the biological environments.

4.3.2. Determination of *In-vitro* Cyctoxicity of Blank and CPT Loaded PDAFBT Nanoparticles

Dose dependent *in vitro* cytotoxicity tests of the blank, camptothecin (CPT) loaded PDAFBT and free CPT against human breast carcinoma MDA-MB-231, MDA-MB-157 and MCF 7 cells with different molecular subtypes and drug sensitivities performed using MTT assay. The reason of choosing three different cell lines was to compare their cytotoxic responses to the same model anticancer drug, using a well known anticancer drug, i.e. CPT, in the presense or absence of drug carriers. In order to analyze the sensitivity of cells to CPT, its chemical interaction with the cellular compartments has to be understood. CPT binds non-covalently to toposiomerase I, a nuclear enzyme which adjusts the topological state of DNA upon replication, -DNA complex and traps this complex. However,it was suggested that this complex can repair itself when degradation occurs through proteasomal pathway and the cells that

can achieve this repair mechanism indicates resistance to CPT.[100] Another important suggestion for the resistance to CPT is alteration of the topoisomerase I with mutation or lower expression.[101] The sensitivity of cells to chemicals was expressed with IC_{50} value which defines the inhibitory concentration of the drug to inhibit the biological process by half. The IC_{50} values obtained from literature shows that, CPT is extremely potent to the MDA-MB-157 cell line with IC_{50} value of 7 nm, while MCF-7 and MDA-MB-231 shows more resistance to CPT with the IC_{50} value of 218nm and 250 nm.[102-103] The effect of free and carried by polymer CPT on these cell lines were tested through the tetradiazole dye based cytotoxicty assays by considering their sensitivies to CPT.

Before the analysis of the toxic effect of CPT loaded nanoparticles on the cancer cells, concentration based cytotoxicity of blank nanoparticles was assessed ranging from 0.312 μM to 40μM of PDAFBT concentration for the concerned cell lines and plotted as in the Figure 4.27. It was observed that while blank nanoparticles do not exhibit significant toxicity to MDA-MB-231 and MDA-MB-157 cells up to 40 μM, a linear decrease at the viability of MCF-7 cells was detected at higher concentrations than 2.5 μM and nearly 40% of the cells were dead at 40 μM PDAFBT nanoparticle solution. Instrinsic cell death mechanism of nanoparticles is not clear however this result suggests that different cell types develop different cytotoxicresponse to nanoparticles as foreign materials and in order to detect efficiency of drug carrier nanoparticles on cancer cells, blank nanoparticles can be used as negative control.

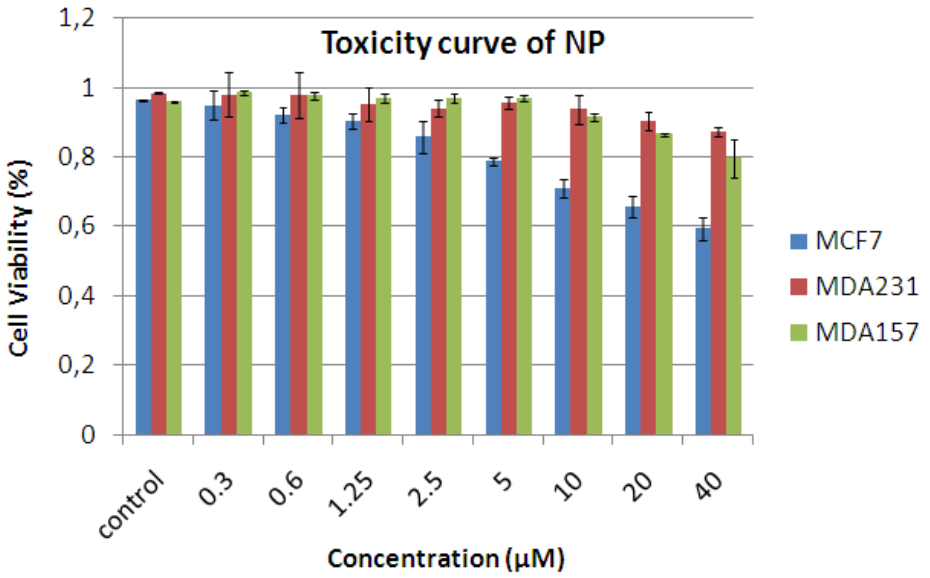

Figure 4.27. Percent cell viability results of PDAFBT nanoparticles on the MCF-7, MDA-MB-231 and MDA-MB-157 cell lines.

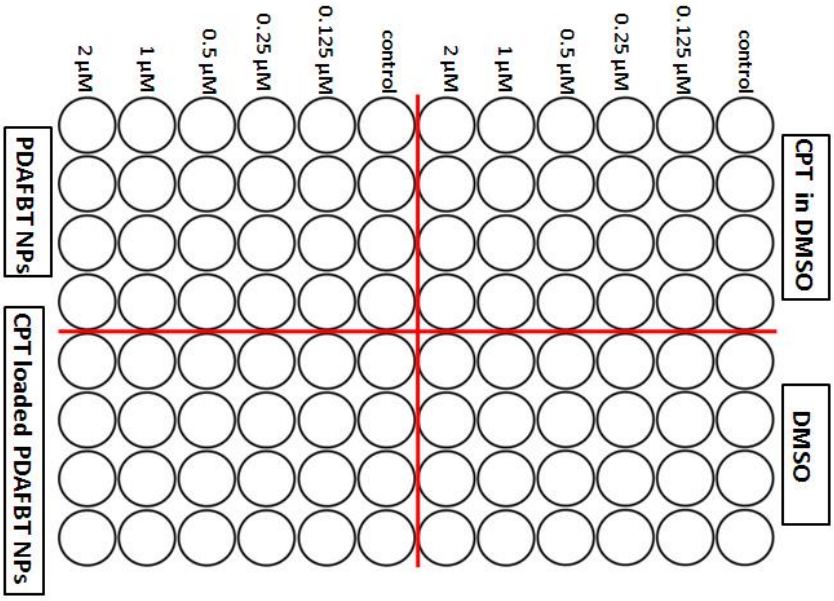

Figure 4.28. Experimental set-up for MTT calorimetric assay in 96 well plates of CPT loaded PDAFBT nanoparticles with positive control of CPT, negative control of DMSO and blank PDAFBT nanoparticles. (Each treatment has three replicates in the set-up.)

As mentioned before percent viability of cells was detected by tetraazolium dye toxicologic assay, named as MTT, which is chemically based on the reduction of

MTT dye to a blue formazan product by mitacondrial dehydrogenases enzyme of live cells.[104] The MTT protocol was applied according to instructions of Invitrogen. The intensity of purple formazan product shows the viability of cells that were plated into 96 well plates (2000 cells) after 24 hours cells were treated with free CPT in DMSO, blank PDFABT nanoparticles, CPT loaded Nanoparticles and DMSO. After 48h treatment, live cells were quantified by measuring the absorbance intensity (optical density) of blue formazan product at 570 nm. In the experimental set-up which is shown in the Figure 4.28, free CPT was used as positive control, DMSO and blank nanoparticles were as negative control to CPT loaded nanoparticles. The cell viability results in percentage of each cell line were demonstrated in the Figure 4.29. Each cell line exhibits generally a similar trend to exposures by decreasing the number of viable cell but the percentage of cell deaths changes with respect to the sensitivity of cell line to PDAFBT nanoparticles and CPT. When the MDA-231 cell line was analyzed, it was seen that while the toxic effect of free CPT on the cells is nearly 35%, toxic effect of blank nanoparticles decreases by half at the same CPT loaded PDAFBT concentrations. In the case of CPT loaded nanoparticles, nearly 70% of cell deathwas observed at 2μM CPT level which is much higher than the sum ofseperatetoxic effects of blank nanoparticles and CPT. This result preliminarily suggests the idea of cell death through synergic effect between nanoparticle and drug, rather than additive effect due to sum of them. IC_{50} values of CPT and CPT loaded PDAFBT NPs were calculated and found as 1.97μM and 1.05μM. This means internalization of the same amount of CPT was more efficient by transporting in PDAFBT nanoparticles rather than in free form. MDA-MB-157 cell line also confirms the toxicity results of MDA-MB-231 cells. Toxicity of PDAFBT Nps and CPT are nearly in the same level with roundly 25% at high concentrations, but CPT loaded nanoparticles kill the nearly 70% of the cells at 2μM CPT concentration. IC_{50} value of CPTloaded nanoparticles was only 1.35μM while IC_{50} value of free CPT was 4.5 μM which shows the high efficiency of delivery of CPT in nanoparticles. However , in MCF7 nanotparticle CPT combination exhibited a relatively slower action on cell compared to other cell lines, and at 2 μM the effect of campothecin was similar to that of nanoparticle CPT complex in one of the experiments but in the other there was a significant difference (Appendix A). Across all concentrations and in all cell lines, PDAFBT-CPT complex exhibited more effect against viability

compared to CPT or PDAFBT alone, suggesting that PDAFBT is a highly effective drug carrier. IC50 values were calculated based on untransformed drug concentrations (Table 5). One possibility is calculate IC50 induction after normalization to controls (i.e., dmso for campothecin and PDAFBT for PDAFBT-CPT) and calculate a single IC50 showing the effect of nanoparticle (Table 5). However, at 2 μM, not all cell lines resulted in 50% reduction in cell viability thus it is difficult to estimate an exact IC50 for MDA157. Thus other methods of drug effectivity, such as Amax and area under curve (AUC) can be explored in the future studies[105]. These initial findings indicate that MDA157 exhibits the most striking effect of the nanoparticle followed by MDA231 and MCF7 cell lines

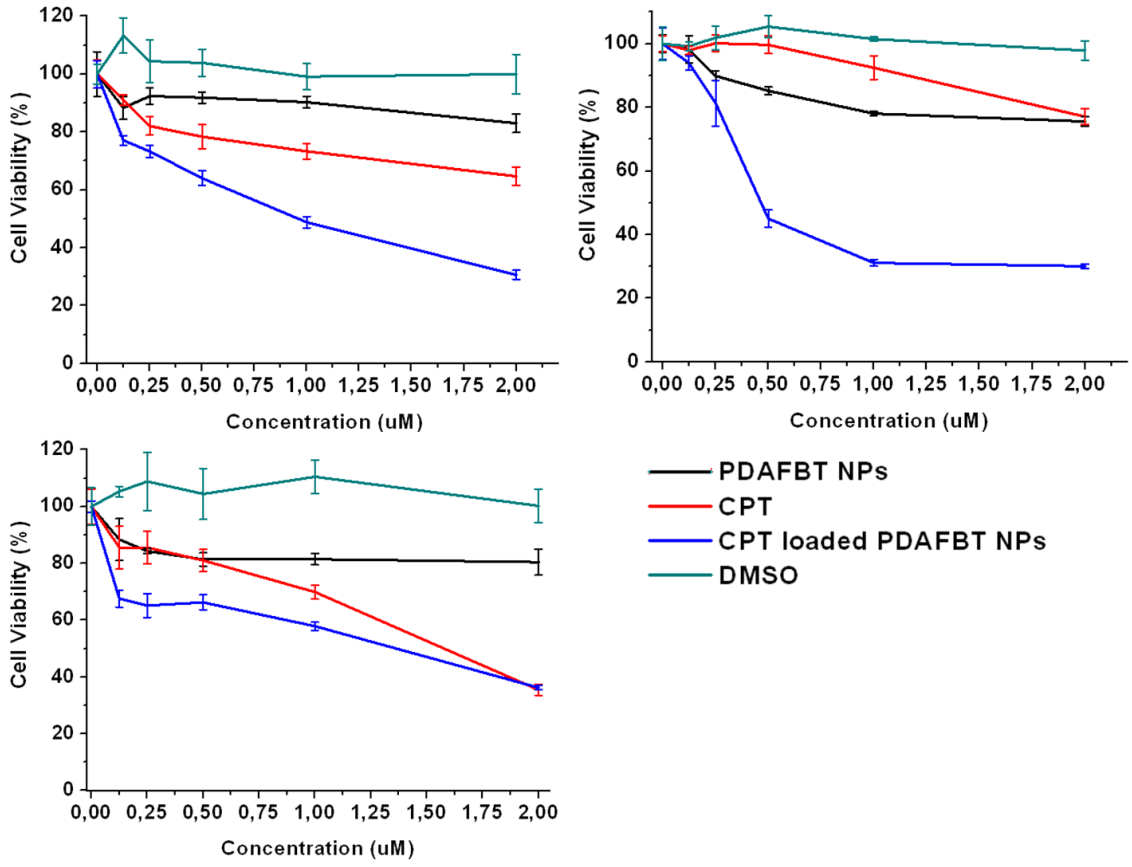

Figure 4.29. Percent cell viability results of **(a)** MDA-MB-231 **(b)** MDA-MB-157 and **(c)** MCF-7 cell lines after 4h MTT treatment.

Cell Line	IC_{50} of free CPT (μM)	IC_{50} of CPT loaded PDAFBT NPs (μM)
MDA-MB-231	1.97	1.05
MDA-MB-157	4.50	1.32
MCF-7	1.48	1.75

Table 6. IC50 values of free CPT and CPT loaded PDAFBT nanoparticles for MDA-MB-231, MDA-MB-157 and MCF-7 cell lines.

A comparison between the sensitivity of the cell lines to an anti cancer drug and morphology of cells can be make by checking the molecular and cellular phenotype of the cells. MDA-MB-231, MDA-MB-157 and MCF-7 cells have differences in their estrogen and progesterone receptor status as well as migratory characteristics that can contribute to the differences observed in NP toxicity and effectivitys[106-108] Therefore future studies are needed to construct a releationship between the morhologies of the concerning cell lines and their sensitivies to nanoparticles carrying CPT.

Cell viability experiments were repeated two-three times with different concentrations and that results for MDA-MB-231 and MDA-MB-157cell lines are in high conformity by exhibiting efficient internalization of CPT through the PDAFBT nanoparticles. (Appendix A) Furthermore, each cell line shows similar response to the same chemicals with changing in viability. The results of sensitivity to CPT of concerning cell lines in these experiments are not same with the literature values reporting the CPT sensitivity of resulting cell lines but sensitivity this maybe due to differences in cell passage numbers and from different batches, phases in the cell cycle also another critical parameter defining the drug sensitivity.[109] It can be preliminarily deduced than from the cytotocity results PDAFBT nanoparticles can be used for diasnogtics approach.

4.3.3. In Vitro and In Vivo Screening of blank PDAFBT and PPFBT Nanoparticles

4.3.3.1.Identification of PDAFBT Treated Cells by BrdU Labeling

5-Bromo-2-deoxyurine (BrdU) is a synthetic thymine analog incorporated to DNA during the cell division and to trace the proliferation of cells. BrdU can quantify the number of newborn cells in the time period of its treatment and labeling BrdU fluorescently provides to screen the cells by fluorescence microscope.[110] DNA incorporated BrdU can be detected by using specific monoclonal primary antibodies and fluorescent dye conjugated secondary antibodies which can bind to these primary antibodies to provide detection of cells by fluorescent screening.

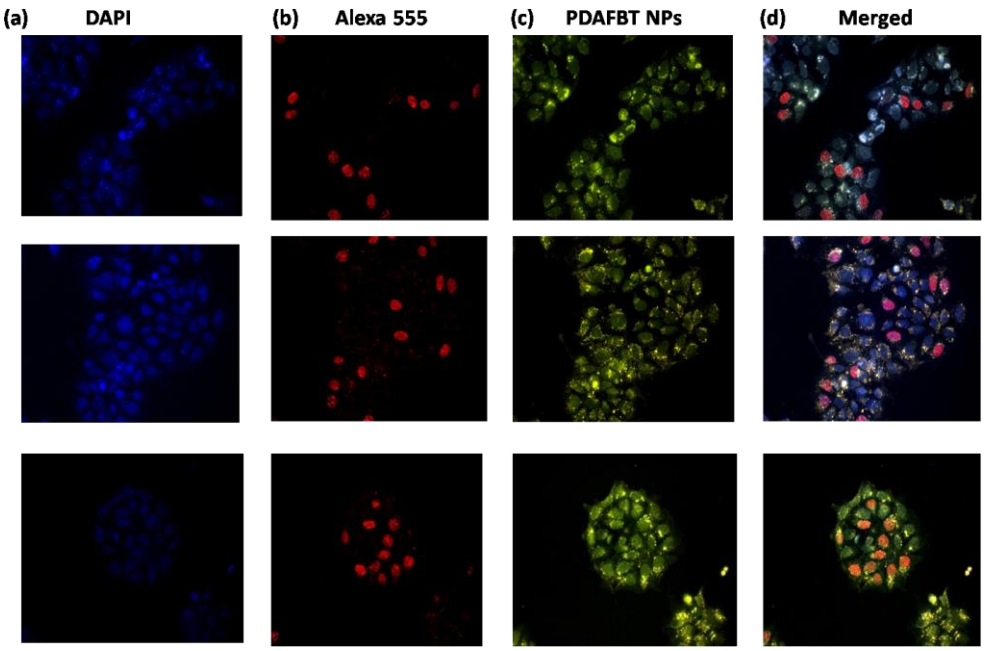

Figure 4.30. Identification of PDAFBTtreated MCF-7 cells through BrdU labeling. **(a)** Stained nuclei with DAPI **(b)** Detection of BrdU incorporation using BrdU Mouse mAB#52925 and Anti Mouse IgG (H+L) #4409, $F(ab')_2$ (Alexa Fluor 555) **(c)** Internalizaed PDAFBT NPs (30μM) into the cells. **(d)** Merged images of (a), (b) and (c). (40X magnification with blue, yellow, red filters.)

Herein, PDAFBT treated MCF-7 cells were screened by fluorescently labeling BrdU and a round estimation was made about the effect of nanoparticles on cell proliferation. In this experiment, BrdU mouse mAB was used as primary antibody to

detect BrdU reagentbound to single stranded DNA and Alexa fluor 555 conjugated anti Anti- Mouse IgG was used as secondary antibody to screen the cells having red emission according to manufacturer's instructions[111] (Cell Signaling). It is important to adjust the time of treatment of BrdU because it is potentially toxic for the cells due to bromide group in its structure. After 48h incubation of the cells with PDAFBT nanoparticles, BrdU reagent was given for 2h. The exposure of PDAFBT NPs and BrdU reagent to MCF-7 cells were shown in the Figure 4.30. In order to to distinguish the cellular boundaries, nuclei were stained with DAPI. Stained nuclei with DAPI (blue) and BrdU (red) (Figure 4.30a-b) can be select effectively. Fluorescent images in the Figure 4.30 (c-d) shows that PDAFBT nanoparticles were internalized efficiently by the cells and they accumulate mostly in the perinuclear reagion of the cells. The cells which make red fluorescence emission are newly proliferated cells after BrdU incorporation. Cell proliferation efficiency after exposure of PDAFBT nanoparticles were not evaluated quantitatively but from the images it can be seen that cell proliferation continues after PDAFBT treatment.Additionally it was observed that, while fluorescent intensity of DAPI decreased enormously after one month storage, there is not any significant change in the brightness of PDAFBT nanoparticles which demonstrates the photostability of PDAFBT nanoparticles for long term period (Figure 4.31)

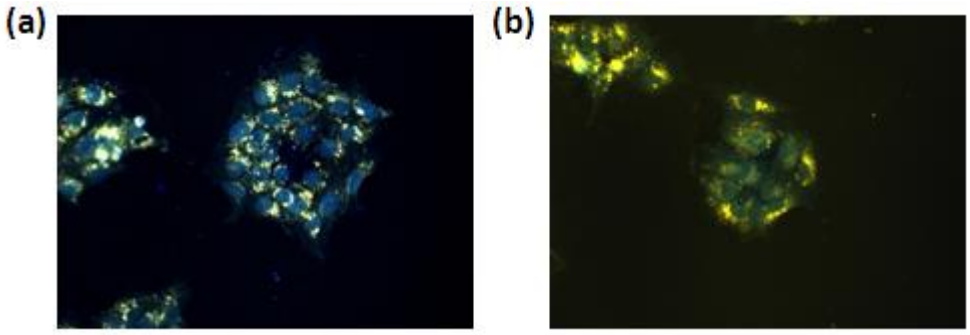

Figure 4.31. PDAFBT NPs internalized MCF-7 cells (a) right after DAPI staining.(b) after one month storage.

4.3.3.2 In Vivo Screening of PDAFBT nanoparticles in Zebrafish Embryos as Model Organism

Embryonic zebrafish is used as an ideal model system for in vivo imaging due their transparency and ability to develop rapid and stereotyped embryonic central nervous system.[112] There are studies reporting exposuring fluorescent organic molecules and fluorescent silica nanoparticleson zebrafish embryos but there is no study consisting whole body imaging of embryonic zebra fish with fluorescent conjugated polymer nanoparticles. [113-114]

Here a preliminarily study, the accumulating of PDAFBT nanoparticles on zebrafish embryos was visualized by fluorescent microscope. Zebrafish embryos at 48h dpf were treated with CPT, DMSO,blank and CPT loaded PDAFBT nanoparticles at different concentrations followed by washing and fixing with paraformaldehyde. After 24 hours exposure, it was observed that there is not significant effect of on the development of zebra fish embryos treated with DMSO and blank nanoparticles while negative effect onsurvial of embryos was encountered treated with free CPT and CPT loaded nanoparticles at 2 μM drug concentration. Zebrafish embryos treated with 0.5μM free CPT and blank nanoparticles and drug loaded nanoparticles revealed that nanoparticles accumulate on the skin of the embryos, particularly ventrally.(Figure 4.32). The intensity of the fluoresence of the NPs allow visualization incontrast to the autofluorescence from the embyros itself. Future studies will involve microinjection of a given amount of blank nanoparticle and drug loaded nanoparticle combination to visualize the effect internally. Also, zebrafish starts feding at 5 dpf, thus nanoparticles might be orally available to the embryos thus effects can be further analyzed.

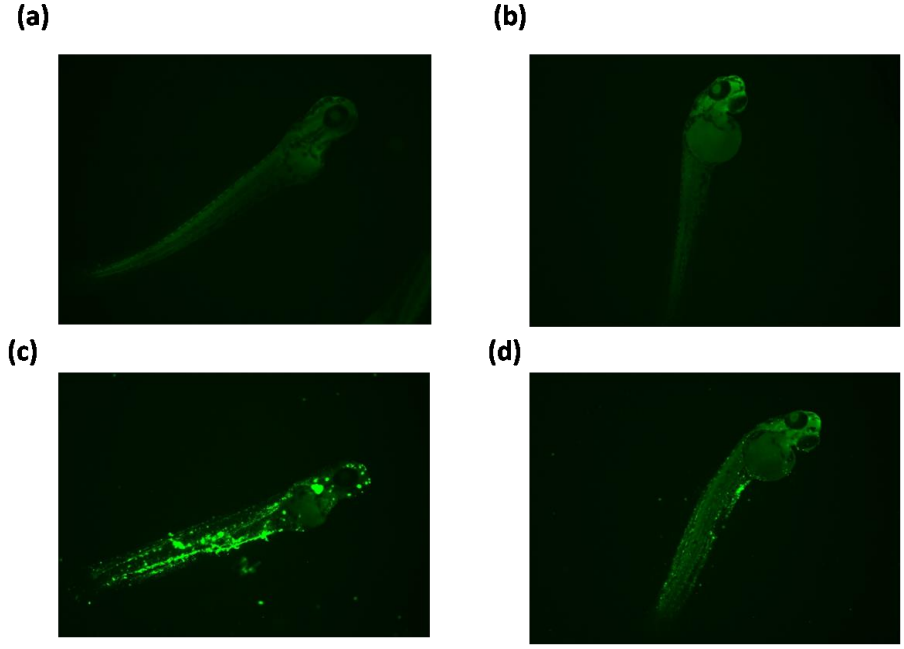

Figure 4.32. Fluorescence microsope images of embryonic zebra fish (48h pf) exposured to **(a)** DMSO (% 1), **(b)** CPT (0.5 μM) **(c)** PDAFBT NPs (2μM) (d) CPT loaded PDAFBT NPs (0.5 μM). ($\lambda_{em=}$ 480-550 nm), 40X)

4.3.3.3.In Vivo Screening and Toxicity Assesment of PPFBT nanoparticles in C. Elegans as a Model Organism

In this part, in vivo visualization and primary toxicity investigation of previously synthesized Poly[9,9-bis{propenyl}fluorenyl-2,7-diyl))-co-(1,4-benzo{2,1,3}-thiodiazole)] (PPFBT) nanoparticles [115] were appliedby using *C. Elegans* as model organism due to its transparency and easy handling. *In vitro* cytotoxicty of PPFBT nanoparticles was assessed previously and IC_{50} value of free CPT and CPT loaded PPBT nanoparticles were found as 0.9 μM and 0.1μM respectively, indicating the high efficiency of internalization of CPT through these nanoparticles.[116] Herein, as a next step of its biomedical applications, a primary study to determine *in vivo* imaging ability and toxicity of PPFBT nanoparticles was conducted. Penetration of PPFBT nanoparticles to adult C. Elegans (L4 phase) was determined after 30 min exposure time and fixation.

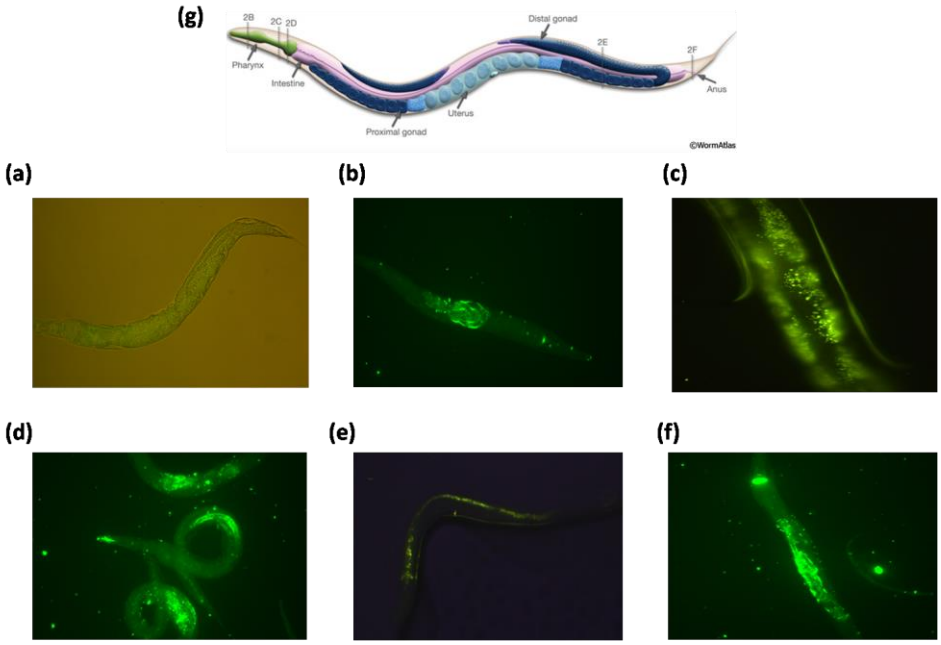

Figure 4.33. (a) Fluorescence microscope images of **(a)** non treated, PPFBT NPs (0.01 mM) stained *C. Elgans* (L4) at (b) 20X **(c)** 40X **(d-f)** 20X magnifications (λem= 480-550 nm) **(g)** Shematic drawing of anatomy of an adult hermafrodite.[117]

Fluorescence images of PPFBT loaded nanoparticles in *C. Elegans* taken by fluorescence microscope with green filter was shown in the Figure 4.33. Images primarily suggest that nanoparticles are efficiently uptaken by worms and accumulate mainly in on the gonad and phyranx of the animal.

Toxic effect of PPFBT nanoparticles on *C. Elegans* was examined primarily by counting of progeny after treatment with 0.01mM nanoparticles for 5 days time period in parallel with untreated control groups. It was observed that PPFBT treated worms at given concentration continue to proliferate like untreated worms with an acceptable decrease as shown in the Figure 3.34. This very primary result is promising to enhance the in vivo studies of PPFBT nanoparticles by optimizing the time and dose dependent applications.

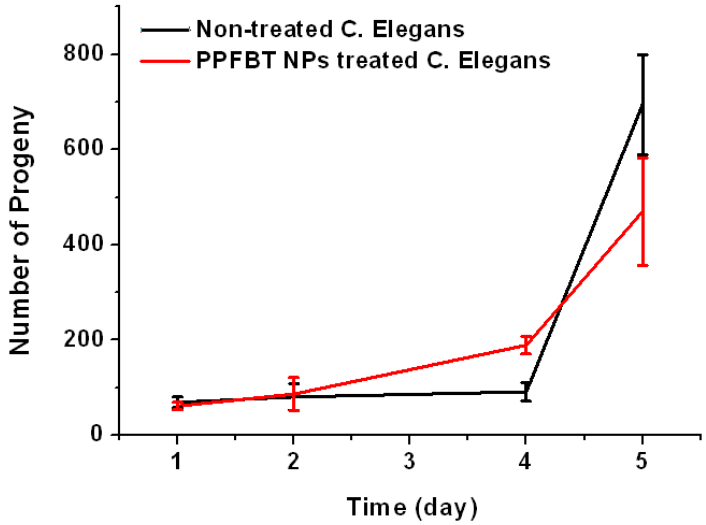

Figure 4.34. Number of progeny of nontreated and PPFBT treated C. Elegans in 5 days time period.

Cell viability assay through MTT and in vitro and in vivo imaging capability results show that these nanoparticles can be deeply analyzed for theranostic applications which is based on imaging guided drug delivery phenomena.

CHAPTER 5

5. CONCLUSION

In this thesis, imaging guided drug carrier system based on conjugated polymers nanoparticleswas developed and their efficiency to deliver water insoluble anticancer therapeutic camptothecin into cells was investigated.

Fluorene based conjugated polymer, PDAFBT, was synthesized through Suzuki Coupling and characterized by H^1-NMR, C^{13}-NMR, ESI-MS, MALDI, FTIR, UV-Vis absorption and Fluorescence spectroscopies. PDAFBT nanoparticles were synthesized through reprecipitation technique and characterized by DLS, TEM, SEM methods and nearly 25nm number avarage size distribution with PDI lower than 0.2 was detected for the uniform nanoparticles In order to obtain drug carried nanoparticles, anticancer drug camptothecin was entrapped into PDAFBT nanoparticles through hydrophobic and $\boldsymbol{\pi}$-$\boldsymbol{\pi}$ interactions. Drug encapsulation efficiency (EE) was found as 92% and 75% for the 1:35 and 1:25 polymer to drug ratios. Through this investigation, drug loading efficiency of PDAFBT nanoparticls (LE) was determined as 2.67±0.3 %. Preliminary drug relase profile which will be strengthen statistically, of PDAFBT nanoparticleswas analyzed and showed that nearly 100 % of loaded CPT was released in 48h time period and release of CPT is not a sudden process. In vitro dose dependent cytoxicity assay MTT on MDA-MB-231, MDA-MB-157 and MCF-7 cells indicates that PDAFBT nanoparticles do not exhibit significant toxicity. IC_{50} values of free CPT and CPT loaded PDAFBT NPs were 4.50μM and 1.35μM for MDA-157 cell line and 1.97μM and 1.05μM for MDA-MB-231 cells which shows efficient internalization of CPT into MDA-MB-157 and MDA-MB-213 cell line through these polymer capsules.Preliminarily in vivo imagings of PDAFBT and PPFBT nanoparticles on embryonic zebra fish and C. Elegans models suggest that efficient internalization of nanoparticles by tissues andin-vivo monitoring of PDAFBT nanoparticles is promising for time and dose dependent treatments as a future direction.

BIBLIOGRAPHY

1. Shotheim ,T. A. ; Elsenbaumer ,R. L. ; Reynolds , J. R., 'Handbook of Conducting Polymers', *Marcel Dekker* , New York , 1998.

2. Strobl, G.R., 'The Physics of Polymers' : 'Concept for Understanding their Structures and Behaviours', Springer, 2007.

3. Sallaneck, W.R.; Friend, R.H.; Bredas, J.L., 'Electronic Structure of Conjugated Polymers : Consequences of Electron Lattice Coupling' *Physics Reports,* no. 319, pp. 231-251, 1999.

4. Dai,L., 'Intelligent Macromolecules for Smart Devices : From Material Synthesis to Device Applications', *Springer,* 2004.

5. Bredas, J. L.; Silbey, R., 'Conjugated Polymers: The Novel Science and Technology of Highly Conducting and Nonlinear Optically Active Materials' ,*Kluwer Academic Publishers*, Drodrect, 1991.

6. Kiess, H., 'Conjugated Conducting Polymers' ,*Springer-Verlag*, New York , 1992.

7. http://www.nobelprize.org/nobel_prizes/chemistry/laureates/1963/speedread.html

8. Shirakawa, H.; Louis, E.J.; MacDiarmid, A.G.; Chiang, C.K.; Heeger, A.J., 'Synthesis of electrically conducting organic polymers: Halogen derivatives of polyacetylene, (CH)x', *J. Chem.Soc. Chem. Commun*., pp. 578-580,1977.

9. Norden, B., Krutmeijer, E, , 'Nobel Prize in Chemistry 2000 : conductive Polymers', *The Royal Sweedish Academy of Sciences*,2000.

10. Lakowicz, J.R., 'Principles of Fluorescence Spectroscopy', 2nd ed. *Kluwer Academic/Plenum*, New York, 1999.

11. Turro, N. J., 'Modern Molecular Photochemistry, University Science Books', Sausalito, CA, 1991.

12. Lakowicz, J.R., 'Principles of Fluorescence Spectroscopy', 3rd ed. *Kluwer Academic/Plenum*, New York, 2006.

13. Burroughes, J. H.; Bradly, D. D. C.; Brown, A. R.; Marks, R.N.; MacKay, K.; Friend, R. H.; Burn P. L.; Holmes, A. B., 'Light Emitting Diodes Based On Conjugated Polymers', *Nature*, no. 347, pp. 539-541, 1990.

14. Perepichka, I. F.; Perepichka, D. F.; Meng, H; Wudl F., 'Light Emitting Polythiophenes', *Adv. Mater.* , no. 17, pp. 2281-2305, 2005.

15. Grem, G.; Leditzky, G.; Ullrich, B.; Lesing, G., 'Realization of Blue Light Emitting Device Using Poly(p-phenylene)', Adv. Mater., vol. 4, no. 1,pp 36-37, 1992.

16. Shu, C. F.; Dodda, R.; Wu, F. I.; Liu, M. S.; Alex, K.; Jen, Y., 'Highly Efficinet Blues Light Emitting Diodes From Polyfluorene Containing Bipolar Pendant Groups', *Macromolecules*, no. 36, pp. 6698-6703, 2003.

17. Bernius, M. T.; Inbasekaran, M.; O'Brien, J.; Weishi, W., 'Proggres with Light Emitting Polymers', *Adv. Mater.*, vol.12, no.23, pp. 1737-1750,2000.

18. Graetzel, M., 'Photoelectrochemical Cells', *Nature*, vol. 414, pp. 338-344, 2001.

19. McGehee, M. D.; Coakley, K. M., 'Conjugated Polymer Photovoltaic Cells', *Chem. Mater.*, vol. 16, pp. 4533-4542, 2004.

20. Padinger, F.; Rittberger, R.S.; Sariciftci, N. S., 'Effects of Postproduction Treatment on Plastic Solar Cells', *Adv. Func. Mater*., vol.14, no. 1, pp. 85-88, 2003.

21. Heeger, A. J.; Schwarz, B. J.; Garcia, M. A. D.; Hide, F., 'New Development in the Photonic Applications of Conjugated Polymers', *Acc. Chem. Res*., vol. 30, pp.430- 436, 1997.

22. Sawager, T. M.; McQuade, D. T.; Pullen, A. E., 'Conjugated Polymer Based Chemosensors', *Chem. Rev*., vol. 100, pp. 2537-2574, 2000.

23. Disney, M. D.; Seeberger P. H.; Zheng, J.; Swager, T. M., 'Detection of Bacteria with Carbohydrate Functionalized Fluorescent Polymers', *JACS*; vol. 126, no.41, pp. 13343-13346, 2004.

24. Swager, T. M.; Yang, J.S., 'Fluorescent Porous Polymer Films as TNT Chemosensors: Electronic and Structural Effects', *JACS*, vol. 120, no. 46, pp. 11864-11873, 1998.

25. Fan, L. J.; Zhang, Y.; Murphy, C. B.; Angell, S.H.; Parker, M. F. L.; Flynn, B. R.; Jones, W. E., 'Fluorescent Conjugated Polymer Wire Chemosensors for Transition Metal Ion Recognition and Signaling', *Coord. Chem. Rev*., vol.253, no. 3-4, 2009.

26. Smela, E.; Inganas, O.; Lundstrom, I., 'Conducting Polymers as Artificial Muscles: Chalenges and Possibilities', *J. Micromech. Microeng*., vol. 3, no. 4, pp. 203-205, 1993.

27. Dennler, G.; Sariciftci, N. S.; Schwaediauer, R.; Bauer, S.; Reiss, H., 'Electromechanical Strain Conjugated Polymer Diodes Under Forward and Reverse Bias', *Appl. Phys. Lett*., vol.86, no.19, pp. 1935-1947, 2005.

28. Friend, R. H.; Gymer R. W.; Holmes, A. B.; Burroghes, J. H.; Marks R. N.; Talliani, C; Bradley D. D. C.; Dos Santos, D. A.; Bredas, J. L.; Lögdlund, M.; Salaneck, W. R., 'Electroluminescence in Conjugated Polymers', *Nature*, vol.397, pp. 121-128, 1999.

29. Bliznyuk, V. N.; Carter, S. A.; Scott, S. C.; Klearner, G.; Miller R. D.; Miller D. C., 'Electrical and Photoinduced Degredation of Polyfluorene Based Films and Light Emitting Devices', *Macromolecules*, vol. 32, pp. 361-369, 1999.

30. Arias, A. C.; Corcoran, N.; Banach, M.; Friend, R. H.; MacKenzie J. D.; Huck, W. T. Z., 'Vertically Segregated Polymer Blend Photovoltaic Thin Film Structures Through Surface Mediated Solution Processing', *Appl. Phys. Lett.*, vol. 80, no. 1695-1698, 2002.

31. Wong, H. M. P.; Wang, P.; Abrusci, A.; Svenson, M.; Anderrson M. R.; Greenham N. C., 'Donor Acceptor Behaviour in a Polyfluorene for Photovoltaics', *J. Phys. Chem. C.*, vol. 111, pp. 5244-5248, 2007.

32. Grice, A. W.; Bradley, D. D. C.; Bernius, M. T.; Inbasekaran, M.; Wu, W. W.; Woo, E. P., 'High Brightnes and Efficiency Blue Light Emitting Diodes', *Appl. Phys. Lett.*, vol. 73, no. 5, pp. 629-631, 1998.

33. Pal, B., Yen, W. C.; Yang, J. S.; Su, W. F., 'Substitiuent Effect on the Optoelectronic Properties of Alternating Fluorene-Thiophene Copolymers', *Macromolecules*, vol. 40, pp. 8189-8194, 2007.

34. Jin, Y.; Kim, J. Y.; Park, S. H.; Kim, J.; Lee, S.; Lee K.; Suh, H., 'Synthesis and Properties of Electroluminescent Polyfluorene Based Conjugated Polymers, Containing Oxadiazole and Carbazole Units as Pendants, for LEDs', *Polymer*, vol. 46, pp. 12158-12165, 2005.

35. Scherf, U.; Neher, D., 'Advances in Polymer Science: Polyfluorenes', *Springer-Verlag*, Berlin, 2008.

36. Charas, A.; Morgado, J.; Martinho, J. M. G.; Alcacer, L.; Lim S. F.; Friend, R. H.; Cacialli, F., 'Synthesis and Luminescence Properties of Three Novel Polyfluorene Copolymers', *Polymer*, vol. 44, 1843-1850, 2003.

37. Xue, C.; Singaravelu, V; Johnson, S.; Saha, R.; Smith, A.; Brewer, W.; Murthy, P.; Bagley S.; Liu, H., 'Highly Water Soluble, Fluorescent, Conjugated Fluorene Based Glycopolymers with Poly(ethylene-glycol) Tethered Spacersfor Sensitive Detection of *Escherichia Coli*', *Chem. Eur. J.*, vol. 15, pp. 2289-2295, 2009.

38. Wu, C. S.; Liu, C. T. ; Chen, Y., 'Multifunctional Copolyfluorene Containing Pendant Benzimidazolyl Groups: Applications in Chemical Sensors and Electroluminescent Devices', *Polym. Chem.*, vol. 3, pp. 3308-3317, 2012.

39. Stevens, M. P., 'Polymer Chemistry: An Introduction', *Oxford University Press*, 3rd ed., New York, 1998.

40. Toshima, N.; Hara, S., 'Direct Synthesis of Conducting Polymers from Simple Monomers', *Prog. ,Polym. Sci.*; vol.20, pp.153-185, 1995.

41. Grunathan, K.; Vadivel Murugan, A.; Marimuthu, R.; Mulik, U.P.; Amalnerkar, D. P.,' Electrochemically Synthesized Conducting Polymeric Materials for Applications Toward Technology in Electronics, Optoelectronics and Energy Storage Devices', *Mater. Chem. Phys.*, vol. 61, 173-191, 1999.

42. Diaz, A. F.; Kanazawa, K. K.; Gardini, G. P., 'Electrochemical Polymerization of Pyrole', *J.C.S. Chem. Commun.*, pp. 635-636, 1979.

43. Kobayashi, M.; Colaneri, N.; Boysel, M.; Wudl, F.; Heeger, A., ' The Electronic and Electrochemical Properties of Poly(isothionapthlene)', *J. J. Chem. Phys.*, vol. 82, 5717-5723, 1985.

44. Vadivel Murugan, A.; Gopinath, C. S.; Vijayamohanan K., 'Electrochemical Studies of Poly(3,4-ethylenedioxythiohene) PEDOT/VS_2 Nanocomposite as cathode Material For Rechargable Lithium Batteries', *Electrochem. Commun*., vol.7, pp. 213-218, 1995.

45. Mayershofer, M. G.; Nuyken, O., 'Living Polymerization of Substituted Acetylenes', *J. Polym. Sci.*, vol. 43, no. 23, 5723-5747, 2005.

46. Zhao, Y.; Campell, K.; Tykwinski R. R., 'Iterative Synthesis and Characterization of Cross-Conjugated iso-Polydiacetylenes', *J. Org. Chem*., vol 67, pp. 336-344, 2002.

47. Scientific Backround on the Nobel Prize in Chemistry 2010: *Palladium Catalyzed Cross Couplings in Organic Synthesis*, The Royal Sweedish Academy of Sciences, 2010.

48. Tamao, K.; Sumitani, K.; Kumada, M., 'Selective Carbon Carbon Bond Formation by Cross Coupling of Grignard Reagents with Organic Halides. Catalysis by Nickel-Phosphine Complexes', *J. Am. Chem. Soc*.; vol. 94, no. 12, pp. 4374-4376, 1972.

49. Heck, R. F.; Nolley, J. P., 'Palladium Catalyzed Vinylic Hydrogen Substitution Reactions with Aryl, Benzyl and Styryl Halides', *J. Org. Chem*., vol. 37, no. 14, pp. 2320-2322, 1972.

50. Miyaura, N.; Suzuki, A., 'Steraoselective Synthesis of Arylated (E) Alkenes by the Reaction of Alk-1-enyborones with Aryl Halides in the Presence of Palladium Catalyst', *Chem. Commun*., pp.866-867, 1979.

51. Miyaura, N.; Suzuki, A., 'Palladium Catalyzed Cross Coupling Reactions of Organoboron Compounds', *Chem Rev*. vol. 95, pp.2457-2483, 1995.

52. King, A.O.; Okukado, N.; Negishi, E., ' Highly General Stereo-Regio and Chemoselective Synthesis of Terminal and Internal Conjugated Enynes by Pd Catalyzed Reaction with Alkynylzinc Reagents with Alkenylhalides', *J. Chem. Socc., Chem. Commun.,* pp.683-684, 1977.

53. Stille, J. K., 'The Palladium Catalyzed Cross Coupling Reactions of Organotin Reagents with Organic Electrophiles', *Angew. Chem. Int. Ed.,* vol. 25, pp. 508-524, 1986.

54. Sonogashira, K.; Tohda, Y.; Hagihara, N., 'Convenient Synthesis of Acetylenes.Catalytic Substitiuons of Acetylenic Hydrogen with Bromoalkenes, Iodoarenes and Bromopyridines', *Tehrahedron Lett,* vol.50,pp. 4467- 4470, 1975.

55. Ikeda, S.; Yamamoto, H.; Kondo, K.; Sato, Y., ' Nickel Catalyzed Tandem Coupling of Chlorotrimethylsilane,.alpha.,.beta.-Enones,Alkynes and Dimethylzinc', *Organometallics,* vol 14, no. 11, pp. 5015-5016, 1995.

56. Landfester, K., 'Miniemulsion Polymerization and the Structure of Polymer and Hybrid Nanoparticles', *Angew. Chem. Int. Ed*., vol. 48, no. 25, pp. 4488-4507, 2009.

57. Landfester, K, 'Semiconducting Polymer Nanospheres in Aqeous Dispersion Prepared by a Miniemulsion Process', *Adv. Mater.,* vol 22, no 9, pp. 651-656, 2002

58. Wu, C.; Szymanski, C.; McNeill J.,'Preparation and Encapsulation of Highly Fluorescent Conjugated Polymer Nanoparticles' *Langmuir,* vol.22, pp.2956-2960, 2006.

59. Tuncel, D.; Demir, H. V., 'Conjugated Polymer Nanoparticles', *Nanoscale,* vol.2, pp. 484,494, 2010.

60. Moon, J. H.; Deans, R.; Krueger, E.; Hancock, H. F., 'Capture and Detection of Labeled Oligonucleotide by Poly(phenylene ethynylene) Particles' *Chem. Commun.*, pp. 104-104, 2003.

61. Fisslthaler E.; Alexander B.; Landfester K.; Sherf U.; List E. J. W.; 'Printing Functional Nanostructures : A Novel Route Towards Nanostructuring of Organic Electronic Devices via Soft Embossing, Inkjet Printing and Colloidal Self Assembly of Semiconducting Polymer Nanospheres' *Soft Matter*, vol. 4, pp. 2448-2453, 2008.

62. Pick, T; Gamerith, S.; Gadermaier, C; Plank, H.; Wenzl, F.P.; Patil, S.; Montenegro, R.; Kietzke, T.; Neher, D.; Sherf U.; Landfester, K.; List, E. J. W., 'Organic Light Emitting Devices Fabricated from Semiconducting Nanospheres', *Adv. Matter*., vol. 15, no.10, pp. 800-8005, 2003.

63. Park, E.J.; Erdem, T.; Ibrahimova V.; Nizamoglu S.; Demir, H.V.; Tuncel D., 'White Emitting Conjugated Polymer Nanoparticles with Crosslinked Shell for Mechanical Stability and Controllable Photometric Properties in Color-Conversion LED Applications', *ACS Nano*, vol. 5, no. 4, 2483-2492, 2011.

64. Kietzke, T.; Neher D.; Kumke M.; Montenegro N.; Landfester K.; Sherf U.; 'A Nanoparticle Approach to Control the Phase Separation Polyfluorene Photovoltaic Devices', *Macromolecule*s, vol. 37, pp. 4882-4890, 2004.

65. Gumbleton, M.; Stephens D.J., 'Coming Out of the Dark: The Evolving Role of the Fluorescence Imaging in Drug Delivery Research', *Adv. Drug Deliv. Rev.*, vol. 57, pp. 5-15, 2005.

66. Stephens, D. J.; Allan, V.J., 'Light Microscopy Techniques for Live Cell Imaging', *Science*, vol. 300, pp. 82-86, 2003.

67. Liu, Z.Y.; Liu, M.; Song, W.L.; Pan, K., Li, J. H.; Bai, Y. B.; Li; t. J., 'Multifluorescent Dye Doped SiO2/Lanthanide Complexes Hybrid Particles' *Matter. Lett.*, vol. 60, pp. 1629-1633, 2006.

68. Zhou, X. C.; Zhou, J. Z.; 'Improving the Signal Sensitivity and Photostability of DNA Hybridizations on Microarrays by Using Dye-Doped Core Shell Silica Nanoparticles', *Anal. Chem.*, vol. 76, pp. 5302-5312, 2004.

69. Hines, M. A.; Guyot, S., 'Synthesis and Characterization of Strongly Luminescing ZnS capped CdSe Nanocrystals', *J. Phys. Chem.*, vol. 100, pp. 468-471, 1996.

70. Wu, Changfeng; Bull, B.; Christensen K.; McNeill J.,' Multicolor Conjugated Polymers Dots for Biological Fluorescence Imaging', *ACS Nano,* vol.2, no. 11, pp. 2415-2423, 2008.

71. Allen T. M.; Culli P. R.; 'Drug Delivery Systems Entering the Mainstream', *Science,* vol. 303, pp. 1818-1822, 2004.

72. Pelicano H.; Martin D. S.; Xu, R. H.; Huang, P.; 'Glycolysis Inhibition for Anti-Cancer Treatment', *Oncogene,* vol. 25, pp. 4633-4646, 2006.

73. Jain; T. K.; Morales, M. A.; Sahoo S. K. Et al ; 'Iron Oxide Nanoparticles for Sustained Delivery of Anti-Cancer Agents', *Mol. Pharm.*, vol. 2, pp. 194-205, 2005.

74. Cuenca, A. G.; Jiang, H.; Hochwald S. N. et al ,'Emerging Applications of Nanotechnology on Cancer Diagnotics and Thearepeutics', *Cancer,* vol. 107, pp. 459-466, 2006.

75. Stohrer, M.; Boucher, Y.; Stangassinger M.; Jain, R. K., 'Oncotic Pressure in Solid Tumors is Elevated', *Cancer Res.*, vol. 60, pp. 4351-4255, 2000.

76. Seymour L. W.; Fery D. R.; Anderson D. et al, 'Hepatic Drug Targeting: Phase I Evoluation of Polymer Bound Doxorubicin', *J. Clin. Oncol.* ; vol. 20, pp. 1668-1676, 2002.

77. Farokhzad, O. C.; Langer R., 'Impact of Nanotechnology on Drug Delivery', *ACS Nano*, vol. 3, no.1, pp. 16-20, 2009.

78. Rong, Y.; Changfeng, W.; Jiangbo, Y.; Xuanjun, Z.; Ye, F.; Zeigler, M. et al, 'Multicolor Fluorescent Semiconducting Polymer Dots with Narrrow Emissions and High Brightness', *ACS Nano*, vol. 7, no.1, pp. 376-384, 2013.

79. Feng, X.; Lv, F.; Liu, L.; Tang, H.; Xing, C.; Yang, Q.; Wang, S.; 'Conjugated Polymer Nanoparticles for Drug Delivery and Imaging', *App. Mater. & Int.*, vol. 2, no. 8, 2429-2435, 2010.

80. Fernando, L.; Kandel, P. K.; Yu. J.; McNeill J.; Ackroyd, P. C.; Christensen K. A., 'Mechanism of Cellular Uptake of Highly Fluorescent Polymer Nanoparticles', *Biomacromolecules*, vol 11, pp. 2675- 2682, 2010.

81. McManus, M. T.; Sharp, P. A.; 'Gene Silencing in Mammals by Small Interfering RNAs', *Nat. Rev. Genet*., vol. 3, pp. 737-747, 2002.

82. Dorset, Y.; Tuschl, T.; 'siRNAs: Applications in Functional Genomics and Potentials as Therapeutics', *Nat. Rev. Drug. Discovery*, vol. 3, pp. 318-329, 2004.

83. Jeong, J. H.; Mok, H.; Oh, Y. K.; Park, T. G.; 'siRNA Conjugated Delivery Systems', *Bioconjugate Chem*., vol. 20, no. 1, pp. 5-14, 2009.

84. Dore, K.; Dubus, S.; et al, 'Fluorescent Polymeric Transducer for the Rapid, Simple and Specific Detection of Nucleic Acids at the Zemptomole Level' ,*J. Am. Chem. Soc*.; vol. 126, no. 13, pp. 4240-4244, 2004.

85. Moon, J. H.; Mendez, E.; Kim, Y.; Kaur, A., 'Conjugated Polymer Nanoparticles for Small Interfering RNA Delivery', *Chem. Commun*., vol. 47, pp. 8370-8372, 2011.

86. Ge, J.; Jacobson, G.B.; Labovkina, T.; Holmberg, K.; Zare, R. N., 'Sustained Release of Nucleic Acids from Polymeric Nanoparticles Using Microemulsion Precipitation in Supercritical Carbon Dioxide', *Chem. Commun.*, vol. 46, pp. 9034-9036, 2010.

87. Wang, F.; Banerjee, D.; Liu, Y.; Zhang, Y.; Suvoln, X., 'Upconversion Nanoparticles in Biological Labeling, Imaging and Therapy', *Anaylst*, vol. 135, pp. 1839-1854, 2010.

88. Kim, S.; Lim, C. K. et al, 'Conjugated Polymer Nanoparticles for Biomedical In Vivo Imaging', *Chem. Commun*., vol. 46, pp. 1617- 1619, 2010.

89. Wu, C.; Stacey, C. H. et al, 'Design of Highly Emissive Polymer Dot Bioconjugates for In Vivo Tumor Targetting', *Angew. Chem*., vol. 123, 3492-3496, 2011.

90. Anderson, G. L.; Boyd, W. A.; Williams, P. L., 'Assesment of Sublethal Endpoints for Toxicity Testing with the Nemadote Caenorhabditis Elegans', *Environ. Toxicol. Chem.*, vol. 20, no. 4, pp. 833-838, 2001.

91. The C. Elegans Sequence Consortium et al, *Science*, vol. 282, pp. 2012-2018, 1998.

92. Lim, S. F.; Riehn, R.; Ryu, W. S.; Khanarian, N.; Tung, C. K.; Tank, D.; Austin, R. H.,' In vivo and Scanning Electron Microscopy Imaging of Upconverting Nanophosphors in Caenorhabditis Elegans'. *Nano. Lett*., vol.6, no.2, pp. 169-174, 2006.

93. Mohan, N.; Chen, C. S.; Hsieh, H. H.; Wu, Y. C.; Chang, H. C.; 'In vivo Imaging and Toxicity Assesments of Fluorescent Nanodiamonds in *Caenorhabditis Elegans*' *Nano Lett*., vol. 10, pp. 3692-3699, 2010.

94. Wall, M E.; Wani, M. C.; Cook, C. E.; Palmer, K. H.; McPhail, A. T.; Sim, G. A.; 'Plant Antitumor Agents.I. The Isolation and Structure of Camptothecin, a Novel Alkoloidal Leukemia and Tumor Inhibitor from Camptotheca acuminata', *J. Am. Chem. Soc.*, vol. 88, no. 16, pp. 3888-3890, 1966.

95. Stork, G.; Shultz, A. G., 'Total Synthesis of dI Camptothecin', *J. Am. Chem. Soc.*, vol. 93, no. 16, pp. 4074-4075, 1971.

96. Herzog, T. J., 'Update on the Role of Topotecan in the Treatment of Recurrent Ovarian Cancer', *Oncologist*, vol. 7, pp. 3-10, 2002.

97. Li, Q. Y.; Zu. Y. G.; Shi, R. Z.; Yao, L. P., 'Review Camptothecin: Current Perspectives', *Curr. Med. Chem.*, vol. 13, pp. 2021-2039, 2006.

98. Opanasopit, P.; Yokoyama, M.; Watanabe, M.; Kawano, K.; Maitani, Y.; Okano T.; 'Influence of Serum and Albumins from Different Species on Stability of Camptothecin-loaded Micelles', *J. Control Release*, vol. 104, pp. 313-321, 2005.

99. Sawyer, A. J. *et al,* "Convection Enhanced Delivery of Camptothecin Loaded Nanoparticles for Treatment of Intracranial Tumors", *Drug Deliv. Transl. Res.* , vol. 1, no.1, pp.34-42, 2011.

100. Desai, S. D.; Wood, L. M.; Tsai, Y. C.; Hsieh, T.; Marks, J.R.; Scott, G.,L.; , Giovenella, B. C.; Liu, L. F., "ISG15 as a Novel Tumor Biomarker for Drug Sensitivity", *Mol. Cancer. Ther.*, vol. 7, pp. 1430-1439, 2008.

101. Brangi, M.; Litman, T.; Ciotti, M.; Nishiyama, K.; Kohlhagen, G.; Takimoto, C.; Robey, R.; Pommier, Y.; Fojo, T.; Bates, S.E.; " Camptothecin Resistance: Role of the ATP Binding Casette (ABC) Mitoxantrone-Resistance Half Transporter (MXR) , and Potential for Glucuronidation in MXR –expressing Cells", *Cancer Res.*,vol. 59, pp: 5938-5948, 2009.

102. Jones, C. B.; Clements, M.K.; Wasi, S.; Daoud, S. S.,"Sensitivity to Camptothecin of Human Breast Carcinoma and Normal Endothelial Cells", *Cancer Chemother. Pharmacol.*, vol: 40, no: 6, pp: 475-483, 1997.

103. Timur, M.; Akbas, S. H.; Ozben, T. , "The Effect of Topotecan on Oxidative Stress in MCF-7 Human Breast Cancer Cell Line", *Acta. Biochim. Pol.*, vol: 52, no:4, pp: 892-902, 2005.

104. Van Meerlo J., Kaspers G. J.; Cloos J., "Cell Sentivity Assays : the MTT assay", *Methods Mol. Bio.*, vol. 237, no.45, pp. 731-735, 2011.

105. Anderson P. L.; "The ABCs of Pharmokinetics", The Body, Test Positive Aware Network, 2005.

106. http://www.cellbiolabs.com/sites/default/files/2FD8C527-3048-812A-2EB950C744EB9D73.pdf

107. http://www.hpacultures.org.uk/products/celllines/generalcell/detail.jsp?refId=92020422&collection=ecacc_gc

108. http://www.lgcstandards-atcc.org/products/all/HTB-22.aspx?geo_country=tr

109. Flowers, J. L.; Hoffman, R.H.; Driscoll, T. A.; Wall, M. E.; Wani, M. C.; Manikumar, G.; Friedman H. S.; Dewirst M.; Colvin O. M.; Adams D.J. , "The Activity of Camptothecin Analogs in Enhanced Histocultures of Human Tumors and Human Tumor Xenografts by Modulation of Extracellular pH", *Cancer Chemother. Pharmacol.*, no. 53, pp: 253-261, 2003.

110. Magavi, S. S.; Macklis J. D., "Identification of Newborn Cells by BrdU labeling and Immunocytochemistry in Vivo", *Methods Mol. Bio.*, no. 438, pp: 335-343, 2008.

111. Ozturk, N. *et al*, "Reprogramming of Replicative Senescence in Hepatocellular Carcinoma Derived Cells", *PNAS*, vol. 103, 7, pp. 2178-2183, 2006.

112. Jontes, J. D.; Emond, M. R., "Fluorescence Imaging of Transgenic Zebrafish Embryos", *Cold Spring Harb. Protoc*., no. 5, 2012.

113. Reddy, E. R.; Banote, R. K.; Chatti, K.; Kulkarni, P., Rajadurai, M. S.; "Selevtive Multocolor Imaging of Zebrafish Muscle Fibers by Using Fluorescent Organic Nanoparticles, *ChemBioChem*, no. 13, pp.1889-1894, 2012.

114. Fent, K.; Weisbrod, C. J.; Wirth-Heller, A.; Pieles, U., "Assesment of Uptake and Toxicity of Fluorescent Silica Nanoparticles in Zebrafish Early Life Stages", *Aquot. Toxicol*., vol.100, no.2, pp.218-228, 2010.

115. Ibrahimova, V., "Synthesis and Characterization of Water Dispersible Conjugated Polymer Nanoparticles", *Thesis, Master of Science*, 2011.

116. Gezici, O., "Multifunctional Conjugated Polymer Nanoparticles As an Anticancer Drug Carrier and A Fluorescent Probe For Cell Imaging", *Thesis, Master of Science*, 2012.

117. http://www.wormatlas.org/hermaphrodite/introduction/Introframeset.html

APPENDIX A

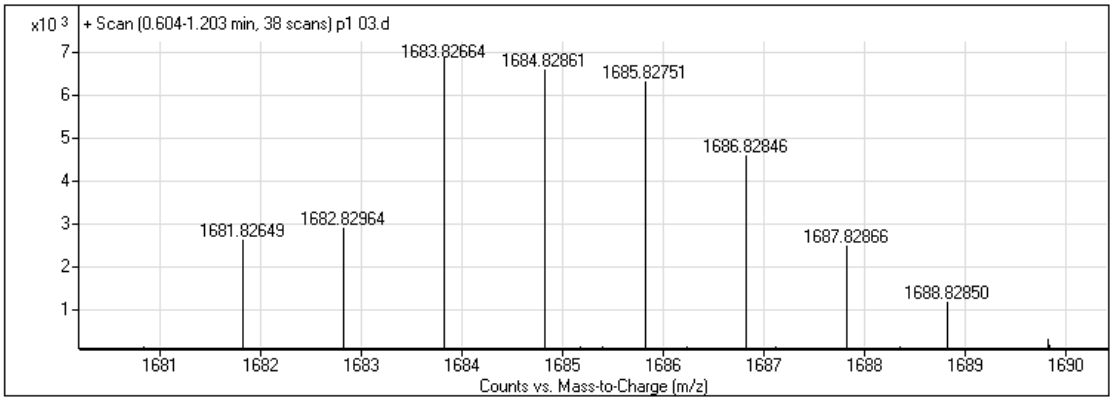

Figure A. 1. ESI-MS spectrum of PDAFBT. ([m/z]+1 = 1684)

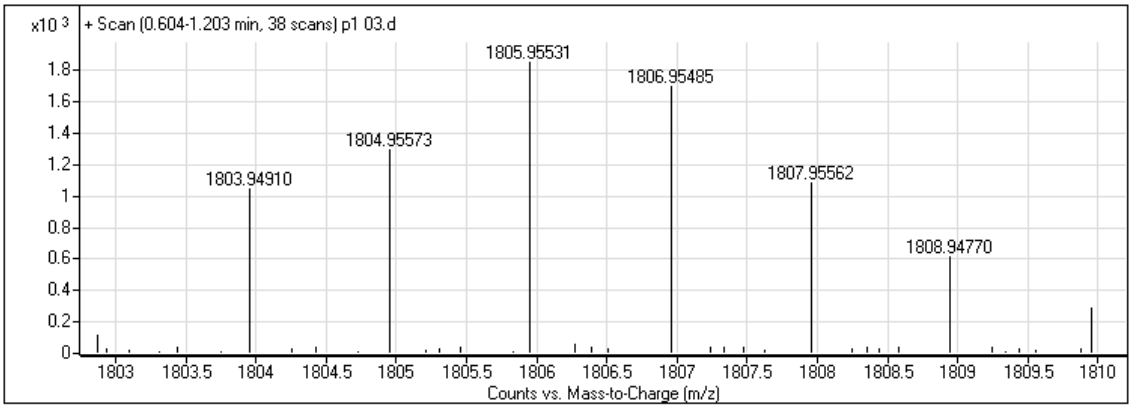

Figure A. 2. ESI-MS spectrum of PDAFBT.([m/z]+1 = 1805)

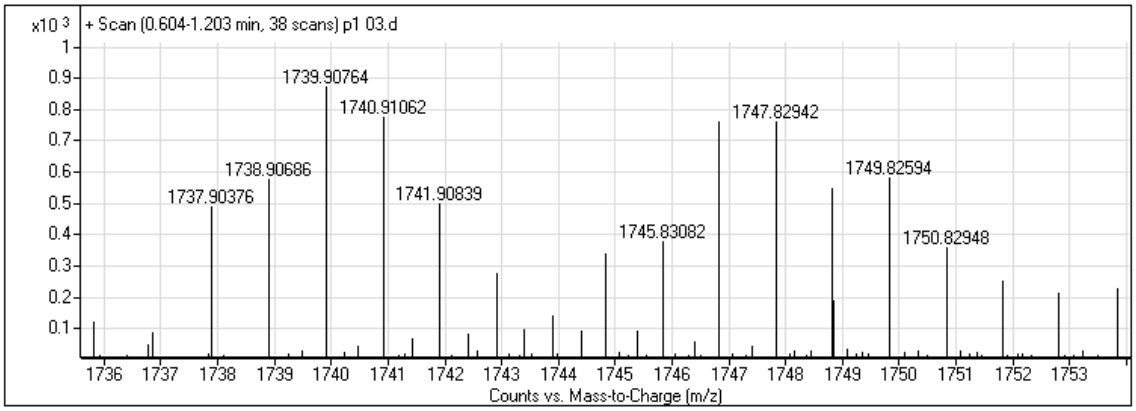

Figure A. 3. ESI-MS spectrum of PDAFBT. ([m/z]+1 = 1739)

		Diam. (nm)	% Number	Width (nm)
Z-Average (d.nm): 83,54	Peak 1:	17,32	100,0	5,915
PdI: 0,224	Peak 2:	0,000	0,0	0,000
Intercept: 0,958	Peak 3:	0,000	0,0	0,000

Result quality : Good

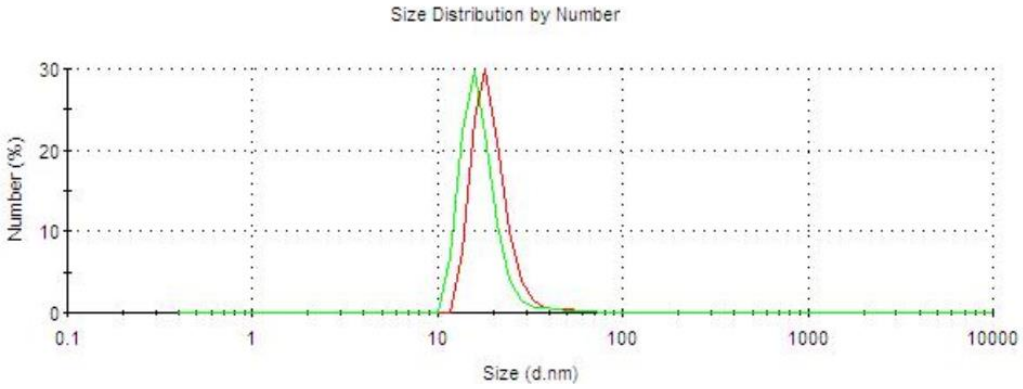

Figure A. 4. Size distrubution histogram of PDAFBT nanoparticles for the detection of their stability in size. (0^{th} day sample -1)

		Diam. (nm)	% Number	Width (nm)
Z-Average (d.nm): 63,55	Peak 1:	18,46	100,0	5,441
PdI: 0,446	Peak 2:	0,000	0,0	0,000
Intercept: 0,943	Peak 3:	0,000	0,0	0,000

Result quality : Refer to quality report

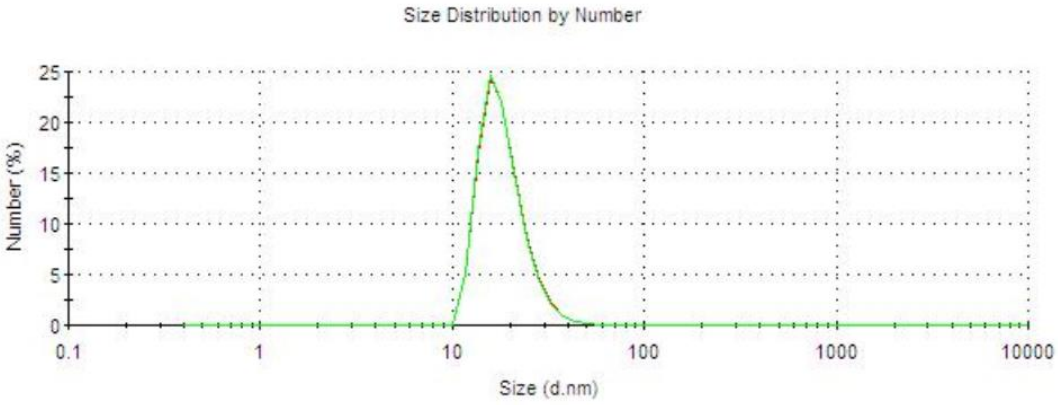

Figure A. 5. Size distrubution histogram of PDAFBT nanoparticles for the detection of their stability in size (0^{th} day , sample-2)

		Diam. (nm)	% Number	Width (nm)
Z-Average (d.nm): 59,74	Peak 1:	11,38	100,0	4,450
PdI: 0,472	Peak 2:	0,000	0,0	0,000
Intercept: 0,949	Peak 3:	0,000	0,0	0,000

Result quality : Good

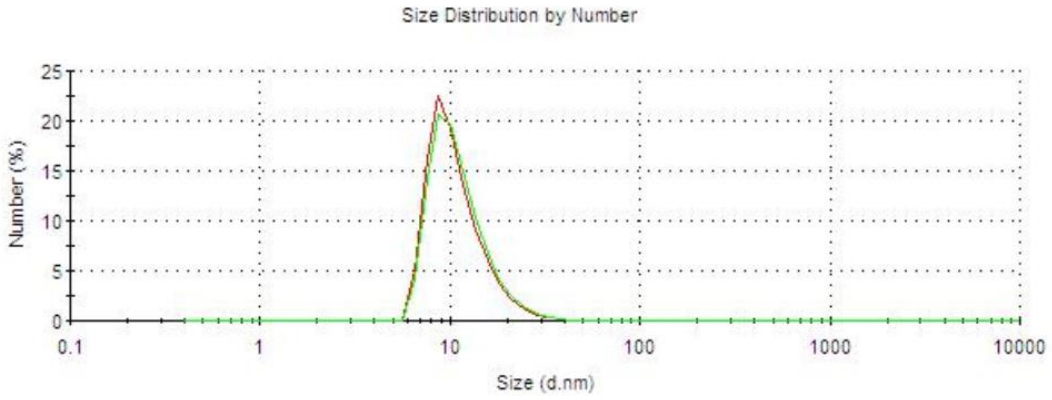

Figure A. 6. Size distrubution histogram of PDAFBT nanoparticles for the detection of their stability in size. (0^{th} day- sample-3)

		Diam. (nm)	% Number	Width (nm)
Z-Average (d.nm): 86,92	Peak 1:	19,08	100,0	8,982
PdI: 0,216	Peak 2:	0,000	0,0	0,000
Intercept: 0,956	Peak 3:	0,000	0,0	0,000

Result quality : Good

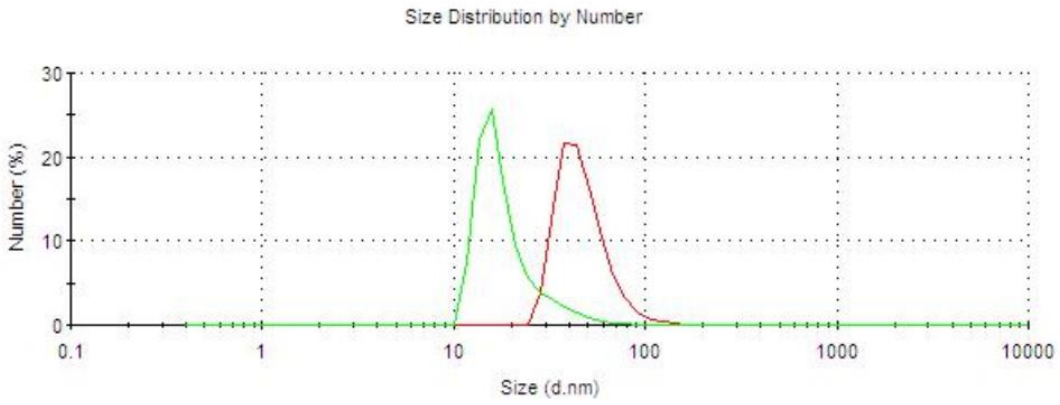

Figure A. 7. Size distrubution histogram of PDAFBT nanoparticles for the detection of their stability in size. (3^{rd} day, sample-1)

		Diam. (nm)	% Number	Width (nm)
Z-Average (d.nm): 82,67	Peak 1:	16,00	100,0	5,794
PdI: 0,222	Peak 2:	0,000	0,0	0,000
Intercept: 0,959	Peak 3:	0,000	0,0	0,000

Result quality : Good

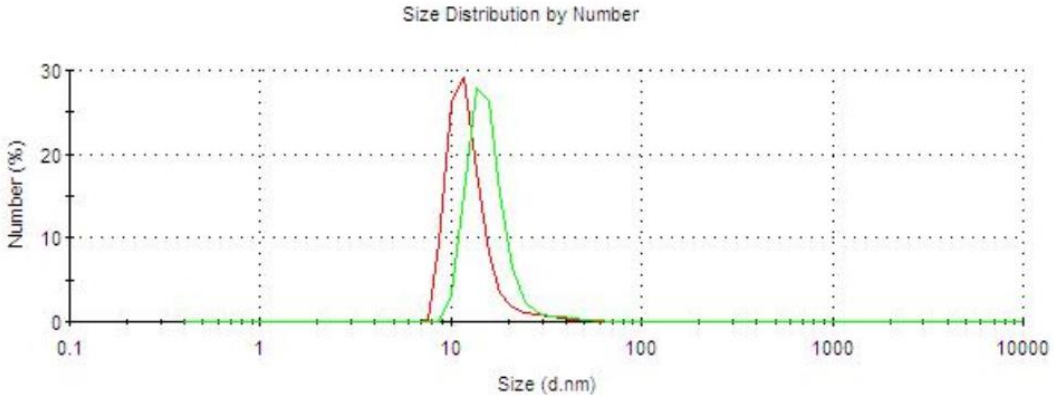

Figure A. 8. Size distrubution histogram of PDAFBT nanoparticles for the detection of their stability in size. (3rd day- Sample-2)

		Diam. (nm)	% Number	Width (nm)
Z-Average (d.nm): 64,29	Peak 1:	15,70	100,0	4,480
PdI: 0,410	Peak 2:	0,000	0,0	0,000
Intercept: 0,951	Peak 3:	0,000	0,0	0,000

Result quality : Good

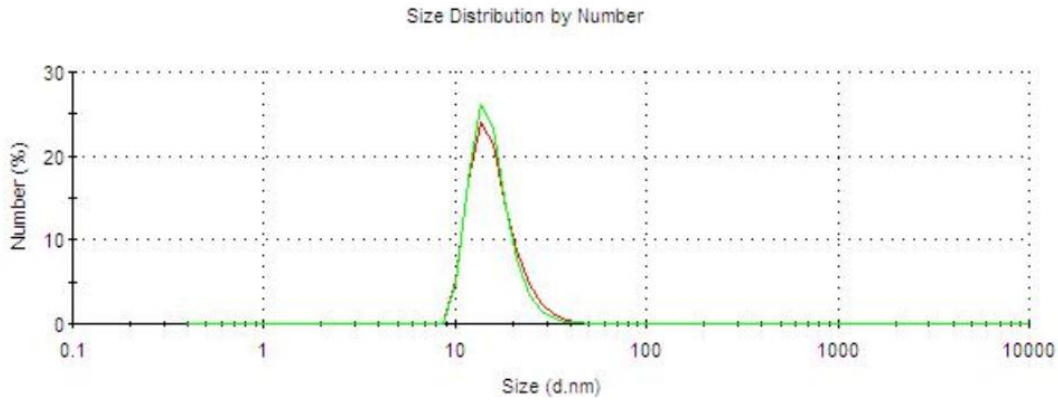

Figure A. 9. Size distrubution histogram of PDAFBT nanoparticles for the detection of their stability in size. (3rd day, Sample-3)

		Diam. (nm)	% Number	Width (nm)
Z-Average (d.nm): 86,92	Peak 1:	19,08	100,0	8,982
PdI: 0,216	Peak 2:	0,000	0,0	0,000
Intercept: 0,956	Peak 3:	0,000	0,0	0,000

Result quality : Good

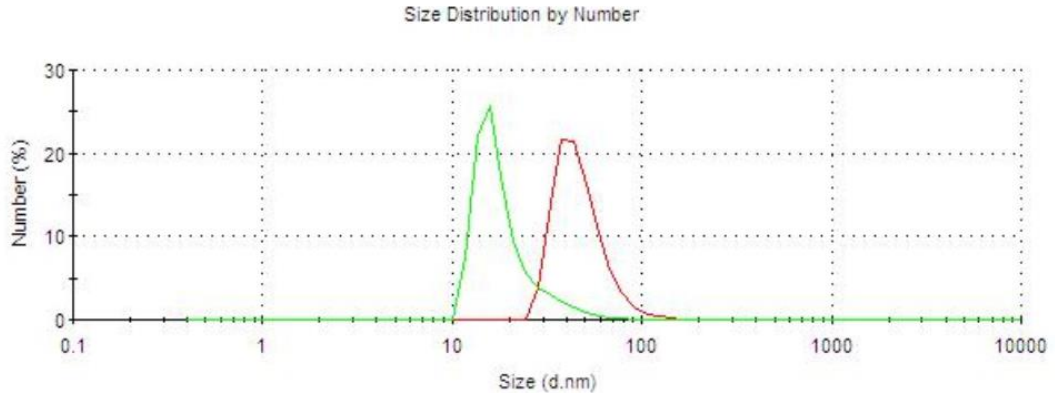

Figure A. 10. Size distrubution histogram of PDAFBT nanoparticles for the detection of their stability in size. (7th day, Sample-1)

		Diam. (nm)	% Number	Width (nm)
Z-Average (d.nm): 82,76	Peak 1:	16,93	100,0	5,536
PdI: 0,240	Peak 2:	0,000	0,0	0,000
Intercept: 0,959	Peak 3:	0,000	0,0	0,000

Result quality : Good

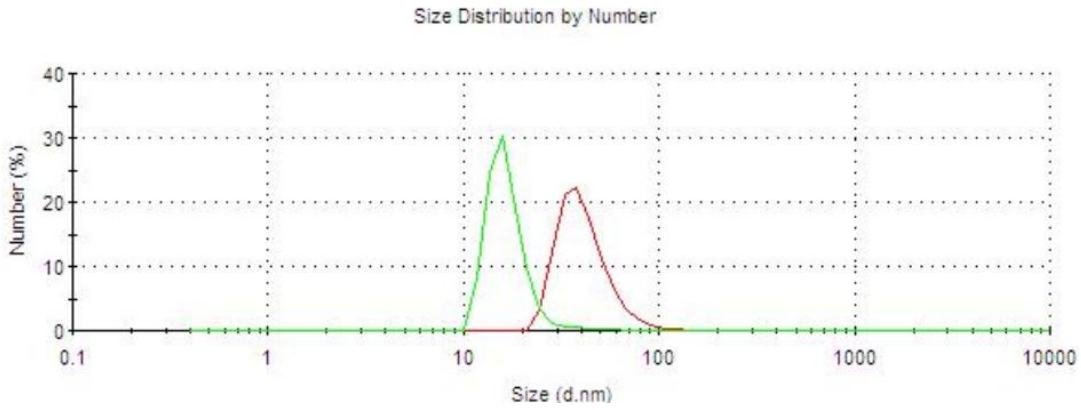

Figure A. 11. Size distrubution histogram of PDAFBT nanoparticles for the detection of their stability in size. (7th day, Sample-2)

		Diam. (nm)	% Number	Width (nm)
Z-Average (d.nm): 64,29	Peak 1:	15,70	100,0	4,480
PdI: 0,410	Peak 2:	0,000	0,0	0,000
Intercept: 0,951	Peak 3:	0,000	0,0	0,000

Result quality : Good

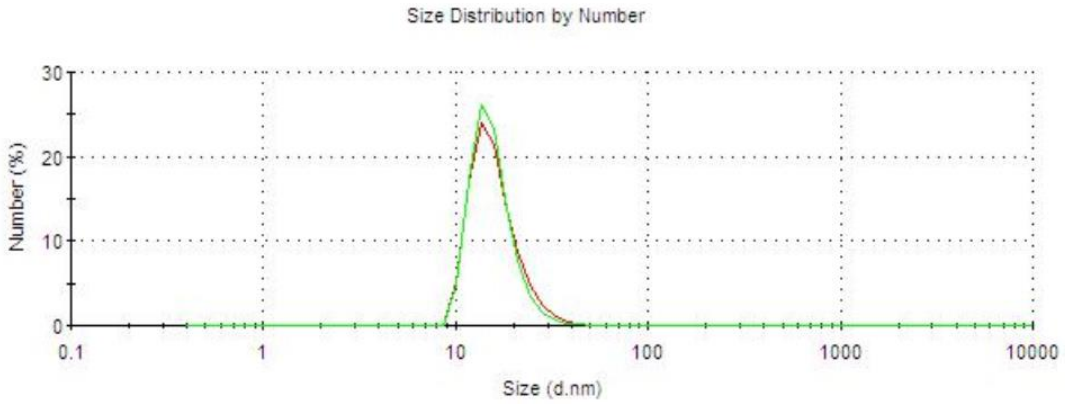

Figure A. 12. Size distrubution histogram of PDAFBT nanoparticles for the detection of their stability in size. (7th day, Sample-3)

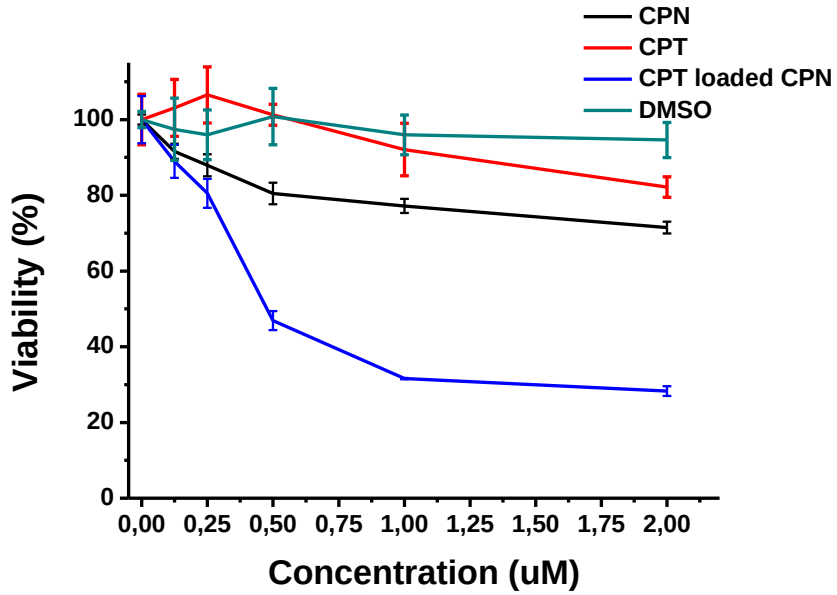

Figure A. 13. Cell Viability Assay of blank and non-loaded PDAFBT NPs on MDA-MB-157. (Replicate-2)

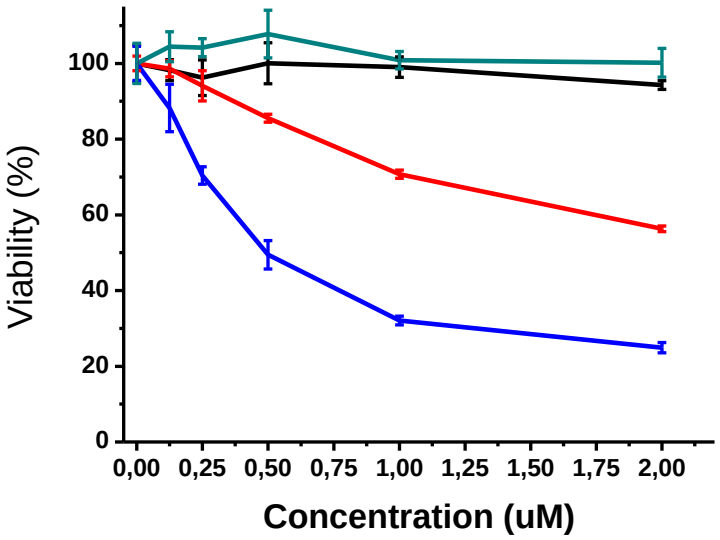

Figure A. 14. Cell Viability Assay of blank and non-loaded PDAFBT NPs on MDA-MB-231. (Replicate-2)

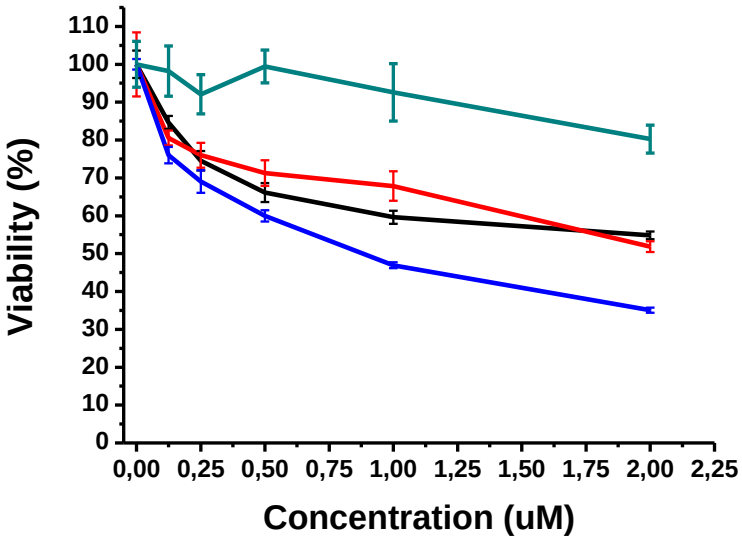

Figure A. 15. Cell Viability Assay of blank and non-loaded PDAFBT NPs on MCF-7. (Replicate-2)